Optimisation of the ONNV Reverse Genetic System

Samuel Jonathan Walby

Submitted in accordance with the requirements for the
degree of Master of Science by Research
The University of Leeds
School of Molecular and Cellular Biology
July 2021

The candidate confirms that the work submitted is their own and that appropriate credit has been given where reference has been made to the work of others.

Acknowledgements

I would like to personally thank my supervisors, Dr Andrew Tuplin and Dr Juan Fontana for their continued ceaseless support, guidance, and keeping me positive throughout. My thanks go out to every member of the Tuplin and Fontana lab groups, as well as all of 8.61, your support sculpted me into a better scientist. Thanks specifically to Dr Fontana and Ben Chadwick for preforming parts of key with within the thesis. Special thanks goes to my fellow MRes Students Joe O'Byrne, Koulla Panayi and Katie Brighton, whom without their friendship and emotional support I may not have made it through. Thank you to Craig Sunman, Will Smith, Indiana Wilson-Brown, Alison Wilson-Brown and Joshua Warnes, all of whom provided me the morale I needed to see the project to the end.
Finally, I'd like to offer my endless gratitude to my parents, Michelle and Gregory Walby, my aunt Melissa Cavill, and my late great uncle Ian Hunter, for their emotional and financial support every step of the way. Thank you for everything, without you, I could never reach these lofty heights.

Abstract

The rate at which emergent Alphavirus epidemics occur globally is increasing. Of the alphaviruses, Chikungunya Virus (CHIKV) is the most geographically and medically prominent, causing number of recent epidemics and increasing in geographic range – due to a range of factors including changing land use, international travel, climate change and mutations associated with changing vector competence. CHIKV's closest genetic relative, O'nyong-nyong Virus (ONNV), has been identified as the causative pathogen of a serious epidemic that affected approximately 2 million people in Sub-Saharan Africa in 1959. However, ONNV has not been well studied, in part due to a paucity of molecular tools and an optimised reverse genetic system.

In the current study replication of three alternative recombinant ONNV infectious clones, expressing different molecular markers of replication, was assessed and optimised across a range of mammalian and mosquito cell lines. We demonstrated that BHK-21, Huh7, RD, C6/36 and U4.4 cells were all permissible to ONNV infection, producing titres ranging from 10^5 PFU/mL to 10^8 PFU/mL. Notably, infectious clones replicating using nsP3-mCherry fusion proteins replicated producing lower titres in C6/36 relative to the other clones over 48 hours. The efficiency of antibodies raised against CHIKV non-structural proteins was demonstrated against ONNV expressed proteins, using both western blot and Immunofluorescence using confocal microscopy.

In order to further validate the reverse genetic systems, for the first time ONNV virions were imaged using negative staining and transmission electron microscopy, and a 3D structure of ONNV virions was generated by image averaging. Comparisons to published CHIKV virus-like particles showed differences in size and icosahedral structure. In summary, for the first time this study optimised the reverse genetic system for ONNV replication, across alternative physiologically relevant cell lines and molecular tools for further investigation of ONNV replication and structure.

Contents

LIST OF FIGURES

LIST OF TABLES

Abbreviations

2ZsG	ONNV_2sg_ZsGreen
$A_{(n)}$	Poly-A tail
ACDP	Advisory committee on dangerous pathogens
Akt	Protein kinase B
ANOVA	Analysis of variances
AUD	Alphavirus unique domain
APS	Ammonium persulphate
BCA	Bicinchoninic acid
BSL	Biosafety level
CCHFV	Crimean-Congo haemorrhagic fever virus
cDNA	Complementary DNA
CHIKV	Chikungunya virus
CPV-1	Cytopathic vacuole type-1
Cryo-EM	Cryogenic electron microscopy
DAPI	4’6-diamidino-2-phenylindone
DENV	Dengue virus
DM	Digital Micrograph
DMSO	Dimethylsulphoxide
DMEM	Dulbecco’s modified eagle’s medium
dsRNA	Double stranded ribonucleic acid
DTT	Dithiothreitol
DOC	Sodium deoxycholate
DRC	Democratic Republic of Congo
EDTA	Ethylenediaminetetraacetic acid
EEEV	Eastern equine encephalitis virus
ELISA	Enzyme-linked immunosorbent assay
EM	Electron microscopy
FBS	Foetal bovine serum
FHL-1	Four-and-a half LIM domain 1
G3BP1/2	Ras GTPase-activating protein-binding protein ½
gRNA	Genomic RNA
HI	Haemagglutinin inhibition test
hpi	Hours post infection
HVD	Hypervariable domain

ICRES	Integration of Chikungunya research
IF	Immunofluorescence
IFN	Interferon
JAK/STAT	Janus kinase-signal transducer and activator of transcription
JEV	Japanese encephalitis virus
kb	Kilobases
kDa	Kilodaltons
MAR	Mono-ADP ribose
MAYV	Mayaro virus
MOI	Multiplicity of infection
MOPS	3-(N-morpholino) propane sulphonic acid
mRNA	Messenger ribonucleic acid
MTT	Thiazolyl blue tetrazoluim bromide
NAP1	Nucleosome assembly protein 1
nsP	Non-structural protein
ONNV	O'nyong-nyong virus
ORF	Open reading frame
P3mCh	ONNV_P3_mCherry
P3ZsG	ONNV_P3_ZsGreen
PAGE	Poly-Acrylamide gel electrophoresis
PAR	Poly-ADP ribose
PBS	Phosphate buffered saline
PI3K	Phosphoinositide 3-kinase
PO	Phenoloxidase
RC	Replication complex
RdRp	RNA dependant RNA polymerase
RNA	Ribonucleic acid
SDS	Sodium dodecyl sulphate
SFV	Semliki Forest virus
SGP	Subgenomic promoter
sgRNA	Sub-genomic ribonucleic acid
SH3	Src homology-3
SINV	Sindbis virus
TATase	Terminal adenylyltransferase
TBEV	Tick-Borne Encephalitis virus
TBP	Tris buffered phosphate
TBS	Tris buffered saline

TEM	Transmission electron microscopy
TIA	TEM Imaging and Analysis
TOSV	Toscana virus
UA	Uranyl acetate
UTR	Untranslated region
VLP	Virus-Like particle
WNV	West Nile virus
YFV	Yellow Fever virus
ZIKV	Zika virus

Chapter 1: Optimisation of the ONNV Reverse Genetic System: Introduction

1.1 What is an Alphavirus?

The genus *Alphavirus* represents enveloped, positive-sense, single-stranded RNA viruses found in the family *Togaviridae*, which are transmitted through the bite of an arthropod vector (Strauss & Strauss, 1994). Alphaviruses are distributed on every continent across the world excluding Antarctica and distribution of individual species are restricted by host-vector restrictions and ecological niches. Alphavirus virions are icosahedral particles formed of a lipid bilayer derived from its host cell, modified with 240 copies of E1 and E2 proteins, which form a heterodimer within it (Strauss & Strauss, 1994). Three E1-E2 heterodimers interact together to form the spike glycoproteins found on the virus surface, which when formed, anchor into the host lipid bilayer (Strauss & Strauss, 1994). The core of the virion is a nucleocapsid, created from an arrangement of capsid proteins that contain the genomic RNA, approximately 11kb (kilobases) long, protecting it from the extracellular environment (Lee *et al.*, 1996).

Medically relevant Alphaviruses cause acute febrile illness that progresses to either encephalitis or polyarthralgia, both debilitating and sometimes fatal conditions. Arthritogenic alphavirus infections debilitate hosts with crippling arthritis that can leave patients debilitated for weeks to months, causing a serious loss of wellbeing and the inability to work during that time. Encephalitic alphaviruses cause similar febrile symptoms, followed by severe neurological symptoms such as confusion, seizures, coma and death, with other specific symptoms for each species (Deresiewicz *et al.*, 1997; Reeves *et al.*, 1958). In both groups, there are efforts being made to discover antiviral treatments and vaccines to prevent infection, but these are ongoing. A greater understanding of alphaviral virus-host interactions is required to discover anti-virals that interrupt the virus lifecycle or elucidate potential viral proteins for use in vaccines.

1.2 Alphaviral Transmission and Emergent Epidemics

Transmission of alphaviruses occurs through the bite or intake of a bloodmeal, allowing virus to pass from the invertebrate vector to the host, or vice versa in a viraemic host. These cycles are sylvatic, requiring an animal host in order to propagate high enough viral titres to cause infection in the next animal host. In an urban epidemic however, the virus is adapted to propagate in human hosts as an amplifying host, causing a higher titre viremia, allowing a vector to take up enough virus to carry it to the next human host and successfully infect them (Barzon, 2018) (Fig.1.1). The rate of infection varies due to certain factors; changes to vector populations and distributions, changes to a vector's environment via climate change or deforestation and rapid adaptation to human hosts, to name a few (Gould & Higgs, 2009; Maciel-de-Freitas *et al.*, 2014; Weaver & Reisen, 2010). By removing the need for an animal host, virions are carried from viremic human hosts to the uninfected at a faster rate, increasing the rate at which an outbreak occurs.

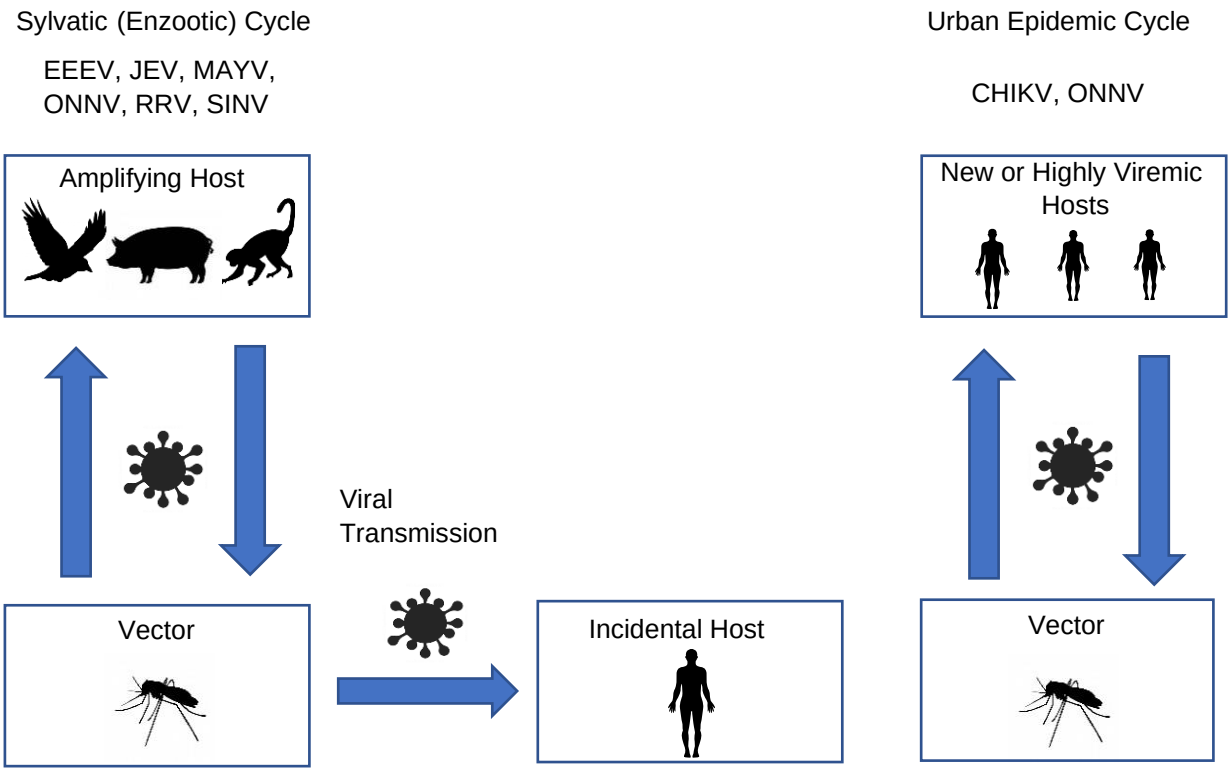

Figure 1.1. Transmission Cycles of Alphaviruses. CHIKV- Chikungunya Virus, EEEV- Eastern Equine Encephalitis Virus, JEV- Japanese Encephalitis Virus, MAYV- Mayaro Virus, ONNV- O'nyong Nyong Virus, RRV- Ross River Virus, SINV- Sindbis Virus

In a globalising world, this increased rate of infection causes emergence/re-emergence of alphaviruses on a more rapid and global scale than previously recorded. Arthritogenic alphaviruses have been reported to cause localised outbreaks or epidemics across the world, often with severe symptoms in hosts (Gould & Higgs, 2009). Smaller outbreaks of sylvatic alphaviruses, infections contracted from wild animals, can be managed with palliative care, such as in Scandanavia where Sindbis Virus (SINV) causes 170 annual cases of disease in humans (Suhrbier *et al.*, 2012). In regions where a vector frequently takes blood meals from humans however, alphaviral infection can become endemic within a population; O'nyong nyong virus (ONNV), an alphavirus isolated to the African Subcontinent, was estimated to have infected two million people in an outbreak between 1959-61 and is now thought to be endemic to those regions (Pezzi *et al.*, 2020; Williams *et al.*, 1965). Evidently, alphaviruses that adapt away from a sylvatic cycle pose a significant risk to public health and greater understanding of transmission in these urban epidemics is essential to effective infection control.

1.3 Alphaviruses

1.3.1 O'nyong nyong Virus

O'nyong nyong virus is an *Alphavirus* closely related to Chikungunya Virus (CHIKV), both of which are in the Semliki Forest antigenic complex (Powers *et al.*, 2000). The virus is primarily transmitted by *Anopholes funestus* and *Anopheles gambiae* mosquitoes, found across sub-Saharan Africa, contributing to the endemic nature of ONNV in the region, notably Uganda and Kenya (LaBeaud *et al.*, 2015). An infection of ONNV known as O'nyong nyong fever typically manifests as a sudden onset fever with headache, rash, severe arthralgia and lymphadenitis, and can be misdiagnosed as Dengue Fever or a CHIKV infection (Kiwanuka *et al.*, 1999).

1.3.2 ONNV Transmission

As described previously, the primary vectors for ONNV are *A. funestus* and *A. gambiae*. This is unique to ONNV as the only alphavirus to be transmitted by *Anopheles* mosquitoes and during outbreaks, infections have been consistently limited to habitats of *A. funestus* and *A. gambiae* (Brault *et al.*, 2004). *A. funestus* and *A. gambiae* are highly anthropophilic species, preferring to feed and rest within human dwellings; these behaviours heighten the frequency of ONNV transmission (Pezzi *et al.*, 2020). ONNV is thought to be maintained in an enzootic

cycle during times between epidemics, but neither the enzootic vector nor an animal reservoir have been confirmed (Powers *et al.*, 2000). ONNV-specific neutralising antibodies have been detected in four duiker species (*Cephalophus* and *Philantomba* spp.) in the Democratic Republic of Congo (DRC), forest buffalo (*Syncerus caffer nanus*) in the DRC and Gabon, and Mandrills (*Mandrillus sphinx*) in Gabon (Kading *et al.*, 2013). These detections were observed in periods without known ONNV epidemic activity, suggesting these species could be vertebrate reservoirs in ONNV's enzootic cycle.

ONNV Non-Structural Protein 3 (nsP) has been implicated in ONNV's unique vector tropism. In chimeric viral constructs of CHIKV and ONNV, a CHIK/ONNV nsP3 chimera was found to be able to infect *A. gambiae*, providing evidence that ONNV's vector specificity is determined by nsP3 (Saxton-Shaw *et al.*, 2013). Attempts made to determine which region provides the specificity were inconclusive but demonstrated a small increase in infection if a chimeric CHIKV had an ONNV carboxyl terminal present. ONNV's carboxyl terminal may be involved in the optimisation of replication in a diverse variety of host cell types in other alphaviruses (Lastarza *et al.*, 1994; Saxton-Shaw *et al.*, 2013).

1.3.3 ONNV Epidemiology and Serology

The first recorded outbreak of ONNV was documented in May 1959; an outbreak of a Dengue-like disease was identified by medical professionals in the Moyo and Arua districts of Uganda. Researchers from the East African Virus Research Institute isolated the virus from *A. funestus* and *A. gambiae*. By comparing regions where these two vectors were present and infection rates, they confirmed these to be the vectors and the virus to be a unique species; CHIKV was initially assumed due to the similarity of symptoms (Haddow, 1960). ONNV spread across eastern Africa, to Kenya, Tanzania, Malawi and Mozambique, estimated to have infected more than two million people with no recorded fatalities, before slowly subsiding (Williams *et al.*, 1965). No cases of ONNV were reported until June 1997, when the first recognised re-emergence of the fever's symptoms appeared in the Rakai district of Uganda, causing acute symptoms including fever, lymphadenitis, skin rash and serious arthritis. Notably, this outbreak was of a smaller proportion and isolated to only Uganda, affecting significantly less people as a result (Lanciotti *et al.*, 1998; Rwaguma *et al.*, 1997). Since then, in 2013 a case of O'nyong nyong fever was reported in a 60 year old German woman whom had been travelling in East Africa; the first confirmed case of an ONNV infection imported to Europe (Tappe *et al.*, 2014). ONNV cases may be misdiagnosed as CHIKV due to their similar symptoms, and infections reliably produce cross-reactive ONNV/CHIKV-neutralising antibodies, as shown by the patient described (Blackburn *et al.*,

1995; Partidos *et al.*, 2012; Tappe *et al.*, 2014).

Seroprevalence analysis of ONNV infections in endemic regions is poorly monitored geographically; seroprevalence studies to identify the presence of ONNV-neutralising antibodies have been performed in Kenya, Cameroon and Nigeria, while other Central African countries where outbreaks have occurred have not had such studies. Furthermore, the seroprevalence data obtained is scarce and not robust, owing to an absence of infection surveillance and cross-reactive ONNV/CHIKV-neutralising antibodies (Pezzi *et al.*, 2019a). Identification of ONNV and CHIKV via Immunofluorescence test, enzyme-linked immunosorbent assay (ELISA), complement fixation test or haemagglutinin inhibition test (HI) is reported to be difficult due to antibody cross-reactivity (Fokam *et al.*, 2010; Woodruff *et al.*, 1978). The cross-reactivity of ONNV/CHIKV-neutralising antibodies has proven to be a fundamental issue when performing serosurveys and reliably diagnosing ONNV. Immunological analyses of ONNV virions has previously demonstrated retention of most of the antigenic sites previously characterised for CHIKV (Blackburn *et al.*, 1995). Investigation into this cross-reactivity revealed a conserved epitope in the B domain of the E2 protein, in which multiple cross-reactive antibodies would bind to neutralise CHIKV, ONNV and other alphaviruses (Fox *et al.*, 2015).

Studies on the seroprevalence of ONNV and CHIKV in Kenya have shown that both are endemic and undiagnosed amongst the population, with a higher seroprevalence in young adults that lowers with age (LaBeaud *et al.*, 2015). Women were also considered more at risk in this study since cultural gender roles within communities where ONNV is endemic have women staying around the home. *A. funestus* and *A. gambiae*, as stated prior are anthrophilic, preferring to feed in homes (LaBeaud *et al.*, 2015; Pezzi *et al.*, 2020). 38% of the positive results in this survey could not differentiate between ONNV and CHIKV, displaying that seroprevalence studies also suffer with the issue of cross-reactivity as discussed previously (LaBeaud *et al.*, 2015). They also do not account for past infections that did not induce an effective immune response in a population, and the generation of false negative results can skew outcomes.

At current time, there are no commercially available molecular tests for detecting an ONNV infection, and there are no international standards in place for molecular detection, molecular assays have been created but have yet to be standardised (Pezzi *et al.*, 2019b).

1.3.4 ONNV Treatment

Treatment for O'nyong nyong fever is palliative and not curative as there are no known curative treatments for the virus, nor an available vaccine. Vaccines are thought to be feasible due to current developments in other alphavirus vaccines, specifically CHIKV. When developing a highly attenuated CHIKV vaccine, a dose was found to produce a strong cross-neutralising antibody response, protecting an A129 mouse against ONNV infection (Partidos *et al.*, 2012). A129 mice are a knockout mouse model incapable of the interferon α/β innate immune response, highlighting that the active immunity was developed due to exposure to the CHIKV vaccine. Recently, these findings were corroborated in a potential CHIKV vaccine trial when ONNV-pseudotyped vectors were neutralised by human sera that had been exposed to a measles-vectored CHIKV vaccine, adding to the idea that a CHIKV vaccine could provide cross-protection against ONNV (Henss *et al.*, 2020).

1.3.5 Chikungunya Virus

Chikungunya Virus is a mosquito-borne alphavirus closely related to ONNV and which is associated with similar symptoms; an acute phase with fever, characteristic rash and polyarthralgia, which can lead to disability for weeks to years as a chronic condition (Pialoux *et al.*, 2007; Queyriaux *et al.*, 2008). Symptoms manifest as more severe in the immunocompromised (elderly and young children) and can cause serious complications such as haemorrhagic fever, meningoencephalitis, febrile seizures, acute encephalopathy and multiple organ failure (Pialoux *et al.*, 2007; Queyriaux *et al.*, 2008; Robin *et al.*, 2008).

1.3.6 CHIKV Epidemiology

Discovered in 1953 after an outbreak in Tanzania, CHIKV had numerous small scale outbreaks across Central and Southern Africa, transmitted by *Aedes aegypti* mosquitos, causing outbreaks when the *A. aegypti* population increased (Vu *et al.*, 2017). In 2004, a large epidemic emerged in Kenya and spread to islands in the Indian Ocean, which led to a large outbreak on La Reunion Island in 2005-2006. La Reunion had a population of 770,000, and by April 2006, 255,000 cases had been reported, with the first deaths (254) caused either directly or indirectly by CHIKV (Josseran *et al.*, 2006; Pialoux *et al.*, 2007). Of note, *Ae. aegypti* was found to be scarce during the epidemic, and a species of mosquito thought to not be a vector, *Aedes albopictus* was identified as the primary vector. La Reunion has a scarce *Ae. aegypti* population, which applied an ecological pressure on CHIKV to adapt to a

new vector for transmission, of which the highly populous *Ae. albopictus* was adapted to (de Lamballerie *et al.*, 2008). Following nucleotide sequence analysis during the epidemic, a novel amino acid substitution from alanine to valine at position 226 in the E1 envelope protein (A226V), enhancing the mutant's ability to be transmitted from *Ae. albopictus* to human hosts (Schuffenecker *et al.*, 2006; Tsetsarkin *et al.*, 2007). Current thinking suggests that another residue, E1-98 controls CHIKV's sensitivity to E1-A226V mutations, in order to modulate the conditions required for E1 fusion loop interactions, thus regulating CHIKV's fusion dynamics with Ae. *albopictus* membranes upon viral entry (Tsetsarkin *et al.*, 2011).

Since 2006, there have been localised CHIKV epidemics in China, Italy, France, multiple Caribbean islands, Brazil, multiple pacific islands and the mainland United States of America, specifically Florida and Texas (Cassadou *et al.*, 2014; Grandadam *et al.*, 2011; Lindh *et al.*, 2019; Pyke *et al.*, 2018; Staples & Fischer, 2014; Wu *et al.*, 2013). *Ae. albopictus* is an expanding invasive species, consequently there are concerns that it may be associated with further autochthonous transmission in temperate regions, previously free of CHIKV infection (Kraemer *et al.*, 2019; Martinet *et al.*, 2019; Wilson & Schlagenhauf, 2016).

1.3.7 Phylogeny of ONNV and CHIKV

ONNV and CHIKV have a connected history; it is hypothesised the two viruses diverged from a common ancestor thousands of years ago, forming their own monophyletic group within the Semliki Forest antigenic complex, and the two are the closest relative of one another (Powers *et al.*, 2000). Phylogenetic analysis of the E1 envelope gene for the viruses was performed, showing a 28% and 13% divergence in their nucleotide and amino acid levels respectively, indicating their phylogenetic distinctness, while simultaneously showing their shared lineage (Powers *et al.*, 2000).

CHIKV's nucleotide sequence has been determined and characterised with comparisons to other alphaviruses, including ONNV. When ONNV and CHIKV's sequenced genomes were compared, both the structural and non-structural proteins displayed an 85% degree of identity, more closely related than any of the other alphaviruses (Khan *et al.*, 2002). Though a comparison between ONNV/CHIK nsP1 (non-structural protein) was not made, the amino acid sequences of ONNV and CHIKV nsP2 displayed a 92% degree of identity (Khan *et al.*, 2002). No sequence comparison was given between ONNV/CHIK nsP3, but both proteins displayed a larger negative charge (-24 and -25 respectively) compared to other alphaviruses such as Semliki Forest Virus (SFV) and Sindbis Virus (SINV) (-10 and -8 respectively) (Khan *et al.*, 2002). A comparison of ONNV/CHIKV nsP4 displayed a 91%

degree of identity, as well as confirmation of the GDD motif, a conserved motif found in other viral RdRps responsible for viral RNA synthesis (Kamer & Argos, 1984; Khan *et al.*, 2002). From these studies, it is clear that ONNV and CHIKV have similar characteristics and interactions, indicating ONNV could provide an effective model system for elucidating CHIKV nsP interactions.

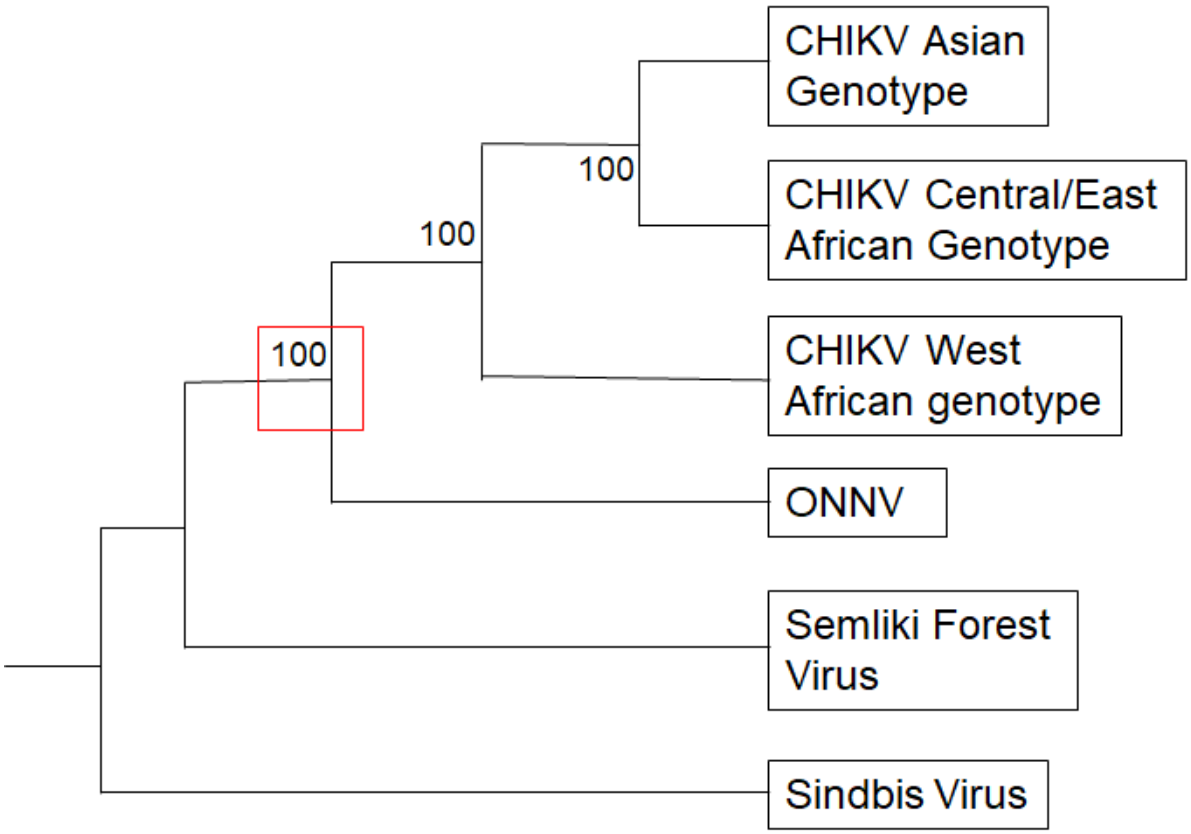

Figure 1.2. Phylogenetic analysis of CHIKV and ONNV generated via PAUP analysis on a 1050bp partial E1 gene sequence. A single distinct clade can be seen, supported by a 100% bootstrap value, for all ONNV isolates, as well as distinct genotypes for CHIKV isolates found in Asia, Western Africa and Central/East Africa. The red square highlights the phylogenetic event in which the common ancestor of CHIKV and ONNV evolved into two distinct species. Figure was adapted from (Powers *et al.*, 2000).

1.4 Alphavirus Replication

Alphaviruses have positive sense, single stranded RNA genomes of around 11kb that encode two open reading frames (ORF). ORF-1 encodes the non-structural proteins and ORF-2, the viral structural proteins. The non-structural proteins are expressed as a single polyprotein, P1234, that is cleaved into four mature non-structural proteins; nsP 1-4, which

are required for successful replication of the virus genome. A smaller P123 polyprotein is produced, comprised of nsP 1-3 (Gorchakov *et al.*, 2008). ORF-2 is transcribed as as 26S subgenomic mRNA, which codes five structural proteins; E1, E2, E3, 6K and capsid protein (Gorchakov *et al.*, 2008). Infection begins with contact between the E glycoprotein and host receptors on the cell surface, which trigger clathrin-mediated endocytosis of the virus into the cell via an endosome (Leung *et al.*, 2011). In the endosome, the E1-E2 complex undergoes a conformational change mediated by the lowering of pH, initiating formation of E1 homotrimers that act as membrane fusion proteins (Helenius *et al.*, 1980; Wahlberg *et al.*, 1992). E1 homotrimers associate with the endosomal membrane and form pores between cellular and viral membranes, through which RNA is released into the cytoplasm (Spyr *et al.*, 1995).

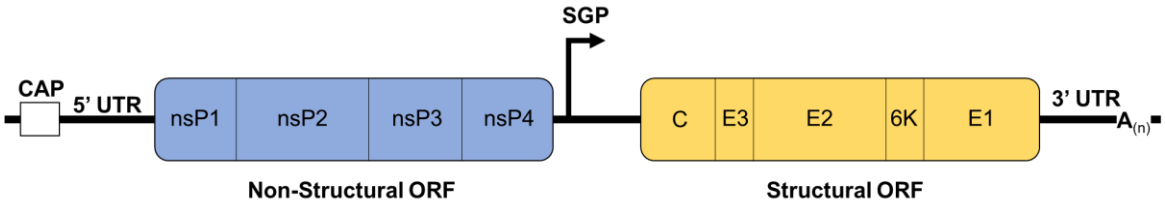

Figure 1.3. Alphavirus genome structure. A single strand, positive sense RNA genome of around 11kb containing a structural and non-structural reading frame, coding for viral proteins. Adapted from (Pietila *et al.*, 2017). A(n), polyA; SGP, subgenomic promoter; UTR, untranslated region.

Following release from the cytoplasm, viral ORF-1 is translated by cellular ribosomes, synthesising non-structural proteins P123 as a polyprotein from the non-structural open reading frame (ORF), terminating at an opal stop codon and P1234 when readthrough of the opal codon occurs. In ONNV, Semliki Forest Virus (SFV) and many CHIKV isolates, the opal termination codon is replaced with an arginine codon, only producing P1234. Both of these are cleaved via proteolytic action from nsP2 as P123/P1234, producing nsP1-4 (Levinson *et al.*, 1990). Following translation, the nsPs migrate to cellular invaginations called spherules, generated by P123, which act as membrane bound replication complexes (RC) (Hellström *et al.*, 2017). Replication complexes use the viral genomic RNA as a template, replicating it into complementary negative sense and full length genomic RNA that is either translated (ORF-1), packaged or templates further negative strand replication. The 26s mRNA leaves the spherule and is translated through cellular ribosomes to synthesise the p130 polyprotein, which is cleaved by capsid autoproteinase, signalase and furin into the 5 structural proteins (Strauss & Strauss, 1994).

Capsid proteins associate with genomic RNA, specifically at the packaging signal, a conserved area of RNA that enhances the specificity of the RNA being encapsidated (Weiss *et al.*, 1989). Once formed, nucleocapsids are free to travel to the plasma membrane where they bind to the spike glycoproteins formed of E3, E2, 6K and E1 (Parrott *et al.*, 2009). The binding of these spike glycoproteins to the nucleocapsid cause the plasma membrane to bud around the virion, releasing the fully formed virus from the cell.

1.5 nsPs, their Functions and Interactions

1.5.1 nsP1

Within the replication complex, each nsP has unique activity; nsP1 is required for initiation of minus-strand RNA synthesis and has methyl/guanylyltransferase enzymatic action to cap genomic and sub-genomic RNA following transcription (Cross, 1983; Cross & Gomatos, 1981) CHIKV nsP1 binds to cholesterol-rich areas of the PM; it has been shown if cholesterol was sequestered out of spherules, nsP1 also relocated, causing a decrease in viral replication (Bakhache *et al.*, 2020). Furthermore, the inhibition of nsP1 membrane affinity inhibits the ability to replicate RNA, displaying that membrane binding is critical to replication (Kallio *et al.*, 2016).

In CHIKV infections, nsP1 binds to negatively charged phospholipids in the PM via an amphipathic helix within the peptide structure, inducing an alpha-helix structure (Gottipati *et al.*, 2020). Association with the plasma membrane in this way induces membrane structural changes, but additional factors are thought to assist in membrane rearrangement (Gottipati *et al.*, 2020). Furthermore, membrane-associated nsP1 complexes were recently isolated, purified and the structure of the complex was structurally characterised using single-particle cryo-electron microscopy (Cryo-EM) to form dodecameric pores (Jones *et al.*, 2021). These pores act to regulate passage in and out of the RC, are predicted to allow passage of proteins smaller than 70-90kDa and ensures the exit of capped viral RNA (Jones *et al.*, 2021). nsP1 is the only nsP to be membrane bound, hence it is responsible for the localisation of the replication complex on the membrane, making it an ideal target in fluorescence imaging to visualise RCs (Ahola *et al.*, 1999; Spuul *et al.*, 2007).

1.5.2 nsP2

nsP2 has an N-terminal domain that has RNA helicase activity and a C-terminal domain that has protease activity. The presence of nsP2 has been observed in the nucleus and cytoplasm of infected cells, can inhibit host cell transcription, and disrupts the JAK/STAT (Janus kinase-signal transducer and activator of transcription) signalling pathway, responsible for the maintaining of Interferon (IFN) secretion, an anti-viral host response to infection (Fros *et al.*, 2010; Fros *et al.*, 2013; Göertz *et al.*, 2018; Peränen *et al.*, 1990). Further exploration displayed that nsP2's C-terminal domain promotes export of STAT1 out of the nucleus in order to inhibit the IFN response, highlighting nsP2's role in inhibiting anti-viral host responses (Göertz *et al.*, 2018).

Inhibition of this protease activity would allow anti-viral host responses to neutralise viral activity; because of this, nsP2 inhibitors are in development. The nsP2pro inhibitors Pep-I and Pep-II have been found to inhibit CHIKV nsP2 as a result and did so in BHK-21 cells at concentrations significantly lower than their cytotoxic concentrations (Singh *et al.*, 2018). These inhibitors were also tested against SINV infection and failed to show a significant change to viral proliferation, indicating their specificity to CHIKV nsP2 (Singh *et al.*, 2018).

1.5.3 nsP3: Macro Domain, AUD and HVD

nsP3 is expressed as a complex three domain structure; the N-terminal macro domain, a conserved middle domain named the alphavirus unique domain (AUD), and the C-terminal hypervariable domain (HVD) (Panas *et al.*, 2014; Shin *et al.*, 2012). The macro domain has the ability to bind RNA, mono-ADP ribose (MAR), poly-ADP ribose (PAR), and displays ADP-ribose 1" phosphate phosphatase activity (Egloff *et al.*, 2006; Malet *et al.*, 2009; McPherson *et al.*, 2017; Shin *et al.*, 2012). CHIKV and ONNV nsP3 have been observed hydrolysing MAR and PAR from aspartate and glutamate residues, and when either are disrupted, cause attenuation in cell culture and reduced virulence in mice, showing this activity to be integral to infection (Eckei *et al.*, 2017; McPherson *et al.*, 2017).

The AUD is less well characterised, it is known to contain an essential zinc-binding domain and mutations here inhibit productive infection (Shin *et al.*, 2012). Furthermore, research using mutagenic alterations of the AUD highlighted RNA-binding activity, hinting at a potential role in RNA synthesis (Gao *et al.*, 2019). Other functional roles are currently unknown (Mutso *et al.*, 2018).

The HVD is largely unstructured and is poorly conserved across all alphaviruses, with regions of binding motifs found throughout. The binding motifs provide a region for protein-protein interactions between virus and host, such as Ras GTPase-activating protein-binding protein 1 and 2 (G3BP1/2), in order to disrupt stress granule formation (Panas *et al.*, 2012). Binding with G3BP1 allows stress granules to bind with the nsP3-G3BP1/2 complex, in order to inhibit the antiviral mechanisms of stress granules (Panas *et al.*, 2012; Scholte *et al.*, 2015). Structurally, the HVD of ONNV nsP3 has been predicted to contain one proline rich region and two G3BP binding sites, akin to those found in CHIKV nsP3 (Götte *et al.*, 2018). Investigation to confirm interaction with these sites in ONNV are scarce; it is theorised that ONNV interacts with proteins containing an SH3 domain but this hasn't been confirmed (Tossavainen *et al.*, 2016). The unstructured region tolerates large deletions and additions, while the binding motifs if interrupted, cause replicative failure (Scholte *et al.*, 2015; Schulte *et al.*, 2016; Varjak *et al.*, 2010).

FHL-1 (four-and-a-half LIM domain 1) was identified as a host protein that co-localises with nsP3 HVD in the cytoplasm of Alphavirus-infected cells, and through knockout trials, was proven to be integral for ONNV/CHIKV infections (Meertens *et al.*, 2019; Meshram *et al.*, 2018; Mutso *et al.*, 2018). Mice with FHL1 deficiency were infected with CHIKV, as well as wild-type littermates and no infectious particles were found within the FHL1 deficient brood after seven days (Meertens *et al.*, 2019). Upon vivisection, necrosis of the skeletal muscles was observed in wild-type littermates, but not in the FHL1 deficient mice; FHL1 deficiencies in humans are associated with myopathies that cause early joint contractures, muscular wasting and adult-onset cardiac-disease (Adam *et al.*, 1993; Meertens *et al.*, 2019; Schessl *et al.*, 2008). With the connection between CHIKV/ONNV's arthritogenic properties, the high rate of expression in skeletal muscles and damage shown in the muscle tissue of mice expressing FHL1, it is thought that FHL1 is a major host factor in CHIKV/ONNV infections and pathogenesis (Meertens *et al.*, 2019; Shathasivam *et al*., 2010).

1.5.4 nsP4

CHIKV/ONNV nsP4 are poorly described in literature, understanding of nsP4 enzymatic activity comes from studies using model alphaviruses such as Sindbis virus (SINV) (Tomar *et al.*, 2006). nsP4 is the RNA dependant RNA polymerase (RdRp), presenting with TATase enzymatic activity to add poly(a) tails onto synthesised RNA and displaying a need for the presence of P123, the precursor polyprotein of nsP1, 2 and 3, referred to in 1.4 (Rubach *et al.*, 2009; Tomar *et al.*, 2006).

Due to the critical role the RdRp plays in RNA synthesis, inhibitors of the RdRp activity as anti-viral treatments are being explored (Foy *et al.*, 2013; Hahn *et al.*, 1989; Kamer & Argos, 1984). In a screen of binding efficacy between CHIKV nsP4 and a panel of FDA-approved molecules, five inhibitors showed stable binding of nsP4, but lacked any *in vitro* study on whether these interactions could be confirmed between the inhibitors and infectious clones (Ghildiyal *et al.*, 2019). Another study discovered inhibition of CHIKV and SINV infection via a drug with a benzimidazole structure, named Compound-A, and was found through reverse genetics to bind to motif B, a functional domain of the RdRp (Wada *et al.*, 2017). Compound-A was found to have a lower safety index (EC_{50}/CC_{50}) than other approved antivirals, suggestions were made for modification of the compound but no further published work is available (Wada *et al.*, 2017). Characterisation of CHIKV nsP4 in it's entirety would give a clearer understanding of function, which would aid in finding potential anti-virals that inhibit such functions.

1.6 Alphavirus Replication Complexes

1.6.1 Replication Complex Structure

Structurally, Alphavirus P123 forms a 50nm bulb-like protrusion from the membrane called spherules, with a constricted neck through which the replication environment and the cytoplasm are connected, and through which synthesised RNA is released (Friedman *et al.*, 1972; Grimley *et al.*, 1972). The role of spherules in genome replication was suggested when observations in infected cells of colocalization between viral RNA synthesis and cytopathic vacuoles (CPVs), large membranous vacuoles containing spherules, were made (Friedman *et al.*, 1972; Grimley *et al.*, 1968; Grimley *et al.*, 1972). Attempts to isolate CPVs were made, revealed RNA-synthesising activity and viral RNA in the same enriched fraction, confirming their role in housing genomic replication (Friedman *et al.*, 1972). With the role defined, further work went into characterising the nsPs' individual roles within genomic replication as described previously, as well as elucidating how alphaviral infection influences and alters host membranes to form spherules (Salonen *et al.*, 2003; Spuul *et al.*, 2007; Thaa *et al.*, 2015)

1.6.2 Spherule Formation

It is currently unknown what interactions are responsible for the membrane curvature that gives RCs their bulb-like shape. Proline-rich regions have been observed within the CHIKV HVD that bind with proteins containing an Src homology-3 (SH3) domain, these are involved in cytoskeletal regulation and signalling pathways (Zarrinpar *et al.*, 2003). A protein found to associate with nsP3 at these regions was Bin1/amphiphysin-2, which has key roles in endocytosis regulation, membrane recycling, cytoskeletal regulation, as well as having the ability to induce membrane curvature (Neuvonen *et al.*, 2011; Peter *et al.*, 2004; Tossavainen *et al.*, 2016). This ability has brought about speculation that amphiphysin is somehow involved in spherule formation, but no studies have confirmed this (Götte *et al.*, 2018).

In SFV, spherules are internalised from the plasma membrane or sub-cellular organelles and are transported via the PI3K-Akt (phosphoinositide-3-kinase-protein kinase B/Akt) pathway to large intracellular cytopathic vacuoles Type-1 (CPV-1), which are modified endosomes and lysosomes, for the purpose of genomic replication (Spuul *et al.*, 2010). This does not occur to the same degree in all alphaviruses; formation of CPV-1s occurs at a low frequency in CHIKV infections in BHK-21 cells, while it is more frequent in SFV infections (Thaa *et al.*, 2015). The frequency at which ONNV produces CPV-1s remains unclear. Indeed, the ONNV RC in general are poorly described in literature, while CHIKV RCs have been studied in a greater depth.

1.7 Project Aims

The project undertaken sought to develop an ONNV reverse genetic system and optimise methodologies for using ONNV as a model to further understand aspects of ONNV replication and structure. I aimed to do this by identifying cell lines that ONNV species can replicate in that would be physiologically relevant to alphaviral infection. Furthermore, I sought to visualise ONNV RCs and nsP subcellular locations through immunofluorescence assay of the ONNV nsPs via confocal microscopy. Finally, I attempted to reconstruct the ONNV virion via Transmission Electron Microscopy (TEM) and compare it to a known alphavirus structure.

Chapter 2: Optimisation of the ONNV Reverse Genetic System: Materials and Methods

2.1 Materials

2.1.1 Continuous Cell Lines

BHK-21 cells are derived from baby hamster (*Mesocricetus auratus*) kidney fibroblasts. Huh7 cells are a human hepatocyte derived carcinoma cell line. RD Cells are a human myocyte derived rhabdomyosarcoma cell line. C6/36 cells are derived from *A. albopictus* larval cells. U4.4 cells are derived from *A. albopictus* larval cells.

2.1.2 ONNV Infectious Clones

ONNV 2sg_ZsG (2ZsG), ONNV P3_ZsG (P3ZsG) and ONNV P3_mCh (P3mCh) were kindly provided by Professor Andres Merits (University of Tartu, Estonia) as cDNA libraries.

2.1.3 CHIKV Replicon Infected Lysates

BHK-21 cell lysate containing CHIKV ICRES (Integration of Chikungunya research) infectious clone and associated proteins was kindly provided by Kate Loveday (University of Leeds, UK).

2.2 Methods

2.2.1 Cell Culture

Monolayers of BHK-21, Huh7 and RD cells were maintained in Dulbecco's Modified Eagle's Medium (DMEM; Sigma-Aldrich), supplemented with 10% (vol/vol) foetal bovine serum (FBS; Gibco), 100 U/mL penicillin and 100 µG/mL streptomycin. The cells were grown at 37^{o}C and in 5% CO_2 in humidified incubators. Mammalian/Human cell lines were passaged using trypsin as cells reached 100% confluency. C6/36 and U4.4 cells were maintained in Liebovitz' medium (Gibco), supplemented with 10% (vol/vol) foetal bovine serum, 10% TBP (Tris-Buffered Phosphate) (Gibco), 100 U/ml penicillin and 100 µG/mL streptomycin. Cells were grown at 28^{o}C and in 5% CO_2. Insect cell lines were passaged using manual force via cell scrapers to loosen adherent cells.

2.2.2 Cell Freezing and Thawing

Mammalian cells were trypsinised and insect cells were scraped, both were resuspended in their respective complete mediums and centrifuged at 1200 xg at room temperature for 5 minutes. Supernatant was removed and cells were resuspended in 10% dimethyl sulphoxide (DMSO; Sigma) and 90% complete media. 1mL aliquots were prepared in cryovials and frozen at -80^{o}C. Aliquots were moved to liquid nitrogen for long term storage. Cells were thawed via a 37^{o}C water bath and transferred to a T25 flask, supplemented with complete media. Cells were expanded to a T75 and T175 respectively once cells reached 90% confluency.

2.2.3 Viral Rescue

Three ONNV infectious clone plasmids were used to generate viral stocks. cDNA was transformed into *E. coli* XL10-Gold Ultracompetent cells (Agilent Technologies) which were propagated at 37^{o}C in tryptic soy broth, and plasmid cDNA was purified using GeneJET Plasmid Maxiprep kits (Thermo Fisher Scientific). The purified cDNA was linearised by 2µg of *Pme* I and the linearised cDNA was purified through a phenol-chloroform extraction. Reverse transcription was performed using SP6 mMessageMachine (Thermo Fisher), the RNA created was purified via Lithium Chloride Precipitation. RNA integrity was confirmed by MOPS (3-(N-morpholino) propane sulphonic acid) gel electrophoresis and quantified by NanoDrop spectroscopy. The purified RNA was then electroporated into 90% confluent BHK-21 cells at 260V, at a capacitance of 25µF and with one pulse. Cells were then incubated at 37^{o}C in 5% CO_2 for 24 hours, from which viral supernatant was aspirated from and plaqued onto BHK-21 cells to determine viral titre. Virus was passaged in competent BHK-21 cells for three days at a time, incubated at 37^{o}C in 5% CO_2. Supernatant was aspirated off, titred, and passage was performed once more. The ONNV infectious clones generated were 2ZsG, P3ZsG and P3mCh.

2.2.4 ONNV Titre Determination via Plaque Assay

BHK-21 cells were seeded in a 12-well plate at $0.1x10^{6}$ cells per well, maintained in Complete DMEM and grown at 37^{o}C and 5% CO_2. At 90-95% confluency, monolayers were washed with PBS and 150 µL of 10x serial dilutions of ONNV, from neat to 10^{-11}, was carefully applied and incubated at 37^{o}C, being rocked every 15 minutes. 1.6% (w/v) methyl cellulose (Sigma) was diluted with complete DMEM. Virus was removed from the cells, monolayers were washed once with PBS and a 1mL 0.8% methylcellulose complete DMEM

overlay was added to each well. Methyl cellulose as an overlay is highly viscous and ensures secreted infectious virions would only infect neighbouring cells. Plaque formation therefore, is defined by infection from serial dilution rather than freshly secreted infectious virions. Cells were incubated at 37ºC for 3 days. Media was removed carefully from cells, which were washed once with PBS and fixed with 4% (vol/vol) formaldehyde. After 30 minutes of fixation, cells were stained with 0.1% (w/v) crystal violet. Crystal violet contains a chromophore that binds to negatively charged cell membranes, while dead cells are washed off before fixation, revealing healthy purple cells and transparent plaques. Monolayers were left to dry and plaques were counted. The following equation was used to determine viral titre:

Viral titre (PFU/mL) = Number of plaques/(dilution factor X volume (mL))

2.2.4.1 72H Cell Line Infection Assay

Mammalian cells were seeded into 6-well plates at $0.5x10^6$ cells per well, maintained in Complete DMEM and grown at 37ºC and 5% CO_2. Insect cells were seeded into 6-well plates at $1x10^6$ cells per well, maintained in Complete Liebovitz' medium and grown at 28ºC. Once confluent, cells were washed with sterile PBS and viral supernatant of each ONNV infectious clone diluted to an MOI (Multiplicity of Infection) of 1 in PBS, made to 1mL, was applied to the PBS-washed monolayers. An MOI of 1 was used to provide one viably infectious virion per cell present. Plates were rocked for 5 minutes and incubated at 37ºC and 5% CO_2 for mammalian cells or 28ºC for insect cells for 1 hour. Viral dilution was removed, washed once with PBS and 2mL of media was applied to the monolayer. 1mL of media was removed from the monolayer and frozen down as timepoint 0 hours, 1mL of fresh media was reapplied to each well and plates were incubated at previously stated parameters for 24 hours. At 24 hours, 1mL of media was taken from each well, frozen down and 1 mL of fresh media was reapplied to each well. This was repeated at 48 hours and 72 hours. Viral titre was then determined via plaque assay as outlined in 2.3.

2.2.4.2 Determination of Wortmannin Cytotoxicity via MTT Assay

Approximately $1x10^4$ BHK-21 cells per well were seeded in a 96 well plate and were incubated at 37ºC in 5% CO_2 overnight in 100µL complete DMEM. Wells were drained and serial dilutions of Wortmannin (Sigma) and DMSO were performed in complete DMEM, producing aliquots of Wortmannin at 400, 200, 100, 50, 25, 12.5 and 0nM, and DMSO dilutions with the same quantity of DMSO as in each Wortmannin dilution. Dilutions were

applied to cells for 3 hours at 37ºC in 5% CO_2. Thiazolyl Blue Tetrazolium Bromide (MTT) (Alfa Aesar) was dissolved in serum free DMEM and run through a sterile filter, drugged media was aspirated out of wells, 100µL of MTT solution was added to each well and the plate was incubated at 37ºC for 30 minutes while wrapped in aluminium foil. MTT solution was discarded and replaced with 100µL DMSO and shaken for 5 minutes at 60rpm to dissolve purple precipitate. Once dissolved, the plate was read using Magellan software (Tecan) at 570nm. The assay was performed three times to provide biological repeats and percentage cytotoxicity of Wortmannin was calculated at each dosage.

2.2.4.3 6H Infection and Drug efficacy

One 12-well plate was seeded with approximately $0.1x10^6$ BHK-21 cells in 1mL of complete media per well on sterile coverslips, which were used at approximately $0.5x10^6$ cells per well. One row of wells was left uninfected as mock cells, one row was infected with 2ZsG at an MOI of 1 and the final row was infected with 2ZsG at an MOI of 1 and treated with 100nM Wortmannin after 90 minutes. The 12-well plate was chilled for 1 hour at 4ºC once the virus was applied to allow the virus to bind to but not enter the cell. The plate was then incubated at 37ºC with 5% CO_2 until the cells were fixed at 0, 2, 4 and 6 hour time points with 4% (vol/vol) formaldehyde in PBS. Once fixed, cells were permeabilised with 0.1% Triton-X100 and probed with anti-CHIKV nsP3 rabbit antibody and anti-rabbit Alexa-Fluor 594 fluorescent antibody. Coverslips were removed from wells and sealed to glass slides using ProLong Gold containing DAPI (4'6-diamidino-2-pheylindole; Invitrogen). Slides were then imaged using a ZEISS LSM 700 laser scanning confocal microscope in Zen imaging software (Zeiss).

2.2.5 Protein Expression Analysis

2.2.5.1 BCA Assay

The BCA (Bicinchoninic acid) assay was performed in order to calculate the total protein concentrations for analysis by Sodium Dodecyl Sulphate Polyacrylamide Gel Electrophoresis (SDS-PAGE) gels by comparing them to a protein standard. The kit used was the Thermo Scientific Pierce BCA Protein Assay Kit (Thermo Scientific) which can detect a broad working range of 20-2000µg/mL at 562nm.

Dilution scheme for standard test tube and microplate protocol Working Range 20-2000µg/mL:			
Tube	**Volume of Diluent (µg)**	**Volume of BSA (µL)**	**Final BSA Conc. (µg/mL)**
A	0	300 of stock	2000
B	125	375 of stock	1500
C	325	325 of stock	1000
D	175	175 of Vial B	750
E	325	325 of Vial D	500
F	325	325 of Vial E	250
G	325	325 of Vial F	125
H	400	100 of Vial G	25
I	400	0	0 (blank)

Table 2.1: Dilution Scheme for Standard BCA microplate protocol.

200µL dilutions of BCA Working Reagent and 25µL of each cell lysate were added to individual wells of 96 well microplate as shown in table 2.2, The plate was covered and incubated for 30 minutes at 37ºC. The plate was then placed in a Tecan Infinite F50 to measure absorbance at 590nm, the closest measurement possible to 562nm the reader was capable of measuring. A standard curve was prepared from these to identify the protein concentrations of the cell lysates.

2.2.5.2 Preparation of Whole Cell Lysate

Cells were washed with PBS and then harvested via scraping in fresh PBS. Suspended cells were centrifuged at 1000 x *g* for 5 minutes. PBS was aspirated from cells, with fresh PBS

being applied and cells were centrifuged again at the same parameters. PBS was aspirated from cells again and cells were resuspended in IP lysis buffer (10mM Tris-HCl pH 7.5, 150 mM NaCl, 0.5mM EDTA, 0.5% NP40, 1x EDTA-free complete protease inhibitor), RIPA buffer (25 mM Tris pH 7.4, 150 mM NaCl, 1% NP40, 0.5% sodium deoxycholate (DOC), 0.1% SDS, 1x EDTA-free complete protease inhibitor) or Leeds lysis buffer (25mM Na^+ β-glycerophosphate, 150mM NaCl, 20mM Tris 7.4 pH, 50mM NaF, 1mM EDTA (Ethylenediaminetetraacetic acid), 10% Glycerol, 1% Triton X-100, 5mM Sodium pyrophosphate tetrabasic decahydrate). Cells were chilled on ice in lysis buffer for 30 minutes, being vortexed every 5 minutes in between. The resulting lysate was cleared of debris via centrifugation at 13,000 x *g* at 4°C for 10 minutes. The pellet was discarded and supernatant was frozen down at -20°C for future use.

2.2.6 Protein Analysis

2.2.6.1 SDS Polyacrylamide Gel Electrophoresis (SDS-PAGE)

SDS PAGE gels were made with either a 10% (3.3mL bis-acrylamide (30%), 2.5mL Tris-HCl 1.5M 8.8 pH, 4mL H_2O, 100µL SDS, 100µL 10% ammonium persulphate (APS), 10µL TEMED) or 7.5% (2.48ml Bis-Acrylamide (30%), 2.5mL Tris-HCl 1.5M 8.8 pH, 4.82mL H_2O, 100µL SDS, 100µL 10% ammonium persulphate (APS), 10µL TEMED) resolving gel, and 5% stacking gel (0.83mL Bis-Acrylamide (30%), 0.63mL Tris-HCl 1M 6.8 pH, 3.4mL H_2O, 50µL SDS, 50µL 10% ammonium persulphate (APS), 5µL TEMED). Protein samples were mixed with 4X SDS sample buffer (1mL 1M Tris-HCl 6.5 pH, 2mL 1M Dithiothreitol (DTT), 0.4g SDS, 20mg Bromophenol Blue, 1.6mL Glycerol, 0.4mL H_2O). Samples were heated at 95°C for 10 minutes to denature and were loaded into gels. Samples were loaded with Prime-Step™ Prestained Broad Range Protein Ladder (Bio-Legend) in an end well. Electrophoresis was performed in 1X SDS running buffer (25mM Tris, 192mM glycine, 0.1% (w/v) SDS) at 200V for 1 hour or until dye had electrophoresed off the resolving gel.

2.2.6.2 Western Blot Analysis

Proteins were transferred from SDS Gels onto PVDF membranes (Sigma) using a Trans-Blot semi-dry cell (Bio-rad) in Towbin buffer (25mM Tris, 192 mM glycine, 20% methanol) for 1 hour at 15V. Membranes were blocked with a 1:1 Odyssey blocking buffer (LiCor) and TBS (Tris-Buffered Saline) and 0.1% Tween 20 solution (TBS-T 0.1%) for 1 hour at room temperature, followed by a 4°C incubation overnight with primary antibody at the appropriate concentration in TBS-T 0.1% and 5% (w/v) Bovine Serum Albumin (BSA). Membranes were

washed three times with TBS-T 0.1%, and probed with appropriate fluorescent secondary antibodies (LiCor) in a 3:1 solution of Odyssey blocking buffer and TBS-T 0.1% for 1 hour at room temperature. Membranes were washed three times with TBS-T 0.1% and left to dry. Imaging was performed using a LiCor Odyssey Sa Infrared imaging system (LiCor).

2.2.6.3 List of Antibodies

Target	Antibody species	Supplier	Catalogue Number	WB Dilution	IF Dilution	Monoclonal or Polyclonal
CHIKV nsP1	Rabbit	Prof Andres Merits, University of Tartu	N/A	1:1000, 1:500	1:1000	Polyclonal
CHIKV nsP3	Rabbit	Prof Andres Merits, University of Tartu	N/A	1:1000	1:1000	Polyclonal
Beta-Actin	Mouse	Sigma Aldrich	A3853	1:10,000	N/A	Monoclonal

Table 2.2: Table of Primary Antibodies used in Western blot probing and IF staining.

Primary Antibody Species	Conjugation	Supplier	Catalogue Number	WB Dilution	IF Dilution	Monoclonal or Polyclonal
Mouse	IRDye 680CW	LiCor	925-68072	1:20,000	N/A	Polyclonal
Rabbit	IRDye 800CW	LiCor	25-32213	1:20,000	N/A	Polyclonal
Rabbit	Alexa Fluor 594	Invitrogen	A-21442	N/A	1:500	Polyclonal

Table 2.3: Table of Secondary Antibodies used in Western blot probing and IF staining.

2.2.7 Immunofluorescence

2.2.7.1 IF Sample Preparation

BHK-21 cells were seeded onto sterile 19mm coverslips in a 12-well plate and incubated at optimal parameters until 90% confluent. Following appropriate infection, monolayers were fixed in 4% formaldehyde at room temperature, while being rocked for 30 minutes minimum. Cells were permeabilised in PBS containing 0.1% Triton X-100 for 10 minutes, being rocked at 4^{o}C, and cells were washed with 1x PBS after. Blocking solution (1% (w/v) BSA in PBS) was applied to cells at room temperature, rocking for 15 minutes, and appropriate primary antibodies at their stated dilutions in blocking buffer were applied to cells and left rocking at 4^{o}C overnight. Cells were washed 3 times with PBS, and appropriate secondary antibodies at their stated dilutions in blocking buffer were applied to cells for 1 hour at room temperature, protected from light. Cells were carefully washed 4 times with PBS, mounted to microscope slides using ProLong Gold with DAPI (4′,6-diamidino-2-phenylindole) (Thermo Scientific), and stored at 4^{o}C.

2.2.7.2 IF Confocal Imaging

Probed cells were imaged using an inverted ZEISS LSM-700 with a x63 oil immersion objective lens. Images produced were processed and analysed via Zen imaging software (Carl Zeiss).

2.2.8 Transmission Electron Microscopy (TEM)

2.2.8.1 Negative Stain Electron Microscopy Grid Preparation

Standard Grade Copper TEM support grids (Sigma-Aldrich) were carbon coated by Martin Wilkinson (Leeds) and underwent glow discharge via a PELCO easiGlow discharge unit prior to use. Grids were applied to viral supernatant gently for 30 seconds to allow for adsorption, then carefully washed with water 4 times, blotting the grid on filter paper immediately after each wash. Grids were gently applied to 1% Uranyl Acetate (UA) to stain grids, excess UA was immediately blotted off. Grids were left to airdry before being imaged.

2.2.8.2 TEM Imaging and Processing

Grids were imaged either via a FEI Tecnai G2-spirit TEM or a FEI Tecnai F20 TEM, due to a mechanical failure of the G2-spirit. Images from the FEI Tecnai G2-spirit were rendered using Digital Micrograph (DM) software, and images from the FEI Tecnai F20 were rendered using TEM Imaging and Analysis (TIA) software. All FEI Tecnai F20 images were obtained by Ben Chadwick (Leeds), who kindly offered his operating expertise. Images were processed, analysed and 3D reconstructions were generated using RELION 3.1.1 software (Sjors Scheres, MRC Laboratory of Molecular Biology).

2.2.9 Statistical Methods

All statistical analyses were performed using GraphPad Prism 9.1.1 (GraphPad Software). Results were to be analysed using the Two-way Analysis of Variances (ANOVA). Two-Way ANOVA was performed to determine the significance of the difference in the results. When making comparisons, P values of >0.05 indicated a statistically significant difference between the results.

2.2.10 Ethics Statement

This research is considered independent and impartial to the best of the student's ability. According to their knowledge and experience, there have been no breach of ethics in relation to the use of patient data, human derived cell lines or animal derived products.

Chapter 3: Optimisation of the ONNV Reverse Genetic System: Results

3.1 Viral Rescue

Viral rescue was performed using the three ONNV (2ZsG, P3ZsG, P3mCh) cDNA libraries as described in 2.2.3. Following RNA purification, 750ng of 2ZsG (2µL) and P3mCh (2.5µL) were run on a MOPS gel to verify RNA integrity (Figure 3.1). P3ZsG RNA was not run due to small RNA yields. Once verified, RNA was transfected into separate BHK-21; 1µg (3.5µL) of 2ZsG RNA, 689ng (19µL) of P3ZsG RNA and 1.125µg (3µL) of P3mCh RNA was used. Transfected titres are shown in Figure 3.2 as Passage 0. Interestingly, the diminished amount of P3ZsG RNA used had no visible effect on viral titre; in all clones the initial titre was ~1x10^7 PFU/mL.

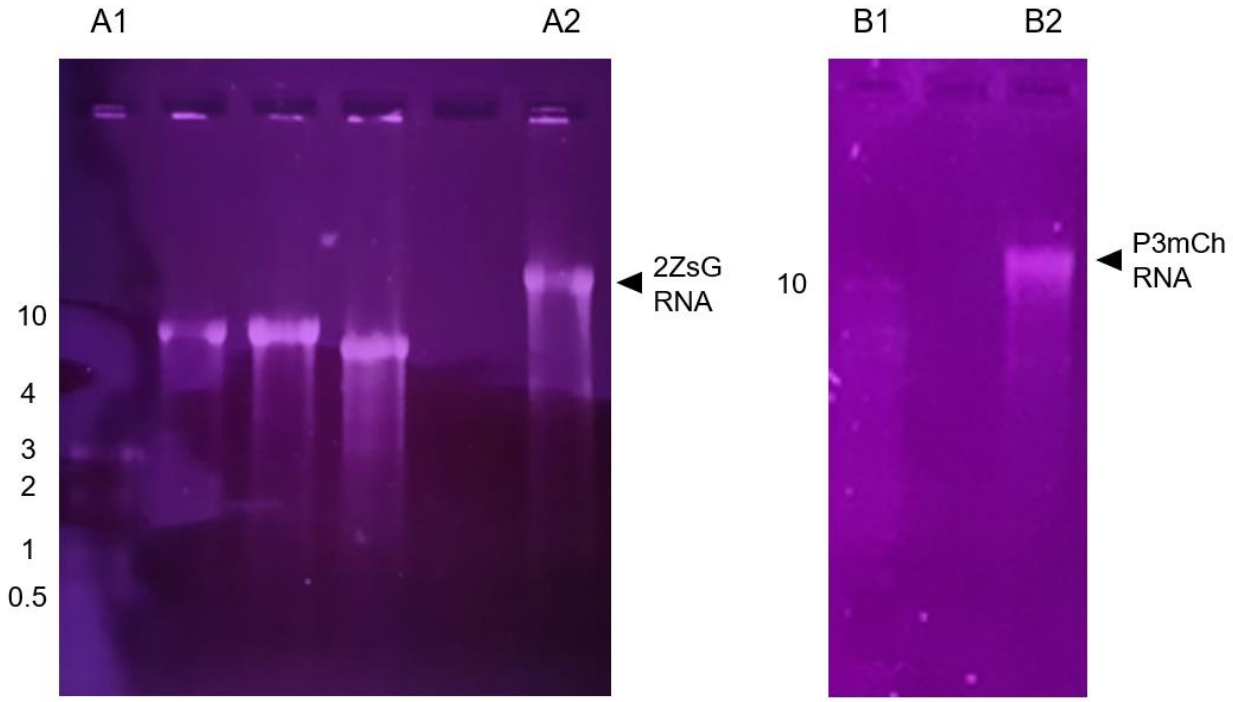

Figure 3.1; Denaturing MOPS Gel RNA electrophoresis of ONNV infectious RNA clones. Gels were submerged in 1X MOPS buffer and electrophoresed at 80V for 1h. Gel A shows 10kb RNA ladder in lane A1 and 550ng 2ZsG RNA in A2. RNA present was visible above the 10kb ladder and formed a single, unified band. Other lanes are not representative of ONNV RNA. Gel B shows 10kb RNA ladder in lane B1 and 750ng P3mCh RNA in B2. RNA present was visible above the 10kb ladder and formed a single, unified band.

2ZsG is an ONNV infectious clone with a second sub-genomic replicon added to the viral genome that encodes for the fluorescent protein ZsGreen (26.1 kDa). As the gene is present in a sub-genomic replicon and not fused to any viral protein, ZsGreen is produced in viral replication and the presence of ZsGreen can be used as a measure of replication. P3ZsG is an ONNV infectious clone with the gene for ZsGreen fused to nsP3, in order to create a nsP3-ZsGreen fusion protein during replication. P3mCh is an ONNV infectious clone with the gene for the fluorescent protein mCherry (26.7 kDa) fused to nsP3, in order to create a nsP3-mCherry fusion protein during replication.

3.1.1 Optimisation of High Titre ONNV Generation

In order to generate high titre stocks of all ONNV clones for further investigations, BHK-21 cells were infected at an MOI of 1 and incubated for 3 days at 37ºC, virus titre was determined by plaque assay in BHK-21 cells. BHK-21 cells were used to generate ONNV as they have shown a propensity for alphavirus infection and production of high viral titres in CHIKV (Davis *et al.*, 1971; Pietila *et al.*, 2017). This resulted in viral titres ranging from 10^5 to 10^8 PFU/mL (Figure 3.2).

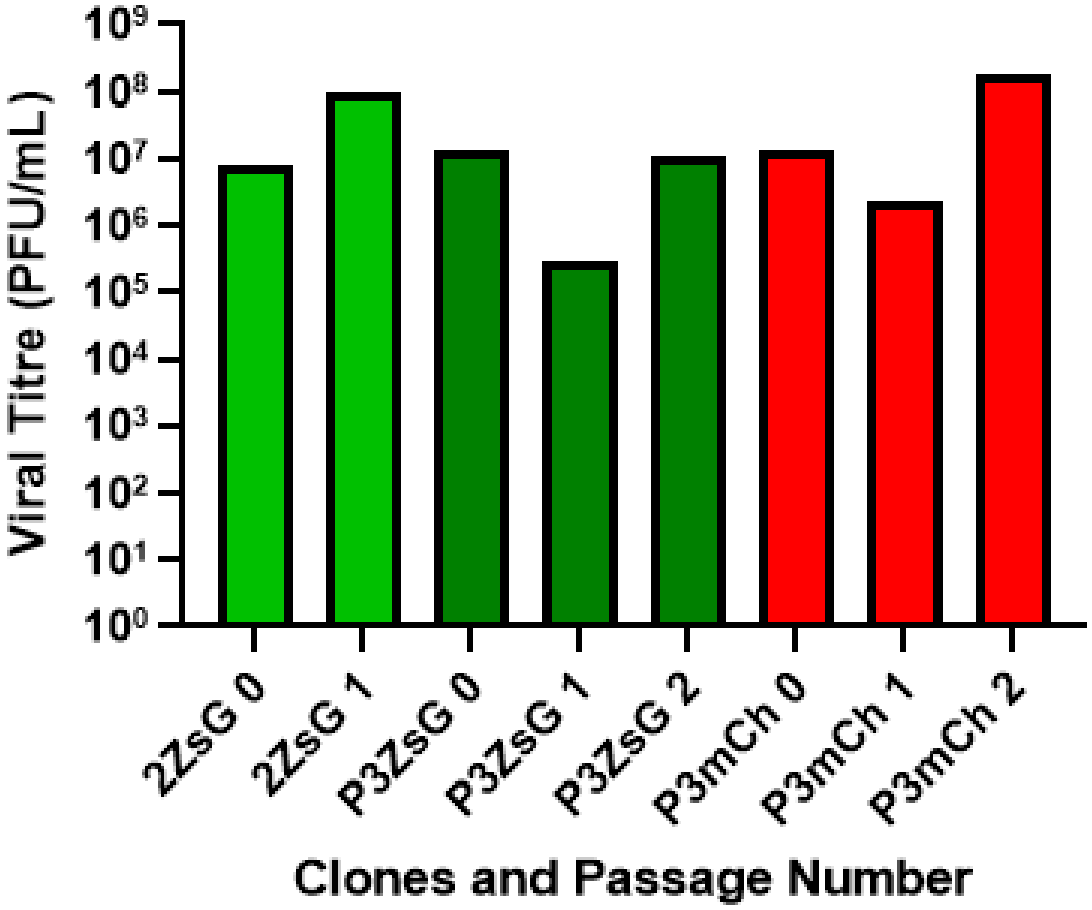

Figure 3.2; Viral titres of all ONNV clones generated via transfection of viral RNA or passage through BHK-21 cells. Passage 0 is representative of transfection.

ONNV infection in BHK-21s produce a large plaque morphology indicative of highly cytopathic virus, often with uneven plaque borders. There were no visible differences in plaque morphology between ONNV clones (Figure 3.3).

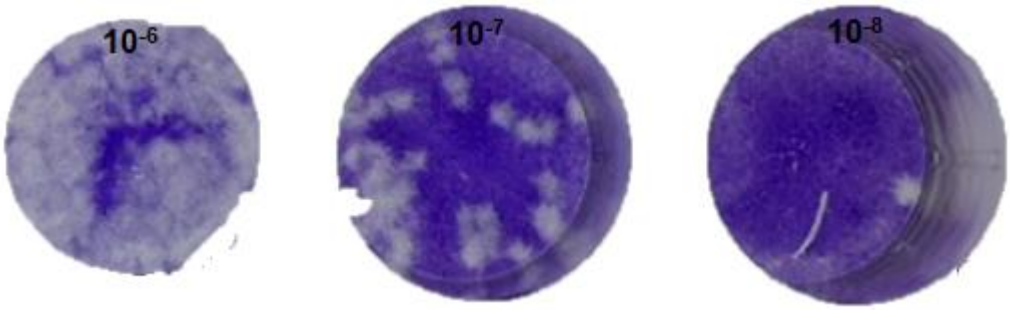

Figure 3.3; Representative Plaque Assay of BHK-Derived P3mCh passaged through BHK-21 cells. BHK-21 cells were infected with a serial dilution of P3mCh of unknown titre (Neat to 10^{-11}). Plaques were visualised with crystal violet, staining the monolayer and revealing transparent virus plaques which were counted. Viral titre was determined at $1.9x10^{8}$. The same procedure was performed to determine the viral titres of other ONNV clones.

3.2 ONNV Infection Study

3.2.1 Characterisation of ONNV infection in different model cells

The characterisation of ONNV infection in different model cells is largely missing from published data, with presumptions being made from CHIKV infection. As a result, we sought to identify cell types that would prove useful in further investigations of ONNV biology. At 80-90% confluency, cells of each chosen cell species were infected with each ONNV clone at an MOI of 1. After a 1 hour incubation, 1mL viral supernatant was aspirated at 24 hour intervals up to 72 hours. A 0 hour control was also taken. Viral titre was determined via plaque assay on BHK-21 cells. BHK-21 cells were used for all plaque assays to provide a standardised method of assessing viral titre.

Huh7, RD and BHK-21 cells were selected as the study's mammalian cell species. BHK-21 cells were selected as they have shown previously to support high alphaviral titres and were regularly used for CHIKV investigations as a model cell line, as fibroblasts are a target cell type for alphaviruses in mammalian infection (Assuncao-Miranda *et al.*, 2013; Pietila *et al.*, 2018; Roberts *et al.*, 2017). BHK-21 cells however, are derived from *M. auratus*, the Golden Hamster, and are not a representative model for human infection, and alternative human cell lines were considered. Huh7 and RD cells were selected as they have been well characterised, have shown previously to efficiently support CHIKV replication and are physiologically relevant to human infection (Gao *et al.*, 2019; Roberts *et al.*, 2017). C6/36

and U4/4 cells were selected as the study's insect cell species. Both C6/36 and U4.4 cells are derived from *Ae. albopictus*, which is not a known vector of ONNV in the wild, but previous work has shown ONNV can infect C6/36 cells, and both cell species are used as model cell species for CHIKV (Bessaud *et al.*, 2006; Roberts *et al.*, 2017). Of note, U4.4 cells have been reported to functionally express an innate immune response to arbovirus infection called a phenoloxidase (PO) cascade, which exhibits antiviral activity and lowering levels of viral replication (Rodriguez-Andres *et al.*, 2012). C6/36 cells have not been reported to display such an immune response.

3.2.1.1 ONNV infect and produce high viral titres in BHK-21 cells in 24h

In all ONNV infections in BHK-21 cells, titres peaked after 24 hours and declined over time. In 2ZsG infection, titre increased by three logs from $1.2x10^5$ to $3.86x10^8$ PFU/mL from 0-24. Viral titre then decreased one log to $1.45x10^7$ PFU/mL at 48 hours and the decrease continued to a titre of $2.03x10^6$ PFU/mL at 72 hours (Figure 3.4). P3ZsG infection follows a similar trend, peaking at $1.14x10^5$ to $9.68x10^7$ PFU/mL at 0-24 hours, a two log increase. Titre then decreased to $2.67x10^7$ PFU/mL at 48 hours and dropped at 72 hours, to $1.6x10^6$ PFU/mL, a log decrease (Figure 3.4). P3mCh infection continued the trend, with a sharp four log increase from $3.9x10^4$ to $5.52x10^8$ PFU/mL from 0-24 hours, which then dropped at 48 hours to $8.85x10^7$ PFU/mL. This decrease continued to 72 hours, dropping to $2.3x10^6$ PFU/mL, a log decrease (Figure 3.4).

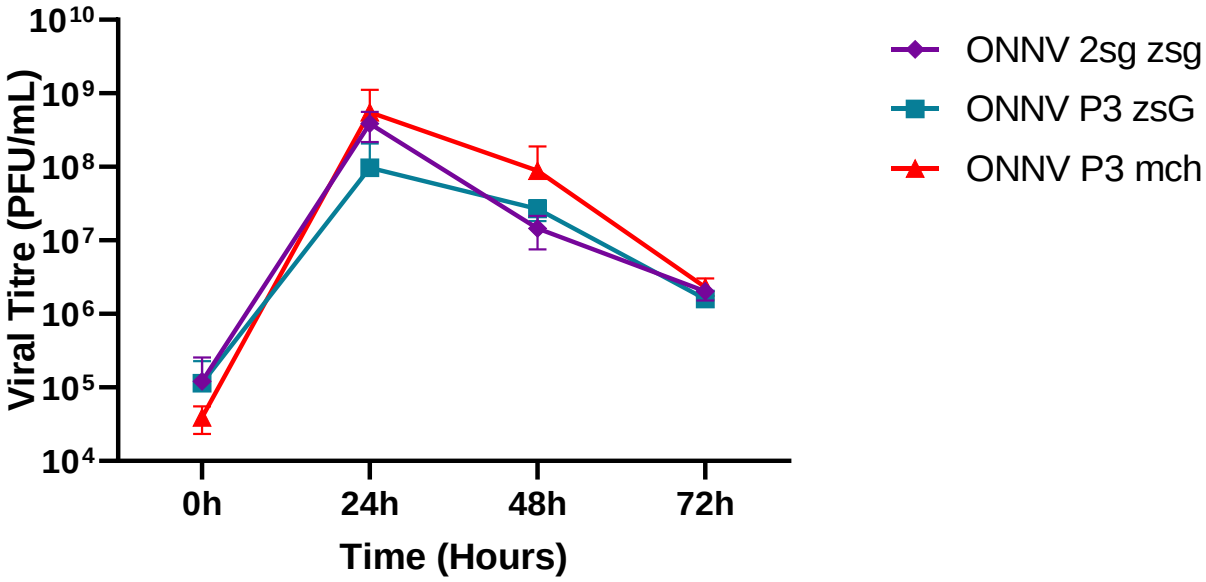

Figure 3.4; Multi-step growth curve of three ONNV clones in BHK-21 cells. Supernatant containing each ONNV clone was used to infect confluent BHK-21 cells at an MOI of 1,

virus-containing supernatant was removed and the titre measured by plaque titre assay. Data are displayed as the means of three independent experimental replicates. Error bars represent standard deviation from the mean.

Two-Way ANOVA was performed to confirm the effect of time and ONNV clone on viral propagation within infected BHK-21 cells. No statistically relevant difference was observed between time and ONNV clones in BHK-21 cells (P=0.3158). As expected, a statistically relevant difference in average titre was seen over time (P=0.0234), and none was seen between ONNV clones (P=0.3489). Simple effects analysis was performed and showed no statistically significant difference between the means of any species or time point.

Overall, this confirms BHK-21 cells are permissible to ONNV infection and show high viral titre within 24 hours, due to highly cytopathic infection. After 24 hours, viral titre decreased dramatically, as the loss of competent cells producing virus lowered overall virus production. Similar to the human cell lines, different ONNV clones had no visible effect on growth kinetics, and BHK-21 cells provided the highest viral titre of any cell type in all ONNV clone, reaching 10^8 PFU/mL.

3.2.1.2 ONNV infect and produce low viral titres in Huh7 cells at 72h

In 2ZsG infection, titre increased from $2.73x10^4$ to $4.9x10^4$ PFU/mL from 0-24 hours, slightly rose to $5.43x10^4$ PFU/mL at 48 hours and increased again to $9.13x10^4$ PFU/mL at 72 hours (Figure 3.5). In P3ZsG infection, titre increased from $1.75x10^4$ to $3.1x10^4$ PFU/mL from 0-24 hours, increased over two-fold to $7.43x10^4$ PFU/mL at 48 hours and the increase slowed to $8.73x10^4$ PFU/mL at 72 hours (Figure 3.5). In P3mCh infection, titre increased from $3.5x10^3$ to $8.16x10^3$ PFU/mL from 0-24 hours, rose to $3.58x10^4$ PFU/mL at 48 hours, and the increase slowed to $6.5x10^4$ PFU/mLat 72 hours (Figure 3.5).

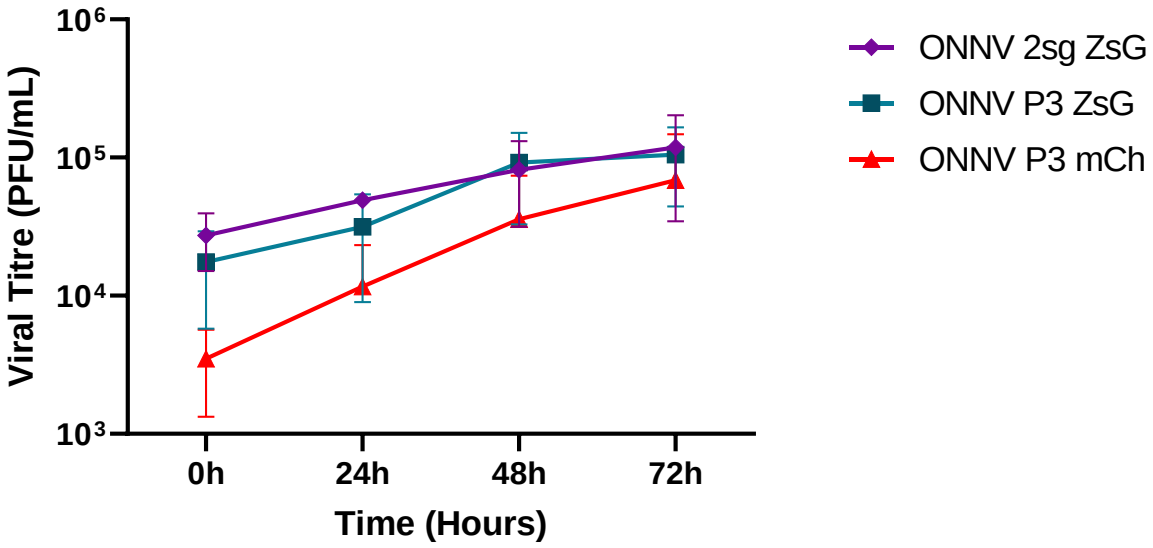

Figure 3.5; Multi-step growth curve of three ONNV clones in Huh7 cells. Supernatant containing each ONNV clone was used to infect confluent Huh7 cells at an MOI of 1, virus-containing supernatant was removed and the titre measured by plaque titre assay. Data are displayed as the means of three independent experimental replicates. Error bars represent standard deviation from the mean.

Two-Way ANOVA was performed to examine the effect of time and different ONNV clones on viral propagation within infected Huh7 cells. No statistically relevant difference was observed between time and ONNV clone in Huh7 cells (P= 0.9748). As expected, a statistically relevant difference was observed in titre over time (P= 0.0149), but one was not observed between clones (P=0.2985). Simple effects analysis showed that there was a significant difference in mean titre between clones 2ZsG and P3mCh at 24 hours (P=0.0317), but this was not the case at 48 and 72 hours. No other mean comparison showed significantly relevant differences.

Overall, these results demonstrate for the first time that Huh7 cells are permissible to ONNV infection, showing viral replication of all ONNV clones. Encouragingly, no significant difference in growth kinetics was observed between the different ONNV clones. However, although Huh7 cells tolerate infection, viral titre never showed a rapid increase, never increasing beyond 10^5 PFU/mL on average. Huh7 cells produce the lowest viral titres of any cell type, regardless of ONNV clone.

3.2.1.3 ONNV infect and replicate efficiently in RD cells in 24h

In 2ZsG infection, titre increased from $4.66x10^4$ to $3.08x10^6$ PFU/mL from 0-24 hours, rose to $5.3x10^6$ PFU/mL at 48 hours and the increase slowed, reaching a titre of $5.82x10^6$ PFU/mL at 72 hours (Figure 3.6). In P3ZsG infection, titre increased over two logs, from $6.61x10^3$ to $3.42x10^6$ PFU/mL from 0-24 hours, which then lowered to $2.27x10^6$ PFU/mL at 48 hours and increased slightly to $2.93x10^4$ PFU/mL at 72 hours (Figure 3.6). In P3mCh infection, titre increased by a two log increase from $1.38x10^4$ to $1.92x10^6$ PFU/mL from 0-24 hours, dropped slightly to $1.5x10^6$ PFU/mL at 48 hours, and then increased to $4.53x10^6$ PFU/mL at 72 hours (Figure 3.6).

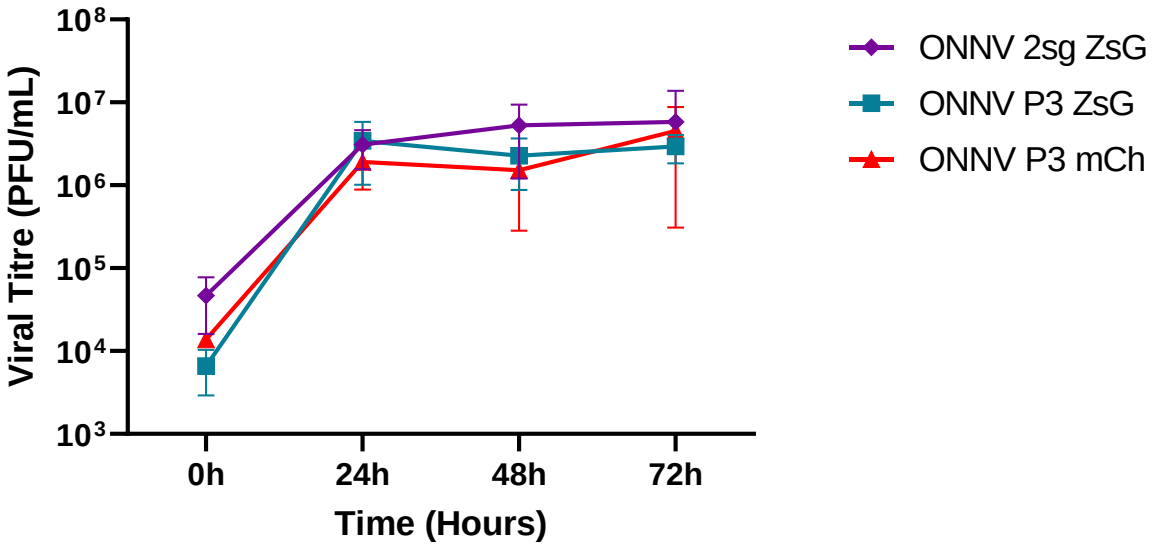

Figure 3.6; Multi-step growth curve of three ONNV clones in RD cells. Supernatant containing each ONNV clone was used to infect confluent RD cells at an MOI of 1, virus-containing supernatant was removed and the titre measured by plaque titre assay. Data are displayed as the means of three independent experimental replicates. Error bars represent standard deviation from the mean.

Two-Way ANOVA was performed to confirm the effect of time and different ONNV clones on viral propagation within infected RD cells. No statistically relevant difference was observed between time and ONNV clone in RD cells (P= 0.8422). Unexpectedly, no statistically relevant difference in average titre was seen over time (P= 0.0847) or between clones (P= 0.5110) in RD cells. Simple effects analysis was performed and showed no statistically significant difference between the means of any clone or time point.

Overall, the results demonstrate for the first time that RD cells are permissible to ONNV infection, showing viral replication of all clones. Viral titres show little change after 24 hours and no statistically relevant difference in replication kinetics was observed between ONNV clones. All titres peak in the 10^6 range, similar to the MOI used to infect with.

3.2.1.4 ONNV infect and replicate at varying rates in C6/36 cells over 72h

In 2ZsG infection, titre increased by a log from $8.58x10^5$ to $3.57x10^7$ PFU/mL from 0-24 hours, decreased to $2.13x10^7$ PFU/mL at 48 hours and titre then stabilised, with the same titre of $2.13x10^7$ PFU/mL at 72 hours (Figure 3.7). In P3ZsG infection, titre increased by two logs, from $1.07x10^5$ to $1.53x10^7$ PFU/mL from 0-24 hours, which then further increased to $3.66x10^7$ PFU/mL at 48 hours and titres decreased to $1.83x10^7$ PFU/mL at 72 hours (Figure 3.7). In P3mCh infection, titre increased 2-fold from $1.88x10^5$ to $5.92x10^5$ PFU/mL from 0-24 hours, and then increased a log to $8.94x10^6$ PFU/mLat 48 hours. This delayed increase continued to 72 hours, with a viral titre of $4.33x10^7$ PFU/mL (Figure 3.7).

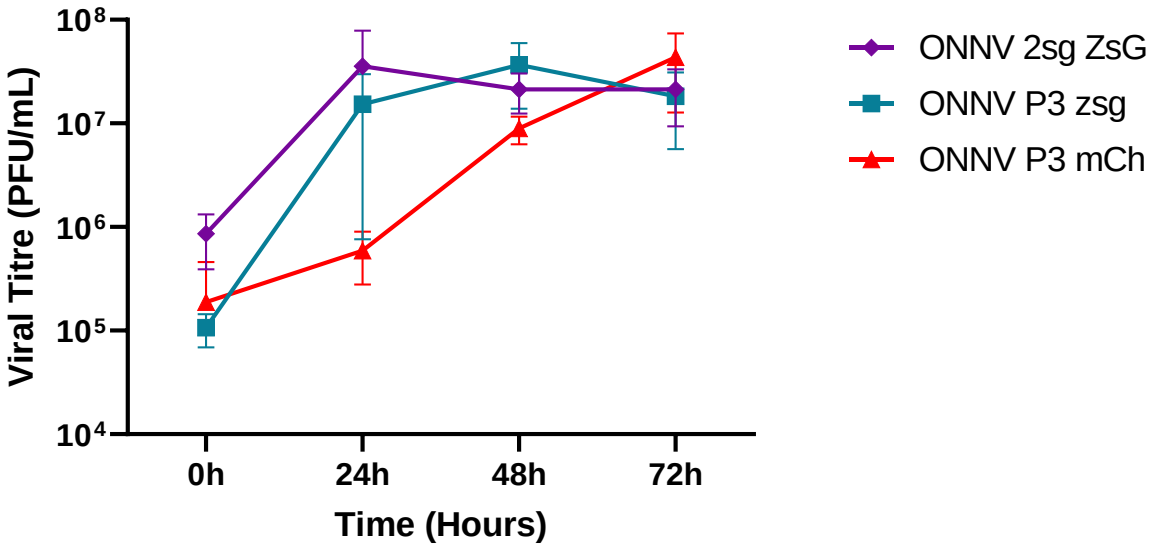

Figure 3.7; Multi-step growth curve of three ONNV clones in C6/36 cells. Supernatant containing each ONNV clone was used to infect confluent C6/36 cells at an MOI of 1 virus-containing supernatant was removed and the titre measured by plaque titre assay. Data are displayed as the means of three experimental replicates. Error bars represent standard deviation from the mean.

Two-Way ANOVA was performed to confirm the effect of time and ONNV clone on viral propagation within infected C6/36 cells. No statistically relevant difference was observed between time and ONNV clones in C6/36 cells (P= 0.0413). As expected, a statistically

relevant difference in average titre was seen over time (P= 0.0155), and more unexpectedly none was seen between ONNV clones (P=0.8114). Simple effects analysis was performed and showed no statistically significant difference between the means of any species or time point.

Overall, the results demonstrate that C6/36 cells are permissible to ONNV infection, showing viral replication of all clones. In the mCh clone, viral titre produced lower titres after 24 hours than ZsG clones; potentially the nsP3-mCh fusion protein may be less efficient in C6/36 cells than the nsP3-ZsG fusion protein and wild-type nsP3 protein. These titres then rise to equal titres at 72 hours. All species eventually reached titres in the 10^7 range, bested only by BHK-21 cells in terms of quantity.

3.2.1.5 ONNV infect and replicate at varying rates in U4.4 cells over 72h

In 2ZsG infection, titre began with a log increase from $4.78x10^4$ to $3.73x10^6$ PFU/mL from 0-24 hours (Figure 3.8). Titre stabilised at 48 hours with an equal titre of $3.73x10^6$ PFU/mL, and rose slightly to $6.03x10^6$ PFU/mL at 72 hours (Figure 3.8). In P3ZsG infection, titre increased one log from $9.7x10^4$ to $2.14x10^6$ PFU/mL from 0-24 hours. Titre then declined to $1.09x10^6$ PFU/mL at 48 hours and rose once more to $3.05x10^6$ PFU/mL at 72 hours (Figure 3.8). In P3mCh infection, viral titre increased from $1.4x10^4$ to $9.95x10^5$ PFU/mL, a log rise between 0-24 hours (Figure 3.8). The rise continued to $1.73x10^7$ PFU/mL at 48 hours, another log increase, and then minimally dropped to $1.25x10^7$ PFU/mL at 72 hours (Figure 3.8).

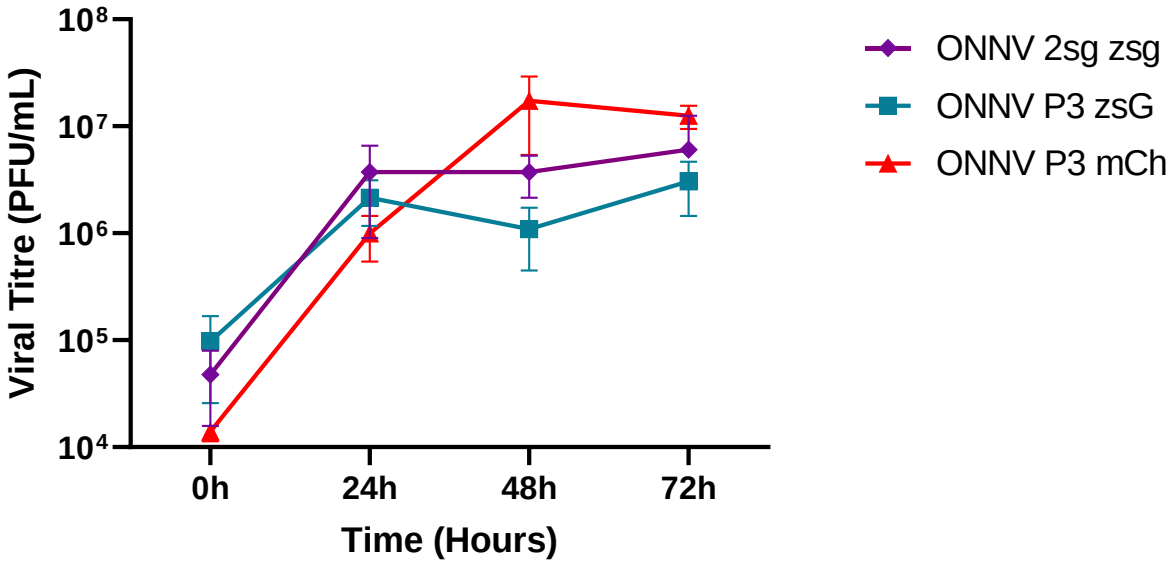

Figure 3.8; Multi-step growth curve of three ONNV clones in U4.4 cells. Supernatant containing each ONNV clone was used to infect confluent U4.4 cells at an MOI of 1 virus-containing supernatant was removed and the titre measured by plaque titre assay. Data are displayed as the means of three independent experimental replicates. Error bars represent standard deviation from the mean.

Two-Way ANOVA was performed to confirm the effect of time and ONNV species on viral propagation within infected U4.4 cells. A statistically relevant difference was observed between time and ONNV clones in U4.4 cells (P= 0.0255). As expected, a statistically relevant difference in average titre was seen over time (P= 0.0379), but interestingly species also showed statistically significant variation (P=0.0117). Simple effects analysis showed that there was a significant difference in mean titre between ONNV_P3_ZsG and ONNV_P3_mCh at 72 hours (P=0.0348), but this was not the case at 48 and 72 hours. No other mean comparison showed significant differences.

Overall, the results display for the first time that U4.4 cells are permissible to ONNV infection. Titres rise to log 10^6 PFU/mL by 24 hours and in ZsG clones stay at a similar level of titre. mCh clone repeats continue to increase and peaked higher than 2ZsG and P3ZsG clones. All titres peaked in the 10^6 range, an approximate log lower than C6/36 cells. This is likely due to the PO cascade innate immune response U4.4 cells display in arboviral infection, as stated previously.

3.3 Cross-Reactive CHIKV Antibody Validation

3.3.1 Optimisation

In order to probe for and isolate ONNV proteins for western blotting and immunofluorescent analysis, effective and reliable antibodies for ONNV were to be identified and validated. Minimal research has been performed working with ONNV and as such, ONNV-specific antibodies were unavailable for use. CHIKV specific antibodies for nsP1 and nsP3 were selected, as the literature reports a one-way antigenic relationship between anti-CHIKV antibodies and ONNV-native proteins (Blackburn *et al.*, 1995; Partidos *et al.*, 2012; Tappe *et al.*, 2014). BHK-21 monolayers were infected with ONNV species at an MOI of 1 and incubated for 24 hours, cells were then harvested and lysed. Mock BHK-21 lysate and BHK-21 lysates containing CHIKV ICRES, P3ZsG and P3mCh proteins were processed via SDS-PAGE and western blotting. BHK-21 cells were chosen as the model for viral infection because they have provided strong replication of CHIKV and CHIKV nsP3 in previous studies (Roberts *et al.*, 2017).

Optimisation of the western blotting process was required, as this was the first time ONNV proteins had been formally detected using anti-CHIKV antibodies, we aimed to elucidate a methodology that provided clear imaging of protein bands. CHIKV nsP1 and nsP3 have a molecular mass of ~60 kDa and 58 kDa respectively, while ONNV nsP1 has a molecular mass of 59.7 kDa, so we expected protein bands at ~60 kDa from the lysates. Though ONNV nsP3 has a molecular mass of 62.4 kDa, in P3ZsG and P3mCh clones, the nsP3-ZsGreen and nsP3-mCherry fusion proteins have molecular masses of 88.5 and 89.1 kDa respectively. In membranes probed for nsP3, we expected bands at ~90 kDa in the P3ZsG and P3mCh infected cell lysates. Beta-Actin has a molecular mass of 42 kDa and was used as a loading control for the presence of cellular protein.

3.2.1.1 TBS is an effective Washing Solution when probing with anti-CHIKV antibodies

Mock BHK-21 lysate and BHK-21 lysates containing CHIKV ICRES, P3ZsG and P3mCh proteins were processed as described in 2.2.6.1. All antibodies were diluted in TBS and membrane washes also performed using TBS. Anti-CHIKV antibodies were diluted at 1:1000, Anti-Beta-Actin antibodies were diluted at 1:10000 and all secondary antibodies were diluted at 1:20000, in 1:3 TBS and blocking buffer.

In Figure 3.9A, two bands were visible at 66 and 52 kDa. Between these, around the 60 kDa level, faint bands of CHIKV and ONNV nsP1 protein were visible, while at around 42 kDa, very faint bands of beta-actin were present. No bands were visible in the BHK-21 mock control. In Figure 3.9B, one band of the protein ladder was visible at 52 kDa. Above and below 52 kDa in the CHIKV and ONNV infected lysates were protein bands, representative of nsP3 and beta-actin respectively. Again, there were no bands in the BHK-21 mock lysate. The membranes did not provide a clear enough representation of the proteins present within the lysate.

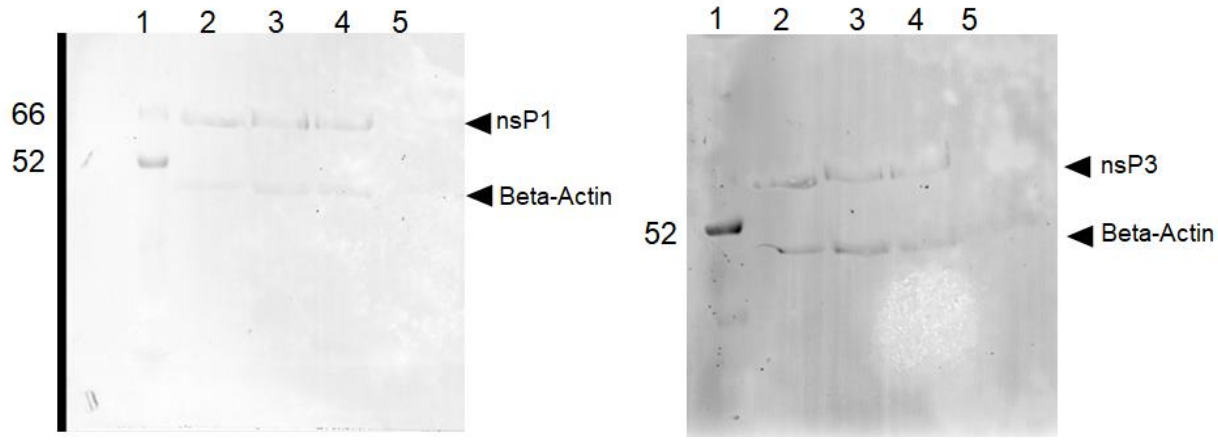

Figure 3.9; Optimisation of the detection of ONNV nsP1 and nsP3 proteins by Western blot analysis from infected BHK-21 cell lysates. SDS-PAGE and transfer to PVDF membranes was performed as described in 2.2.6.1. Membranes were probed with anti-Beta-Actin and anti-CHIKV nsP1 (A) or anti-CHIKV nsP3 (B) antibodies, and probed after with anti-mouse and anti-rabbit secondary antibodies in TBS and blocking buffer. Molecular masses are displayed in kilodaltons (kDa). 1= Protein Ladder, 2= CHIKV-Replicon BHK Lysate, 3= P3ZsG BHK lysate, 4= P3mCh BHK lysate, 5= Mock BHK lysate.

3.2.1.2 TBS-T 0.1% is an effective Washing Solution when probing with anti-CHIKV antibodies

The same protocol was followed as in 3.2.1.1, but with the substitution of PBS as a wash solution and use of TBS-T 0.1% as an alternative. All antibodies were diluted in TBS-T 0.1% and 5% BSA. Antibody dilutions remained as reported in Section 2.2.6.3 and diluted in TBS-T (0.1% vol/vol).

In Figure 3.10 membrane A, bands at around 60 kDa were present in all CHIKV and ONNV lysates representing nsP1, with no band present in the mock BHK lysate. Distinct bands at around 42 kDa were present in all lysates, representing beta-actin. In membrane B, a band was present in the CHIKV replicon around 60 kDa, representative of CHIKV nsP3. In the ONNV_P3 lysates, two distinct bands were present above 95 kDa, presumed to be ONNV nsP3-ZsGreen/mCherry fusion proteins respectively. In all lysates, a band was present at 42 kDa, representative of beta-actin. Of note in both membranes was the addition of non-specific bands of protein.

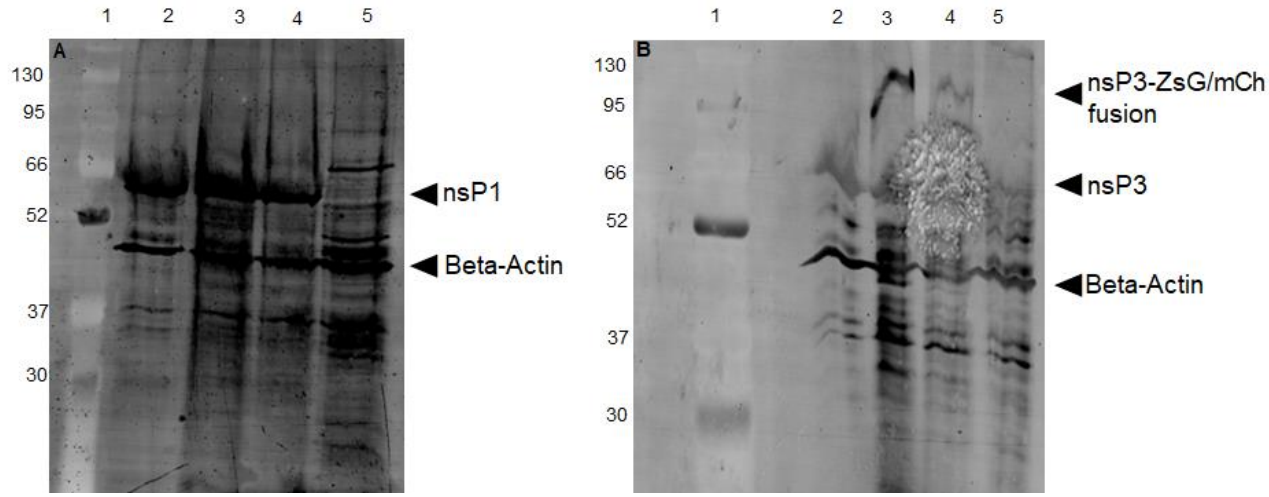

Figure 3.10; Western Blots of 25µg of BHK-21 cell lysate with TBS-T 0.1% as a Washing Solution. SDS-PAGE and transfer to PVDF membranes was performed as described in 2.2.6.1. Membranes were probed with anti-Beta-Actin and anti-CHIKV nsP1 (A) or anti-CHIKV nsP3 (B) antibodies and probed after with anti-mouse and anti-rabbit secondary antibodies in TBS-T 0.1% and 5% BSA. Molecular masses are displayed in kilodaltons (kDa). 1= Protein Ladder, 2= CHIKV-Replicon BHK Lysate, 3= P3ZsG BHK lysate, 4= P3mCh BHK lysate, 5= Mock BHK lysate.

Evidently, displaying all expected protein bands and all bands of the protein ladder made using TBS-T 0.1% the washing solution of choice for further western blots. The addition of Tween-20 was supposed to prevent non-specific protein-protein interactions, as it more effectively does in 3.2.2 and 3.2.3, but bands of antibody-specific proteins were more readily detected than blots without Tween-20 in washing solutions. It is unclear why this is the case.

3.3.2 Anti-CHIKV nsP1 antibodies bind efficiently with ONNV nsP1

As stated in 3.2.1, studies and serological testing have seen a one-way antigenic relationship between anti-CHIKV antibodies and ONNV-native proteins in patients with CHIKV antibodies present in their sera (Blackburn *et al.*, 1995; Partidos *et al.*, 2012; Tappe *et al.*, 2014). In order to determine if anti-CHIKV nsP1 primary antibodies can be used to detect ONNV nsP1 effectively, cell lysates infected with CHIKV replicon or ONNV infectious species underwent SDS-PAGE gel electrophoresis, protein transfer and probing with anti-CHIKV nsP1 antibodies.

In figure 3.11, the protein ladder was visible with bands from 30 to 175 kDa. Between 66 kDa and 52 kDa, a strong band of protein was present in all CHIKV/ONNV infected lysates, representative of nsP1. There was no band for nsP1 present in the mock BHK lysate. Between 52 kDa and 37 kDa, a strong band of protein was present in all lysates, representative of beta-actin. Non-specific bands of protein weakly were present in all lysates.

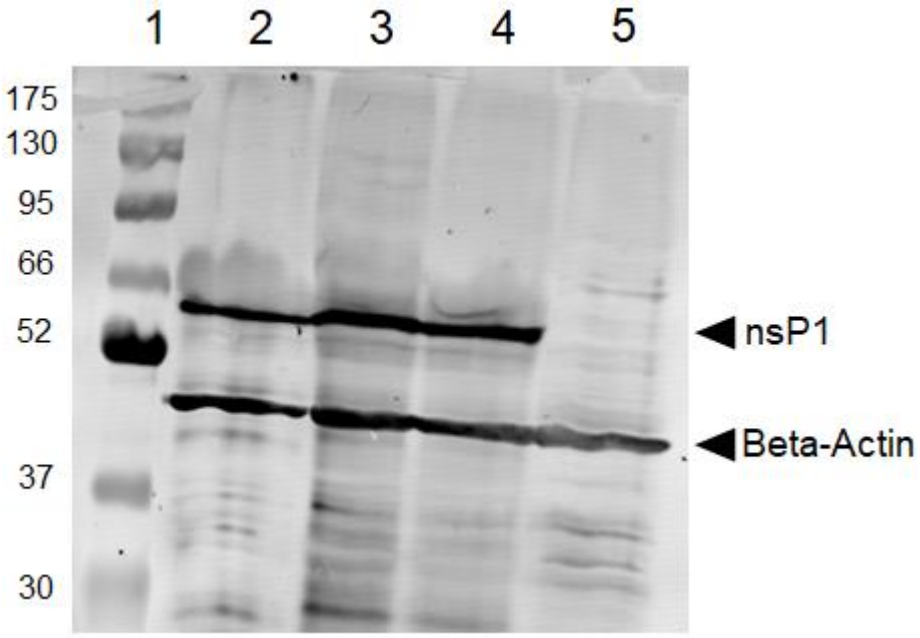

Figure 3.11; Western Blot of BHK-21 cell lysate probed with anti-CHIKV nsP1 antibody. SDS-PAGE and transfer to PVDF membrane was performed as described in 2.2.6.1. Membrane was probed with anti-beta-actin and anti-CHIKV nsP1 (1:500) antibodies. Secondarily probed with anti-mouse and anti-rabbit secondary antibodies. Molecular masses are displayed in kilodaltons (kDa). 1= Protein Ladder, 2= CHIKV-Replicon BHK Lysate, 3= P3ZsG BHK lysate, 4= P3mCh BHK lysate, 5= Mock BHK lysate.

The nsP1 band in the CHIKV-infected lysate acts as a positive control, and uninfected BHK lysate acts as a negative control. ONNV nsP1 is shown clearly in both ONNV-infected lysates, confirming that anti-CHIKV nsP1 antibodies are effective at binding with ONNV nsP1 proteins.

3.3.3 Anti-CHIKV nsP3 antibodies bind efficiently with ONNV nsP3

In order to determine if anti-CHIKV nsP3 primary antibodies can be used to detect ONNV nsP3 effectively, cell lysates infected with CHIKV replicon or ONNV infectious species underwent SDS-PAGE gel electrophoresis, protein transfer and probing with anti-CHIKV nsP3 antibodies.

In figure 3.12, between 52 kDa and 66 kDa, there were murky protein bands at around 60 kDa in CHIKV and ONNV infected lysates that represent nsP3. Of note, there were faint bands close to 95 kDa in ONNV infected lysates that represent nsP3 bound with their respective fluorescent marker proteins. No nsP3 protein was present in the mock BHK lysate. Between 37 kDa and 52 kDa, clear bands of protein were present in all lysates, representing beta-actin. As with Figure 3.11, there were non-specific protein bands across all lysates.

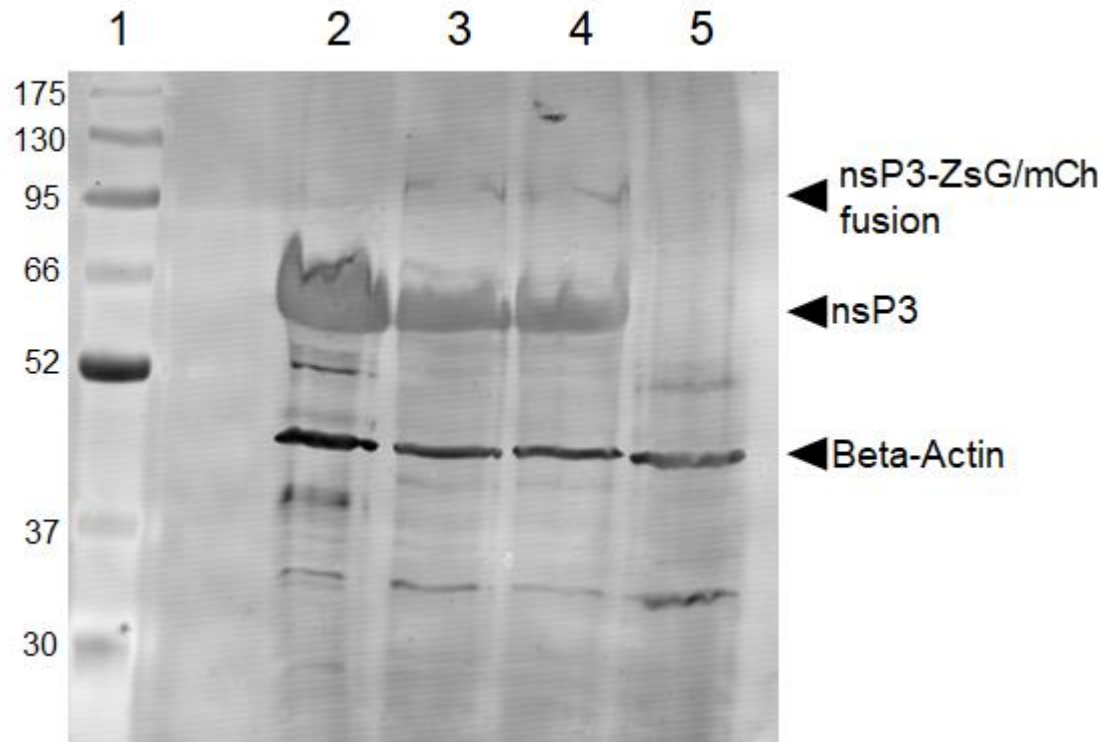

Figure 3.12; Western Blot of BHK-21 cell lysate probed with anti-CHIKV nsP3 antibody. SDS-PAGE and transfer to PVDF membrane was performed as described in 2.2.6.1. Membrane was probed with anti-Beta-Actin and anti-CHIKV nsP3 (1:1000) antibodies. Secondarily probed with anti-mouse and anti-rabbit secondary antibodies. Molecular masses are displayed in kilodaltons (kDa). 1= Protein Ladder, 2= CHIKV-Replicon BHK Lysate, 3= P3ZsG BHK lysate, 4= P3mCh BHK lysate, 5= Mock BHK lysate.

The presence of the nsP3 band in the CHIKV-infected lysate acted as our positive control, and the lack of a band in the mock BHK-21 cell lysate acted as our negative control. As stated, ONNV nsP3 seems divided between the band around 60 kDa, representative of nsP3, while the small quantities of protein at ~95 kDa would represent the fluorescent nsP3 fusion proteins. Though this confirms anti-CHIKV nsP3 antibodies effectively bind with ONNV nsP3 proteins, it raises the question of how there are non-fluorescent nsP3 proteins present in those lysates.

To summarise, TBS-T 0.1% provided the clearest western blots when used as a washing buffer and antibody diluent. Using this information, it was clearly demonstrated that both anti-CHIKV nsP1 and nsP3 antibodies can be used to effectively probe for ONNV nsP1 and nsP3 proteins in western blots.

3.3.4 48H Immunofluorescence of Infection

The viral entry, replication process and egress of ONNV infection is presumed to be similar to that displayed of other alphaviruses such as CHIKV. In CHIKV, nsP1 remains permanently bound to plasma membranes while nsP3 interacts with host proteins across the cytoplasm, whereas nsP sub-cellular localisations in ONNV infection are poorly described (Gottipati *et al.*, 2020). Once we validated that anti-CHIKV nsP1 and nsP3 antibodies effectively bind with ONNV nsP1 and nsP3 in western blots (Figure 3.11 and Figure 3.12), attention turned to the antibodies' use in immunofluorescence assays. IF assays are useful for the analysis of the virus replication cycle, as they identify the localisation of viral proteins at set hpi, which in turn allows for interpretation of virus-host protein interaction at various times in the replication process. The antibodies would have to show affinity for ONNV nsP1 and nsP3 in their natively folded state in order to work effectively in IF assays.

In order to elucidate the subcellular locations of ONNV nsPs during infection, as well as validate that anti-CHIKV nsP1 antibodies were effective for ONNV IF assays, an ONNV infection in BHK-21 cells was performed using P3mCh at MOI-1 and 10, fixed at 6, 12, 24 and 48 hours. BHK-21 cells were chosen to be infected as they readily infect with ONNV and in CHIKV infection, large amounts of nsP3 have been visualised prior (Roberts *et al.*, 2017). We used two MOIs of virus to exemplify the difference between a low and high viremia in infection. Cells were permeabilised and probed with 1:1000 anti-CHIKV nsP1 rabbit antibodies and 1:500 anti-rabbit Alexa-Fluor 488 fluorescent antibody (Figure 3.12). DAPI was used to intracellularly stain nuclei.

Mock panels A-E showed mock BHK-21 cells probed in the manner described. In all Mock panels, nuclei were intracellularly stained blue and cytoplasm showed weak green background fluorescence and a weak red background fluorescence. Cell physiology was typical of fibroblasts in all images, with large nuclei and elongated cells.

MOI-1 panels A-E showed BHK-21 cells infected with P3mCh at an MOI of 1. MOI-1 panel A failed to stain effectively with DAPI and therefore nuclei were less visible. MOI-1 panel B showed typical cell physiology, distinct blue nuclei and the presence of nsP1, but the distinct presence of localised collections of nsP3 were visible, localised near nuclei within the cytoplasm. In MOI-1 panel C, cell physiology was visibly changed, with thinner, pseudopod-like protrusions from cells. Nuclei were intracellularly stained with a weaker nsP3 presence diffuse across the cytoplasm but most notably, the presence of nsP1 was of a similar intensity to MOI-1 panel B, with roughly circular puncta of a higher intensity at the edges of

the cell membrane which varied in size. In MOI-1 panel D, the characteristics seen in MOI-1 panel C were visible, but nsP3 presence was more intense than MOI-1 panel C and was gathered in localised collections near nuclei. In MOI-1 panel E, we saw similar physiology to MOI-1 panel D. nsP1 had lowered in intensity diffuse across cells but still showed circular pockets of intensity on the plasma membrane. nsP3 was present in small puncta, smaller than in other images, and was diffused weakly throughout the cells.

MOI-10 panels A-E showed BHK-21 cells infected with P3mCh at an MOI of 10. MOI-10 panel A showed typical BHK physiology and minor background red fluorescence. Green fluorescence was of similar intensity as in mock images. MOI-10B showed typical cell physiology. nsP1 was visible across all cells and was visibly more intense than MOI 10A, with a very intense region of activity in the topmost cells. nsP3 presence mirrored that seen in MOI-1 panel B, but smaller collections of nsP3 were seen across cells away from the nucleus. MOI-10 panel C showed a change in cell physiology for some cells, rounding and losing their fibroblastic shape. Cells maintaining their physiology mirrored those in MOI-10 panel B. These cells show intense nsP1 presence and localised nsP3 puncta around the nucleus. MOI-10 panel D showed further changes in physiology, with thin pseudopod-like extensions on the outside of cells. nsP3 formed puncta in some cells near the nucleus, but was also weakly diffused across cells. nsP1 presence was slightly reduced when compared to MOI-1 panel C, but circular pockets of intensity on the plasma membrane were similar to those seen in MOI-1 panels C, D and E. In MOI-10 panel E, physiology continued to be irregular. nsP3 was no longer gathered near the nucleus and was weakly diffused across the cells. nsP1 presence was significantly less intense than previous panels, and small circular pockets of cytoplasm separated from cells were visible with nsP1 in them.

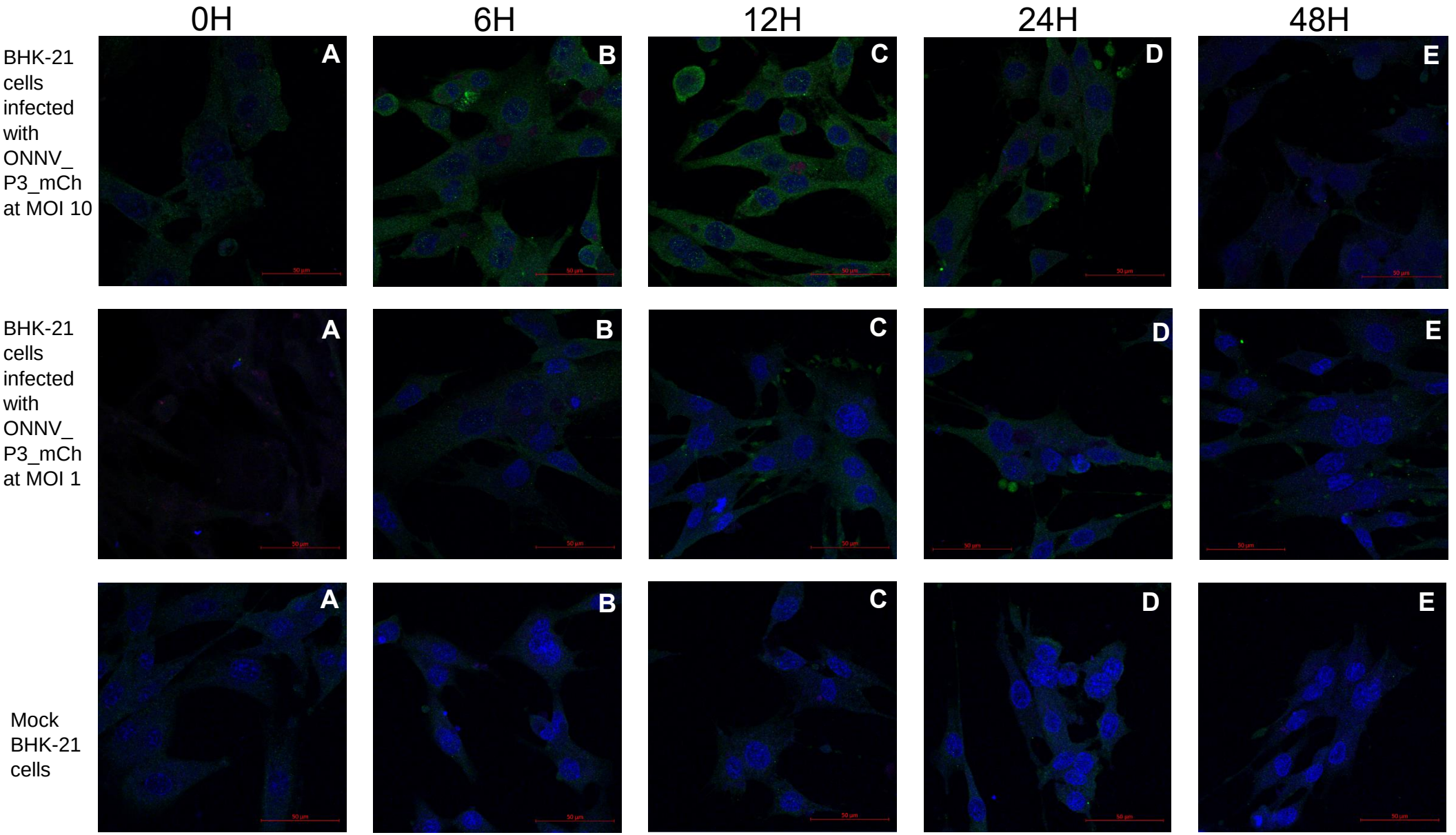

Figure 3.13; Fluorescence Microscopy of ONNV nsP1/3 in BHK-21 cells over 48 hours. Merged confocal Imaging of mock BHK-21 cells, BHK-21 cells infected with P3mCh at MOI-1 and BHK-21 cells infected with P3mCh at MOI-10 at 6, 12, 24 and 48 hours. Cells were infected with ONNV at an MOI-1 or 10 and incubated at 37^{o}C and 5% CO_2. Cells were fixed and probed with 1:1000 anti-CHIKV nsP3 rabbit antibody and 1:500 anti-rabbit Alexa-Fluor 488 fluorescent antibody (Green). Nuclei are stained with DAPI (Blue). The nsP3-mCherry fusion protein was also visualised (red). Separate channel images of the 6, 12, 24 and 48 ours at both MOI are shown on the next page.

FF

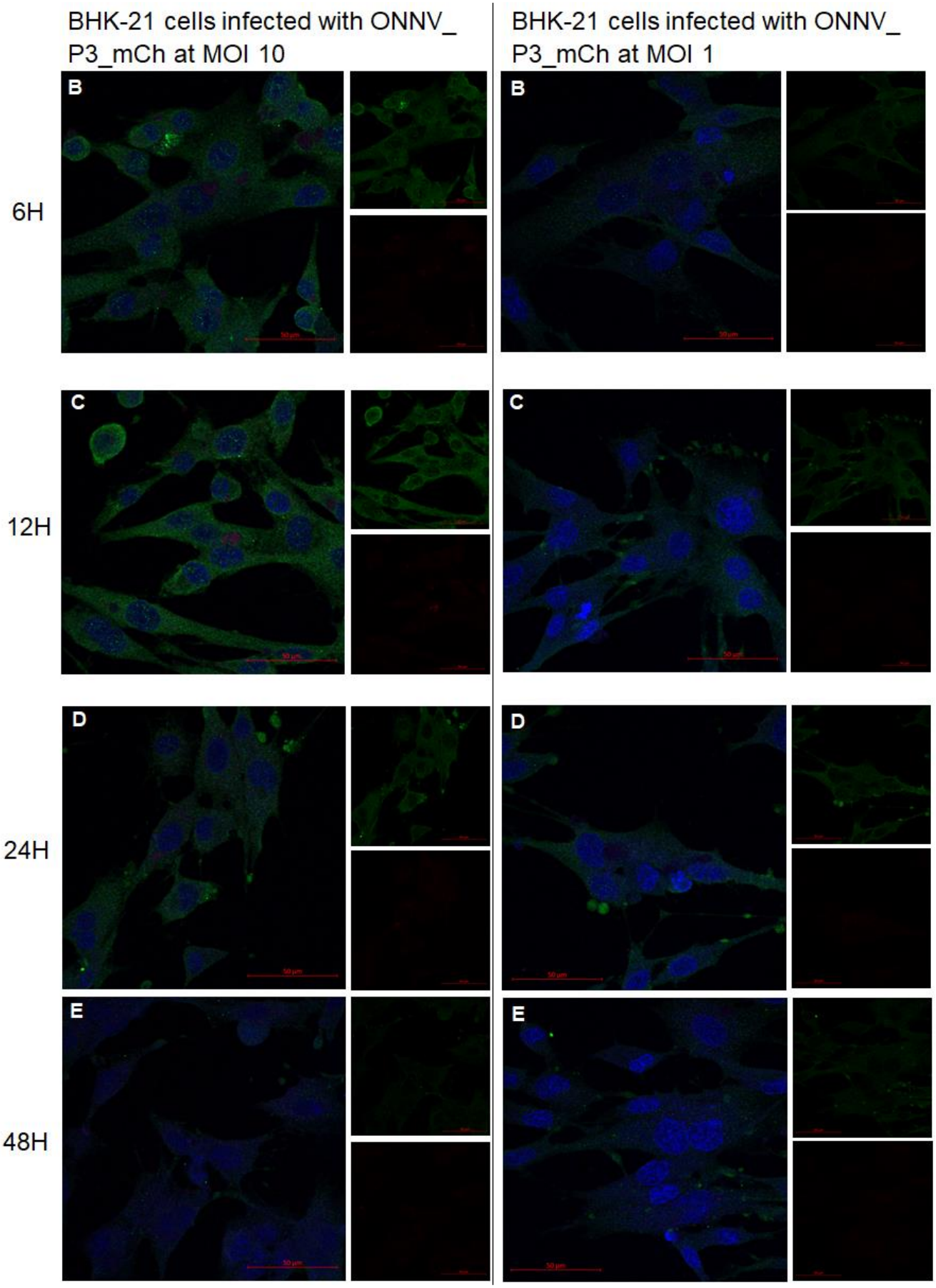

Figure 3.13B; Fluorescence Microscopy of ONNV nsP1/3 in BHK-21 cells over 48 hours. Merged images are identical to Figure 3.13, with green and red fluorescence channels split, showing ONNV nsP1 and nsP3-mCherry respectively.

The changes to cell physiology and circular membranous pockets on the plasma membrane were likely sequelae of apoptosis; the pseudopod-like extensions seen 24 hours may have been apoptopodia. Furthermore, blebs of cytoplasm and plasma membrane form as the cytoskeleton dissociates from the plasma membrane, the circular membrane pockets seen 12 and 24 hours in MOI-1 and MOI-10 respectively could have been these blebs filled with nsP1. nsP1 is permanently bound to plasma membranes during ONNV infection and was noticeably more present in MOI-10 infections than MOI-1 infections.

The behaviour of nsP3 to localise around the nucleus was seen in CHIKV infection, but the quantity and shape differed between cell types, some forming puncta and rods (Roberts *et al.*, 2017). In BHK-21 cells, nsP3 only formed large puncta around the nucleus visually 6hpi in MOI-10 infection, but was only visible 24 hours in MOI-1 infections.

Though not typical of all cells imaged, potential evidence of syncytia was visualised in 3.3.2, specifically in ONNV infection at an MOI-10, 48 hours. Interestingly, multinucleated mass of cellular membrane and nuclei were observed (Figure 3.14). Multi-nucleated cells of these proportions are referred to as Syncytium, or a polykaryocyte. nsP1 acted as a useful plasma membrane marker in this instance, showing us that the syncytium present had a membrane border. Unfortunately, the syncytium was larger than the range of magnification used and as such, a definitive size of the syncytium could not be determined. nsP1 was seen lining the perimeter of the plasma membrane, with multiple distinct spots scattered across the syncytium. nsP3 was present both within and outside the syncytium, but was intensely present around the nuclear material.

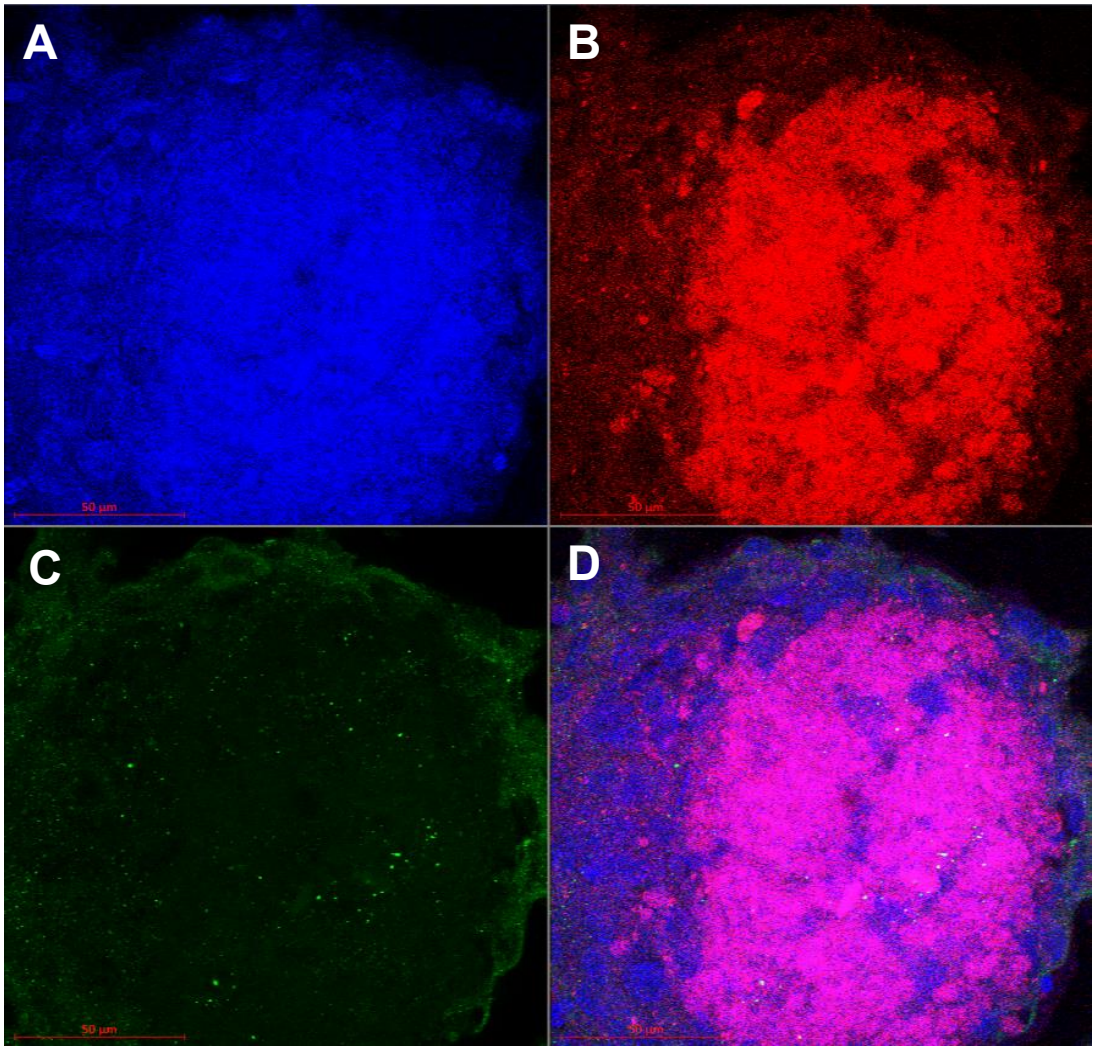

Figure 3.14; ONNV Infection at an MOI of 10 in BHK Cells after 48 hours, displaying the presence of syncytia formation. A) DAPI staining of the nuclei, B) Red fluorescence of nsP3-mCherry protein, C) ONNV nsP1 probed with anti-CHIKV nsP1 antibody, secondarily probed with Alexa-fluor 594 secondary antibodies. D) Merged image of fluorescence channels.

To summarise, in MOI-1 infections 12 hours post-infection, membrane-bound sections of the cytoplasm were filled with nsP1, almost all of them connecting to the plasma membrane. These were seen 24 and 48 hours also. nsP3 on the other hand, migrated from spherules and aggregated around the nucleus, which occured visually at 6 hours in MOI-10 infections, but was only visible by 24 hours in MOI-1 infection. Syncytia were formed by 48 hours in MOI-10 infections, this was the first reported evidence of ONNV-induced syncytia formation. Finally, we confirmed that CHIKV nsP1 antibodies provided effective binding to ONNV nsP1 *in vitro*, validating their further use in IF assays.

3.4 Replication Complex Study

3.4.1 Wortmannin MTT Assay

It is currently unknown whether ONNV spherules are internalised during infection, as other alphavirus spherules such as CHIKV and SFV are, to create cytopathic vacuoles (CPV-1). Wortmannin, a PI3-Kinase inhibitor, has been shown previously to inhibit mechanisms that internalise spherules into CPV-1s (Pietila *et al.*, 2018). In studies performed on the replication complex of SFV, understanding where spherules are localised is integral for knowing which membranes to isolate (Pietila *et al.*, 2018). For future studies focused on isolating the ONNV spherules to further characterise the nsPs in their native environment, this knowledge would be ideal. In order to clarify whether or not ONNV spherules are internalised during infection, we must first assess the toxicity of Wortmannin in BHK-21 cells, which was to be determined via MTT assay. BHK-21 cells were chosen as to replicate a previous study in which Wortmannin was used to block spherules to the plasma membrane is SFV infection.

The lowest average viability of cells in Wortmannin was 400nM (91.7%). The highest average percentage viability of cells in Wortmannin was 200nM (110.2). As all average percentage viabilities shown via MTT are above 80%, 100nM was used in published literature studies and was chosen for future investigations (Pietila *et al.*, 2018).

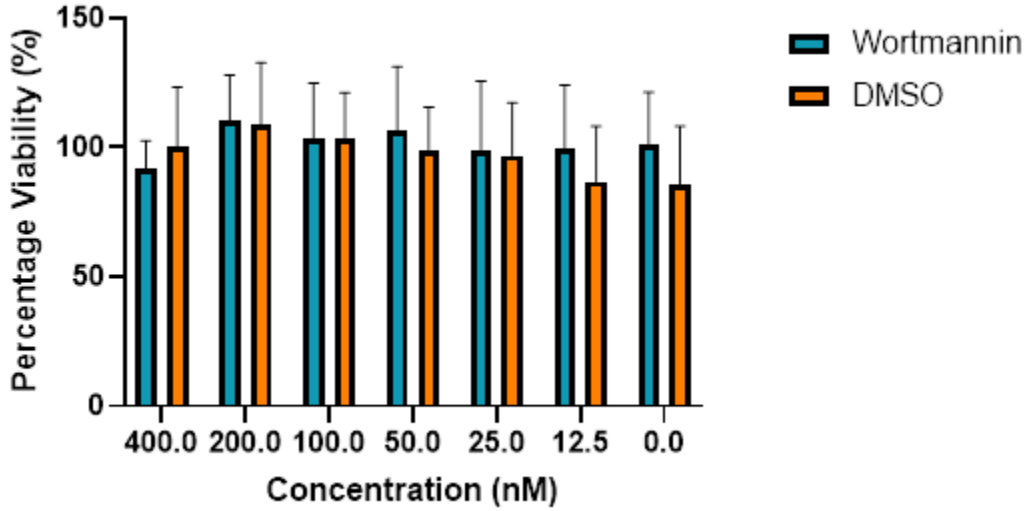

Figure 3.15; Percentage viability of BHK-21 cells in Wortmannin. Concentrations of Wortmannin and DMSO from 400-0 nM were diluted down in complete DMEM and incubated on cells for 3 hours (n=3).

3.4.2 Fluorescence Microscopy of BHK-21 cells infected with ONNV and treated with Wortmannin, at 6 hours

In order to determine whether or not spherule internalisation was occurring during ONNV infection, as well as validate the use of anti-CHIKV nsp3 antibodies for ONNV IF assays, nsP3, a constituent protein of the replication complex was selected. Again, BHK-21 cells were used to simulate conditions described in prior studies. BHK-21 cells were infected at MOI-1 with 2ZsG and cells were fixed at 0, 2, 4 and 6 hours. In parallel, another set of BHK-21 cells followed the same procedure for infection and were treated with 100nM Wortmannin after 90 minutes to prevent spherule internalisation. Timepoints for fixation and Wortmannin dosage were chosen to mirror parameters in prior published study (Pietila *et al.*, 2018). Cells were permeabilised and probed with 1:1000 anti-CHIKV nsP3 rabbit antibodies and 1:500 anti-rabbit Alexa-Fluor 594 fluorescent antibody (Figure. 3.16). DAPI was used to stain nuclei.

As expected, control cells at 0hpi (Figure 3.16 A and E) showed no visible presence of nsP3. Cells fixed at 2 hours (Figure 3.16 B and F) showed intense nsP3 presence around the plasma membrane. In 3.16 B, nsP3 was present around the plasma membrane, as well as around the nucleus. In 3.16 F, nsp3 was present around the plasma membrane unevenly, forming small circular pockets. Cells fixed at 4 hours (Figure 3.16 C and G) showed nsP3 throughout the cytoplasm, or in small, faint, circular puncta. Cells fixed at 6 hours showed nsP3 throughout the cytoplasm in some cells, whilst dense puncta of nsP3 were observed in others.

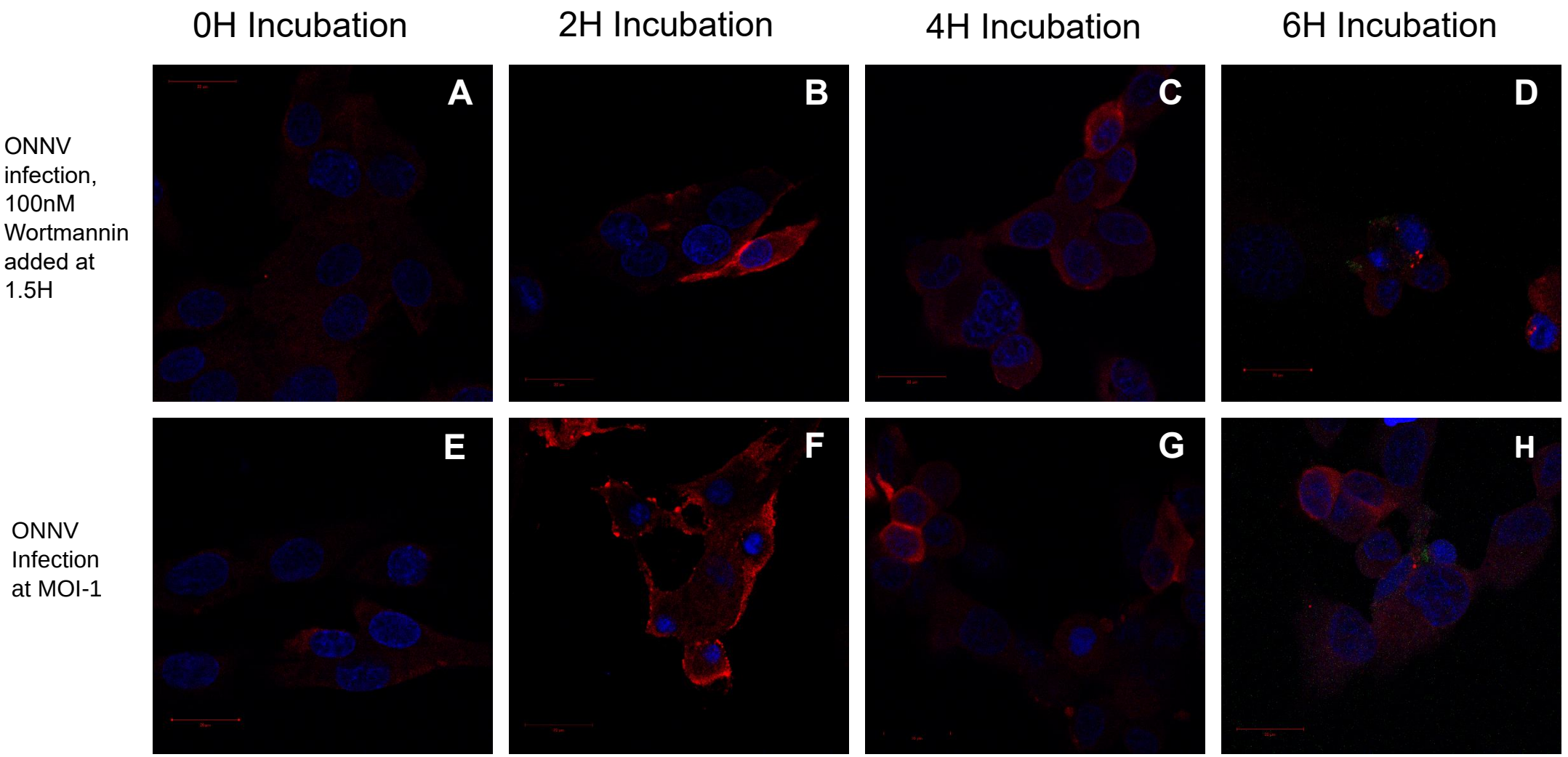

Figure 3.16; BHK-21 cells infected with ONNV at MOI-1, with and without 100nM of Wortmannin after 90 minutes. BHK-21 cells observed under a Zeiss 700 LSM confocal microscope at 40X in oil immersion. ONNV nsP3 is shown in red (1:500 anti-rabbit Alexa-Fluor 594 fluorescent antibody). Nuclei are shown in blue (DAPI). ZsGreen is shown in green in 6H incubation, ZsGreen detection was not used for other images. Figure shows presumed spherule formation at 2 hours, with nsP3 dispersal across the cytoplasm after 4 hours and dense clustering near nuclei after 6 hours. All scale bars are 20μm across.

In the control untreated ONNV infection, nsP3 was present in spherules by 2 hours, but had migrated across the cytoplasm by 4 hours and by 6 hours were beginning to form small puncta near the nucleus. When ONNV-infected cells were treated with Wortmannin, the distinct collection of nsP3 was not seen, but was instead dispersed throughout the cytosol, with puncta at 6 hours still present. The migratory nature of nsP3 across the cytoplasm means no conclusions about spherule internalisation could be inferred from the images. However, the migration of nsP3 towards the nucleus forming puncta mirrors prior published data that shows similar activity in CHIKV infection in Huh7 cells (Roberts *et al.*, 2017). This also corroborates the observations and conclusions made about nsP3 in Figure 3.13. nsP3's migration from spherules to the cellular environment supports previously published theories about the multifunctional nature of nsP3 in alphaviral replication (Gao *et al.*, 2019; Götte *et al.*, 2018; Panas *et al.*, 2014; Scholte *et al.*, 2015). Finally, the study confirms that CHIKV nsP3 antibodies provided effective binding to ONNV nsP3 *in vitro*, validating their further use in IF assays.

3.5 TEM Imaging of ONNV Isolates

3.5.1 TEM Negative Stain Imaging of ONNV clone isolates

The capsid structure of many alphaviruses have been studied in detail using imaging techniques such as cryo-electron microscopy (Cryo-EM) and X-ray crystallography. Though it is presumed that ONNV has a similar structure to other alphaviruses, it has to date not been confirmed in the published literature. In order to clarify the nature of ONNV's capsid structure, negative staining at 1% and transmission electron microscopy (TEM) and Negative Staining using an FEI Tecnai G2 spirit transmission electron microscope was performed. 2ZsG, P3ZsG and P3mCh infected viral supernatants were imaged.

ONNV virions surrounded by a darkened halo awere visible via negative staining. Virions present were around 60-70nm in diameter and looked approximately circular, similar to other alphaviruses. Some capsids appeared damaged (e.g. Figure 3.17B). However, damaged virions were also ~60-70nm in diameter. Of note, virions showed pleiomorphic features (Figure 3.19), in contrast to what has been described for other alphaviruses (Mancini *et al.*, 2000; Sun *et al.*, 2013).

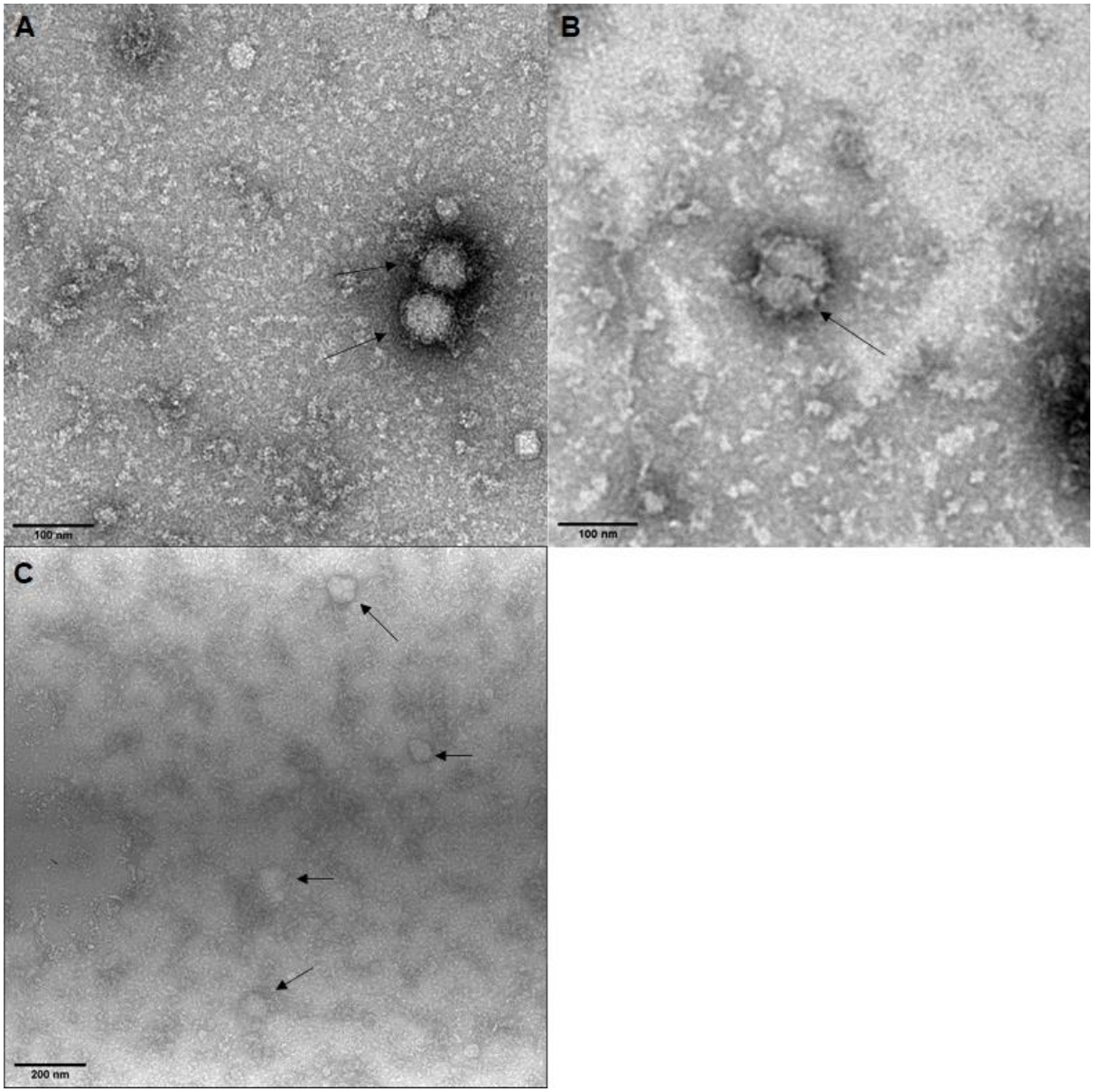

Figure 3.17; TEM Imaging of ONNV Infectious clones, stained with 1% UA. A) 2ZsG at x68000 magnification. B) P3ZsG at x68000 magnification. C) P3mCh at x30000 magnification. Arrows highlight the presence of ONNV virions of VLPs.

To summarise, ONNV virions are 60-70nm in diameter, displaying symmetrical capsid and there are no visible differences between the three ONNV species as expected.

3.5.2 3D Reconstruction of the 2ZsG Capsid via RELION

TEM imaging cannot provide detailed information about the protein structure or icosahedral symmetry present within the virion. In order to determine the 3D protein structure of the ONNV virion, TEM Electron Micrographs obtained of 2ZsG virions using the FEI Tecnai F20 were processed via RELION image processing software. ONNV virions were selected in micrographs, 74 particles were selected from 39 micrographs. 2D classification reconstruction was performed, resulting in the selection of 65 virions for 3D reconstruction. Particles were then used to generate an icosahedral reference, and subjected to 3D refinement, resulting in a map, at a final resolution of 32 Å (Angstroms) (Figure 3.18).

The ONNV virion reconstruction is consistent with a protein map that forms both pentamers and trimers; surrounding each pentamer are five trimers, and surrounding each trimer are three pentamers. When compared to other alphaviral structures, this is unusual, as alphaviruses present a hexamer and pentamer structure, with each hexamer surrounded by six pentamers. It is unknown as to whether this is unique to ONNV. Figure 3.19 shows a comparison between our ONNV reconstruction and a previously generated CHIK VLP. The CHIKV virion diameter is approximately 700 Å in diameter, the previously reported size of alphavirus virions, while the generated ONNV virion diameter is approximately 500 Å. This does not equate to the size displayed in previous electron micrographs, leading us to believe that the model generated may not be truly representative of 2ZsG.

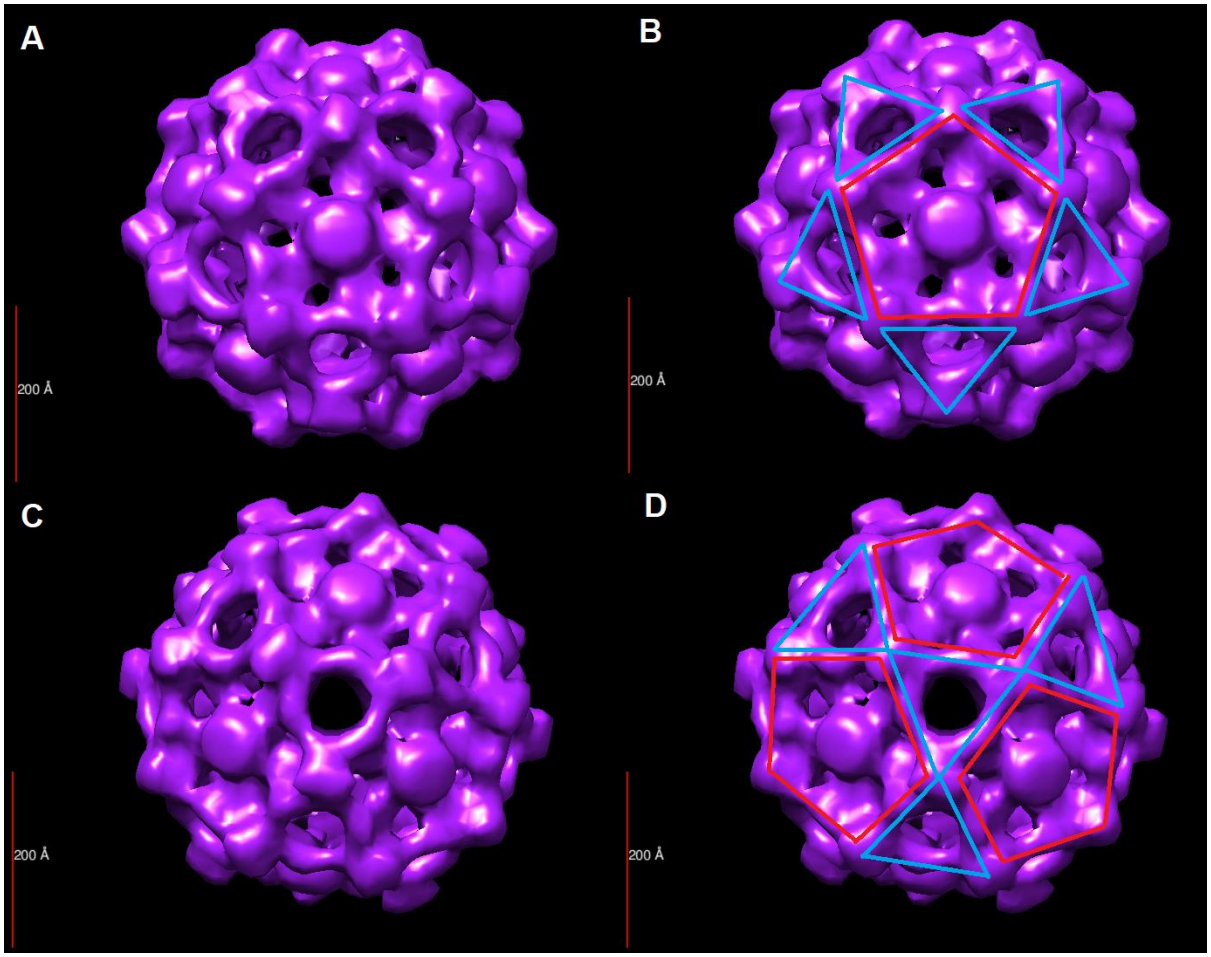

Figure 3.18; Negative staining 3D Reconstruction of the 2ZsG Virion. A) Pentamer structure present in the ONNV protein map. B) Highlights the structure in a clearer manner. C) Trimer structure present in the ONNV protein map. D) Highlights the structure in a clearer manner. Reconstruction was presented at a resolution of 32 Å. Red=Pentameric structure, Blue=Trimeric structure. Images used to generate the structure were taken by Ben Chadwick (University of Leeds), Digital Reconstruction via RELION was performed by Dr Juan Fontana (University of Leeds).

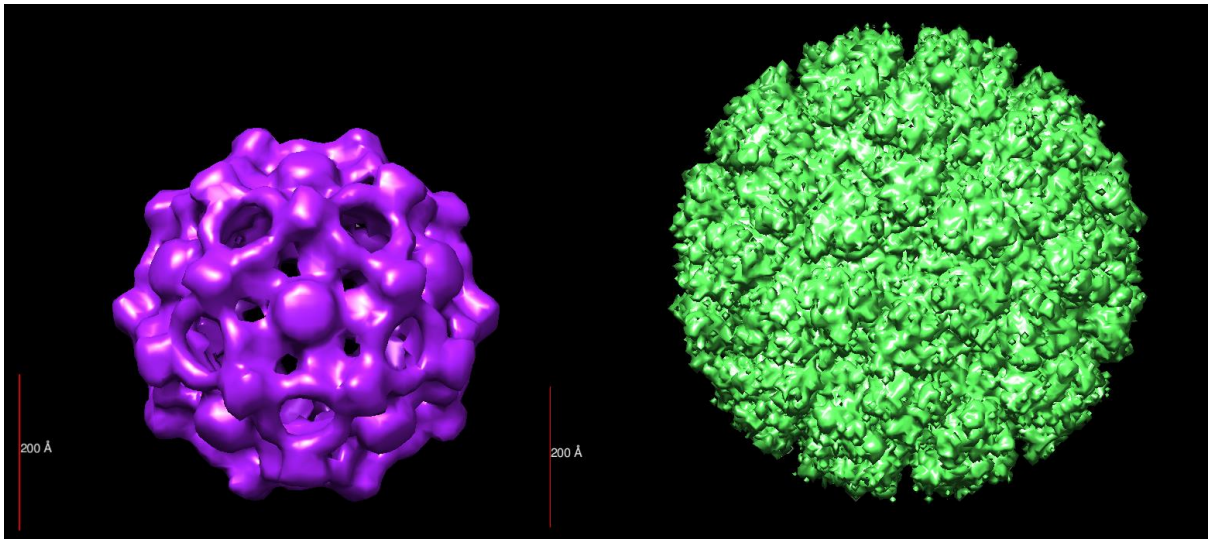

Figure 3.19; Comparison of the negative stain 3D reconstruction of ONNV with previously published CHIKV VLP (Virus-Like Particle) Reconstruction. ONNV virion is presented in purple, CHIKV VLP is presented in green. CHIKV VLP protein map (Sun *et al.*, 2013) was generated from 36,236 particles by cryo-EM. The resolution of the average is 5.3 Å. ONNV virion protein map was generated from 65 virions acquired via TEM.

Chapter 4: Optimisation of the ONNV Reverse Genetic System: Discussion

4.1 Summary of Results

The aim of this study was to optimise reverse genetic systems and molecular tools for ONNV studies, to be used as a model system for other alphaviruses. Optimisation of ONNV propagation was performed using different ONNV infectious clones and cell lines, including establishment of ONNV infection in U4.4 cells, the results of these indicate preferences for ONNV propagation. Tools such as antibodies to be used as markers were validated via SDS-PAGE and western blotting, use of these antibodies and western blot analyses with ONNV proteins were optimised. Imaging methodologies such as immunofluorescent confocal microscopy and transmission electron microscopy were also validated, allowing insight into ONNV protein-cell interactions. A 3D model of the ONNV capsid was generated, presenting a potential protein structure.

Currently, ONNV is significantly understudied in comparison to other alphaviruses. Within the published literature there is a significant lack of information regarding cell permissibility, characterisation of viral entry, replication and egress in relevant cell lines and virus-host protein interactions. Studies performed characterise infection in vectors or murine models, the latter of which have not proven representative of human disease (Keene *et al.*, 2004; Seymour *et al.*, 2013). Furthermore, there are minimal papers reporting the development of tools for use with any ONNV system; ONNV-specific antibodies are largely missing from papers, using cross-reactive antibodies developed against other alphaviruses such as the use of anti-SINV E2 antibodies, which provided cross-reactivity with ONNV E2 proteins, which displays a need for such tools (Keene *et al.*, 2004). Cell lines that are permissible to ONNV infection are reported in few papers and have varying methods and time points, which would benefit from optimisation (Chan *et al.*, 2020; Keene et al, 2004). Full protein sequences are available for polyprotein P1234 and the structural polyprotein, but sequences and structures of the cleaved native proteins are not available, and most protein interactions or subcellular locations documented are presumed by structural similarity to other alphaviruses. This lack of information and standardised tools for research has dark implications when paired with the increasing risk of alphaviral epidemics; in 20 years, cases of CHIKV infection that were once isolated to *Ae. aegypti* habitats geographically, to autochthonous cases now worldwide due to factors such as globalisation and international trade, and climate change (Nasci, 2014; Kraemer *et al.*, 2019). ONNV's shared homology

with CHIKV poses the possibility that ONNV could have a change in vector also, through similar microevolution, and become a similar global health threat.
ONNV makes an effective model system for alphaviruses, especially CHIKV. Comparative analysis of structural and non-structural protein sequences between CHIKV and ONNV showed an 85% similarity, showing ONNV's closely shared lineage with CHIKV (Khan *et al.*, 2002). Furthermore, CHIKV is a BSL-3 (biosafety level-3) pathogen, which requires BSL-3 conditions at all times when using CHIKV, which can prevent the use of techniques such as cryo-electron microscopy. ONNV can provide a model that is phylogenetically similar to CHIKV whilst usable in BSL-2 conditions.

4.2 ONNV shows different rates of replication between different Cell Lines

Multi-step growth curve assays over multiple time points in BHK-21, Huh7, RD, C6/36 and U4.4 cells demonstrated that ONNV replicates at different rates depending on the cell line. BHK-21 cells are derived from baby hamster (*Mesocricetus auratus*) kidney fibroblasts. Huh7 cells are a human hepatocyte derived carcinoma cell line, while RD Cells are human myocytes derived from rhabdomyosarcoma. C6/36 and U4.4 cells are derived from *A. albopictus* larval cells. The production of infectious titre was used as a measure of ONNV replication. All five cell lines were chosen as they have previously been used in propagation and analysis of alphaviral lifecycles. Of the mammalian cell lines, BHK-21 cells were chosen for further use in the study as, although not a human cell line, they are physiologically representative of fibroblasts, cells typically targeted in alphaviral infection. They also showed the highest viral titre of all cell lines, peaking at 10^8 PFU/mL at 24 hours. Comparatively, BHK-21 cells infected with CHIKV strains produced an average titre of 10^7 PFU/mL at 24 hours, while at 48 hours onwards plateaued at 10^8 PFU/mL, which decreased in titre dependant on CHIKV strain (Sudeep *et al.*, 2019). These comparisons between CHIKV and ONNV titres may suggest a more aggressive and cytopathic infection caused by ONNV, it's possible CHIKV's modulation of host anti-viral responses are less efficient than ONNV's. Further research into the alphavirus anti-viral response could elucidate this.

Huh7 cells produced the lowest viral titres of any cell line, an interesting contrast to the use of Huh7 cells as a model cell line for CHIKV infection, CHIKV has previously produced titres around $1x10^6$ after 24 hours in Huh7 cells (Roberts *et al.*, 2017). This higher titre in CHIKV corroborates to murine and non-human primate studies where infectious virus was found within the liver of infected animals and was found to be a site of initial viral replication in murine models (Couderc *et al.*, 2008; Labadie *et al.*, 2010). In murine models, ONNV showed minimal to no damage to liver integrity, with only microgranuloma formation,

implying an immune response but not active viral replication (Seymour *et al.*, 2013). These studies, along with the titres generated in this study imply ONNV and CHIKV have different native sites of replication in mammalian infection. Because of this, we believe the use of Huh7 cells as a model for ONNV infection is limited.

RD cells produced a viral titre of 10^6 PFU/mL at 24 hours and sustained this level of titre over 72 hours in all infectious clones. In replication kinetics studies of CHIKV strains using RD cells, titres took between 48 and 72 hours to peak, reaching titres between 10^6 and 10^8 PFU/mL (Sudeep *et al.*, 2019). ONNV titres peaking after 24 hours is indicative of muscle cells, of which RD cells are an effective model for, being a site of initial viral replication in ONNV infection. Furthermore, in murine models of both CHIKV and ONNV infection, muscle cells are infected in acute infection; RD cell lines would make for a better physiological model for muscle cell pathogenesis of alphaviral infection (Couderc *et al.*, 2008; Seymour *et al.*, 2013).

As ONNV is a mosquito transmitted arbovirus, we felt it was also important to understand viral replication in mosquito cell lines. U4.4 cells on average produced a 1-log lower titre when compared to C6/36 cells. We hypothesise that reduced titres in U4.4 cells is due to the PO cascade immune response; inhibition of which was found to lead to higher virus genome levels, inferring it has a suppressive effect on viral replication (Rodriguez-Andres *et al.*, 2012). An innate immune response of a similar nature has not been reported for C6/36 cells, these titres are therefore a model for viral replication both in and out of the presence of an effective immune response in insect cells. The necessity for models of infection in alphaviral vectors, especially ONNV, is present in publications. Both cell lines are derived from *Ae. albopictus*, a relatively new vector for CHIKV, but native ONNV infection in the wild has not been reported. ONNV infection in these cell lines infers the potentiality ONNV genetic adaptation to *Ae. albopictus* as a vector for infection. Furthermore, *Ae. albopictus'* geographic distribution and habitat suitability have been changing due to both climate change and human globalisation (Kraemer *et al.*, 2019). *Ae. albopictus*-associated CHIKV infections have occurred across the world now, as mentioned in 1.3.6, and *Ae. albopictus*' geographical distribution is predicted to spread broadly across Europe, the Northern United States, highland regions of South America and East Africa within the next 30 years (Kraemer *et al.*, 2019). CHIKV's genetic adaptation to Ae. albopictus, as mentioned in 1.3.6, occurred due to a novel amino acid substitution from alanine to valine at position 226 in the E1 envelope protein, there is precedence for this to occur again in ONNV, as crossover between habitats *of Ae. albopictus* and *A. gambiae* occur in Central and East Africa (Schuffenecker *et al.*, 2006; Wiebe *et al.*, 2017; Kraemer *et al.*, 2019). Comparing E1 amino

acid sequences between CHIKV and ONNV, ONNV E1 protein contains this alanine at position 226; a valine substitution that causes a similar increase in *Ae. albopictus* vector competency is possible (Tsetsarkin *et al.*, 2007; UniProt, 2021).

It may have been more physiologically appropriate to have assessed titre in a cell line derived from *A. funestus* or *A. gambiae*, such as Mos. 55, Sua1B and 4a-3B (Marhoul & Pudney, 1972; Muller *et al.*, 1999). Mos. 55 cells have previously been infected successfully with ONNV, and 4a-3B cells also express the precursor molecule to the PO cascade, Prophenoloxidase, both of which could provide a physiologically representative cell line for vector infection (Marhoul and Pudney, 1972; Müller *et al.*, 1999).

The replication of ONNV could have been assessed via an infection time course using 2ZsG and quantitative live-cell imaging. This would give an image of ONNV replication within cells, quantified by fluorescence; expression of ZsGreen would be representative of viral replication. Ultimately, this would not be representative of replication for the nsP3 fusion species of ONNV, therefore plaque assay analysis of viral titre was a suitable method to determine ideal cell lines and time points for further investigation. However, the optimisation of these infectious clones does provide more tools for ONNV infection analysis going forward; an IncuCyte Zoom system could be used to image fluorescent virus in live cells, giving a more native image of the infection cycle.

4.3 Anti-CHIKV Antibody Validation

4.3.1 Anti-CHIKV nsP1 Antibodies can be used to detect ONNV nsP1

Anti-CHIKV nsP1 antibodies were used to probe ONNV nsP1 to determine their efficacy. Figure 3.11 shows specific binding of the anti-CHIKV nsP1 antibody to ONNV and CHIKV nsP1 protein in BHK-21 cell lysate with bands between 66 kDa and 52 kDa. Using the ONNV non-structural polyprotein P1234 amino acid structure, cross-comparing CHIKV nsP1 amino acid structure to identify ONNV nsP1's amino acid structure and calculating the molecular mass, ONNV nsP1 is 59.7 kDa (UniProt, 2021). CHIKV nsP1 is 60 kDa (UniProt, 2021). When both nsP1 sequences were compared, there was a 91.4% match in sequence. Polyclonal antibodies are developed to bind to different epitopes of a specific protein, consequently a higher amino acid sequence similarity provides more matching epitopes from the target antigen for the antibody to bind to. There are factors to be considered for the use of polyclonal antibodies for western blots. As polyclonal antibodies bind to numerous

epitopes on an antigen, they are much more sensitive and can detect proteins at low abundance, but can cross-react with unrelated proteins. This ability for alphavirus antibodies to cross-react with similar alphaviruses has been reported in the literature, such as the use of monoclonal antibodies for SINV E2 protein that cross-reacts with ONNV E2 protein, and cross-reactive anti-CHIKV antibodies neutralising ONNV antigens in murine models (Keene *et al.*, 2004; Partidos *et al.*, 2012).

In the alphaviral RC, nsP1 binds to negatively-charged phospholipids in the plasma membrane and anchoring itself within the neck of the spherule (Gottipati *et al.*, 2020; Jones *et al.*, 2021). nsP1 is also required to initiate minus-strand RNA synthesis (Cross & Gomatos, 1981). These two features, being bound to the spherule and integral to minus-strand RNA synthesis make nsP1 an optimal marker protein for spherule formation, RC activity and therefore, viral replication. The results have therefore validated the use of CHIKV nsP1 antibodies for western blotting. Western blots prove to be a useful tool in characterising protein expression, quantification, and subcellular location, which has been demonstrated in previous alphavirus studies (Pietila *et al.*, 2018).

4.3.2 Anti-CHIKV nsP3 Antibodies can be used to detect ONNV nsP3 and Fluorescent Fusion Proteins

Anti-CHIKV nsP3 antibodies were used to probe ONNV nsP3 to determine their efficacy. Figure 3.12 shows specific binding of the anti-CHIKV nsP3 antibody to ONNV and CHIKV nsP3 protein in BHK-21 cell lysate with bands between 66 kDa and 52 kDa. Using the ONNV non-structural polyprotein P1234 amino acid structure, cross-comparing CHIKV nsP3 amino acid structure to identify ONNV nsP3's amino acid structure and calculating the molecular mass, ONNV nsP3 is 62.4 kDa (UniProt, 2021). CHIKV nsP1 is 58 kDa (UniProt, 2021). When both nsP1 sequences were compared, there was a 67.8% match in sequence. The same considerations made for working with polyclonal antibodies made in 4.3.1 apply here, but a lower sequence similarity means blots for ONNV nsP3 should have reduced signal and sensitivity when compared to CHIKV nsP3. This is hard to judge due to the quality of western blots.

nsP3 is a multi-functional protein that is highly conserved within alphaviruses. It binds to host proteins G3BP1/2 in order to bind with stress molecules and inhibit their antiviral mechanisms (Panas *et al.*, 2012; Scholte *et al.*, 2015). nsP3 binds to RNA and is also theorised to be integral to viral RNA synthesis, potentially playing a role in the trafficking of

nucleocapsids to the plasma membrane and as such, is expected to migrate across the host cell (Gao *et al.*, 2019). Using a mutant CHIKV genome with alterations in the AUD (P247A/V248A), purifying and isolating the AUD of mutant and wild type CHIKV and using radiolabelling of RNA to measure binding efficacy, it was found that impaired binding of sgRNA (sub-genomic RNA) to the AUD impeded viral replication (Gao *et al.*, 2019). Furthermore, comparing sub-cellular localisations of nsP3 capsid and dsRNA in mutant and wild type CHIKV infection, colocalised at 8hpe (hours post electroporation) in clusters which then accumulated at the plasma membrane at 12 and 16hpe in wild type while the mutant produced reduced levels of capsid that were never sequestered to the plasma membrane (Gao *et al.*, 2019). This concretely solidified the idea that nsP3 plays a critical role in all stages of CHIKV RNA synthesis and potentially virus assembly, while displaying the multifunctionality of nsP3 within alphavirus replication.

Notably, in both ONNV-infected lysates, a faint band can be seen at around 95 kDa, which is representative of ONNV nsP3 with fluorescent proteins ZsGreen or mCherry bound to them (Figure 3.12). ZsGreen and mCherry have molecular masses of 26.1 kDa and 26.7 kDa respectively, which when added to ONNV nsP3's molecular mass is 88.5k Da and 89.1 kDa respectively. It is unclear why only a small fraction of the fluorescent ONNV nsP3 have their fluorescent proteins attached. There is a possibility of cleavage within the cellular environment or it could have occurred in the lysis/denaturing of the proteins for western blot. If fluorescent proteins are cleaved at a point in the cellular environment, their fluorescence would not be indicative of ONNV nsP3 localisation. To identify this, an IF assay using the anti-CHIKV nsP3 antibodies validated here could be used to characterise co-localisation of ONNV nsP3 and the fluorescent marker proteins, previous alphavirus studies have performed similar confirmations (Cristea *et al.*, 2006). In order to validate the genetic integrity of infectious clones, their genomes should be sequences. Nonetheless, the western blot validated the use of anti-CHIKV nsP3 antibodies for detection of ONNV nsP3.

It must be noted that investigations into the ONNV RC are limited by an absence of antibodies to detect nsP2 and nsP4. Antibodies for each would provide tools to gain more refined insight into the functions of the RC and its proteins during infection. The development of antibodies for other nsPs could prove challenging. Methods developed for creating nsP4 purifications using a bacterial expression system synthesise a heterogenous mix of nsP4 and cellular proteins, which would require further purification before use as an antigen for antibody development. (Rubach *et al.*, 2009). Purification itself poses further challenges, such as preventing non-native changes to the protein structure. nsP4 antibodies should be prioritised, as alphaviral nsP4 is known to be integral to RNA synthesis and yet is poorly

described in the literature (Hahn *et al.*, 1989; Kamer & Argos, 1984). nsP4 is the RNA-dependant RNA Polymerase (RdRp) in alphavirus replication, it is responsible for the synthesis of negative strand RNA from a positive strand RNA template. nsP4 requires P123, the polyprotein of nsP1, nsP3 and nsP3 to replicate minus strand RNA, and possesses TATase (Terminal Adenylyl transferase) activity to create the poly(A) tail, referred to in 1.5.4 (Rubach *et al.*, 2009; Tomar *et al.*, 2006). Information about nsP4's host protein interactions and co-localisations with other virus proteins could clarify aspects of ONNV replication. The use of cross-reactive antibodies developed against other alphaviral species is a possible solution to this issue; effective use of anti-SINV E2 antibodies cross-reactivity with ONNV E2 proteins has been described, which supports this. These could be validated for use as was performed in 3.2.2 and 3.2.3.

4.4 Immunofluorescence Microscopy of ONNV infection

4.4.1 nsP1 and nsP3 do not colocalise permanently in ONNV infection

In order to both elucidate the subcellular locations of ONNV nsPs during infection and validate anti-CHIKV nsP1 antibodies for use in ONNV IF assays, ONNV infection at MOIs of 1 and 10 in BHK-21 cells, visualised via immunofluorescence (Figure 3.13). These results show that by 12 hours in the ONNV infection cycle, nsP3 migrates across the cytoplasm and aggregates around the nucleus. These aggregates are notably absent of nsP1; in an MOI 10 infection at 12 hours, a visible region devoid of nsP1 is present where the nsP3 aggregates are.

As expected, nsP1 in ONNV infection binds to the plasma membrane and persists throughout infection. CHIKV nsP1 in the literature is described as having affinity for the plasma membrane of infected cells and this characteristic is seen across both MOIs in ONNV infection (Kumar *et al.*, 2018). In CHIKV infection, RCs are intermittently internalised into CPV-1 vesicles; however, this was not seen in ONNV infection over 48 hours, suggesting this characteristic may not be conserved between these species (Thaa *et al.*, 2015). nsP1 forms dodecameric pores at the opening of the spherules, regulating passage between the internal RC and cellular environments, in which it is irreversibly bound to the to plasma membrane, which is likely why we see association throughout infection (Jones *et al.*, 2021).

nsP3 is known for having multiple roles within the CHIKV replication process such as RNA binding, zinc binding and the regulation of stress granules to suppress anti-viral host responses (Gao *et al.*, 2019; Panas *et al.*, 2012; Shin *et al.*, 2012). The presence of ONNV nsP3 near the nucleus as puncta within the perinuclear area supports the idea, presented in the literature, that ONNV nsP3 also performs similar roles (Götte *et al.*, 2018; Panas *et al.*, 2014). Figure 3.16 demonstrated further that nsP3 initially localised at the plasma membrane at 2 hours and migrated into the cellular environment at 4 hours. The lower levels of nsP3 associated with the RC, highlighted by the minimal colocalization seen, is similar to that observed in CHIKV infection, but puncta size varies between the species. In CHIKV at 12 hours, puncta are >5μm on average, while those observed in ONNV infection could be much larger (Gao *et al.*, 2019). While it is possible cell lines used here display different levels of nsP3 cytoplasmic aggregates in infection, this could suggest a larger response to host anti-viral responses. In CHIKV and SFV, cytoplasmic nsP3 aggregates are reduced in mutants that fail to bind Ras-GTPase-activating protein (SH3-domain)-binding protein (G3BP), normal binding of which inhibits the formation of stress granules as a host anti-viral mechanism (Götte *et al.*, 2018; Panas *et al.*, 2014; Panas *et al.*, 2012). Evidently, nsP3 provides a natural resistance to host antiviral responses and likely does so in ONNV infection. As mentioned prior, aggregation of nsP3-mCherry in the perinuclear area may not be representative of all nsP3 sub-cellular localisation if the nsP3-mCherry fusion protein is cleaved in the cell, as Figure 3.12 may suggest.

The formation of syncytia was observed in ONNV infection at MOI-10, at 48 hours. Described prior, syncytia are large, polynucleated cells formed via the fusion of infected cells. Syncytia form when infected cells incorporate the fusion proteins of viruses to their plasma membrane into the external environment. When they make contact with neighbouring cells, fusion proteins make contact with their corresponding cell receptor proteins and fusion is initiated, forming a polynucleated syncytia. This can occur between any number of cells. ONNV syncytia at 48 hours were large (over 100 μm), as displayed by figure 3.13, it would have been useful to observe early stage syncytia of significantly fewer cells to exemplify the process of syncytia formation. Though not recognised regularly in the literature as characteristic of alphaviral infection, syncytia formation has been observed in the neuroblastoma cell line SH-SY5Y cells when infected with CHIKV. The cells displayed the formation of syncytia between 36-48 hours, which is around the time syncytia was observed in ONNV infection (Dhanwani *et al.*, 2012).

Visualisation of nsP3 could have been performed using fluorescent live-cell imaging, using the nsP3-fluorescent fusion protein ONNV species for infection. This would allow live

imaging of the infection cycle; however without a fluorescent tag on other nsPs, it would not be possible to visualise colocalization of nsPs. Probes for cellular organelles could also be validated and adopted for use with IF assays to identify interactions or localisation of viral proteins around or within organelles. The western blot of ONNV nsP3 performed in this study (Figure 3.12) showed both whole and cleaved nsP3-fluorescent fusion proteins, suggesting cleavage within the cellular environment. If this is the case, images using nsP3-mCherry fluorescence such as Figures 3.13 and 3.14 will not provide accurate information about nsP3 localisation in infection, as mentioned in 4.3.2.

As the nature of investigation was to gain an understanding of possible nsP1 and 3 colocalisation, we believe confocal immunofluorescence was the appropriate choice, but hesitant to make conclusions about nsP3 localisation due to cleavage of fluorescent fusion proteins.

4.4.2 The nature of CPV-1 formation in ONNV infection

Internalisation of the RCs in alphaviral infection creates CPV-1 vesicles, which contain large numbers of spherules, as such, they are the major site for ONNV genome replication and an area of localisation for nsPs. The formation of CPV-1 vesicles is the same in all alphaviral infections, but the processing of them differs; RCs are internalised in SFV infection while in CHIKV and SINV infections, spherules predominantly stay on the plasma membrane (Frolova *et al.*, 2010; Spuul *et al.*, 2010; Thaa *et al.*, 2015). ONNV shows a higher degree of amino acid homology with CHIKV than SFV, so it was presumed RCs would also be internalised early in ONNV infection (Khan *et al.*, 2002; UniProt, 2021). For further study of the ONNV RC and individual nsPs, the localisation of RCs at different time points in the ONNV infection cycle would be paramount for knowing when to begin isolation of the RCs and which membranes they predominantly reside on. Isolation of RCs would allow for further insight into the alphaviral replication process. Once SFV RCs were isolated, in vitro replication assays were performed and found RCs to be capable of synthesising SFV gRNA, but could not utilise exogenous template RNA (Pietila *et al.*, 2018). Insights into alphavirus replication such as this could be verified in more medically relevant models, like ONNV. Furthermore, isolated RCs also would allow investigation into the interconnected nature of the RdRp mentioned prior, an understanding of all nsPs is required as all four are required for RNA synthesis (Pietila *et al.*, 2018).

In the current study, an analysis of early ONNV infection in BHK-21 cells, treated with 100nM of the PI3K inhibitor Wortmannin, visualised via immunofluorescence (Figure 3.16),

demonstrated the migration of nsP3 from RCs to form puncta near the nucleus of cells. Alphavirus RCs are endocytosed in a PI3K and actin-myosin dependant manner, forming small internalised vesicles, which fuse with late endosomes and are transported by microtubules to the perinuclear area to form CPV-1s (Spuul *et al.*, 2010). When cells are treated with Wortmannin, the PI3K prevents internalisation, blocking RC internalisation. Investigations found SFV viral replication was not halted by this, and an increase in RNA production was observed (Pietila *et al.*, 2018; Spuul *et al.*, 2010). If RCs are blocked to the plasma membrane by wortmannin's presence, we can infer that nsP3's cellular localisations are not a visualisation of the internalisation of RCs, rather a localisation independent of RCs.

The migration of nsP3, rather than a permanent localisation to the RCs meant we were unable to accurately track the localisation or potential relocation of RCs during the 6 hour experiment. The early time points in comparison to other IF assays in this study was to mirror previous studies on alphavirus RCs, showing RC formation and internalisation within 6 hours; RC isolation techniques in SFV were performed after 4 hours (Pietila *et al.*, 2018; Spuul *et al.*, 2010). nsP3 migration has been documented prior in alphaviruses; in SFV infection of BHK-21 cells, nsP3 migrated from the plasma membrane but was associated with RCs, denoted by dsRNA presence (Spuul *et al.*, 2010). However, cytoplasmic aggregates separate from RCs have been observed in other alphavirus species and the levels of association vary depending on species (Götte *et al.*, 2018). As previously mentioned, in CHIKV and SFV, nsP3 binding to Ras-GTPase-activating protein (SH3-domain)-binding protein (G3BP), is associated with the inhibition of stress granule formation, a pro-viral protein-protein interaction (Götte *et al.*, 2018; Panas *et al.*, 2014; Panas *et al.*, 2012). Evidently, nsP3 provides pro-viral action in response to host antiviral responses out of RCs, while also playing a role in viral replication when present in RCs. The question we asked when designing this experiment was, "Do ONNV RCs internalise during infection, similar to some alphaviruses?", and as such, the information gained does not definitively answer our question.

To answer the question posed, a membrane-bound aspect of the RC could act as a marker protein to highlight the presence of spherules on the plasma membrane, as well as localise with spherules if they are relocated to CPVs. Described earlier, nsP1 binds to the plasma membrane to form pores that segregate the RC environment from the cytoplasm, making it an optimal marker protein for RCs. This has already proven effective, as shown in Figure 3.13. An alternative to nsP1 would be using dsRNA (double stranded RNA) as a marker molecule for RCs; dsRNA are the template for positive strand viral RNA, and sub-genomic RNA, and translation of the dsRNA takes place within the RC in alphaviral infection, previous

studies have demonstrated its worth as an RC marker molecule (Frolova *et al.*, 2010).

4.5 ONNV Virion Structure and Potential Complications

Using TEM images of ONNV virions, a 3D reconstruction of the ONNV virion was created from 65 particles, at a resolution of 32 Å, displaying an icosahedral arrangement of trimers and pentamers on the virion surface. Typical alphavirus structure, as displayed by CHIKV in figure 3.19 displays an icosahedral arrangement of pentamers and hexamers, though it must be noted the CHIKV average was generated from 36,236 CHIKV virions and is accurate to 5.3 Å, allowing for heightened structural accuracy. There is a notable difference in diameter also, the generated ONNV structure is much smaller (~50nM) than TEM micrographs visualisations of other alphavirus virions (60-70nm). It was concluded that the 3D structure generated for ONNV may not be an accurate representation of the ONNV capsid. The minimal size of the ONNV average and relative lack of glycoproteins could suggest the structure is that of the nucleocapsid, this is further supported by a previous structural study of CHIKV nucleocapsid structures, which shows an icosahedral structure formed of E1, E2, E3 and 6K viral proteins (Yap *et al.*, 2017).

Reconstruction quality and reliability are often difficult to judge, with reconstructions of structures differing between published papers. The first initial judgement of whether the structure is correct is a comparison between the input images and the reconstruction itself. For our reconstruction, we find the reconstruction falls short on size, in electron micrographs ONNV virions show to be 60-70nm, but this itself is not an accurate way of measuring virion size.

There are areas where our reconstruction faced setbacks that affected the quality of the reconstruction. First, the number of isolated virions used to generate the initial 3D structures was small; Determination of SFV's virion structure used 5276 particles to determine the virion structure to a 9 Å resolution, and notably, in the resulting work, found fusion proteins across the spike proteins to be 10 Å (Mancini *et al.*, 2000). The number of particles picked for reconstruction greatly heightens the resolution required to identify important structures present on the virion surface. Our structure was generated from 65 images at a resolution of 32 Å, this resolution may not be enough to fully display the expected hexamer/pentamer structure of alphaviruses. This could be rectified by either increasing the number of virions used to generate the structure, and/or examine the ONNV virion using Cryo-EM. Cryo-EM has been used previously to produce high-resolution structures of icosahedral virion structures, including alphaviruses, at resolutions nearing the atomic level, at 3-4 Å (Baker *et*

al., 1999; Guo & Jiang, 2014). Vitrification of samples ensures a more native and representative structure for EM, this would clarify whether or not sample preparation or negative staining of the virions has altered their structure somehow (Guo & Jiang, 2014). This would also work to either validate or discredit the 3D structure generated, as well as its size.

4.6 Future Work and Conclusions

At time of writing, there are no licensed treatments or vaccines for any alphaviruses. This represents a significant humanitarian and economic risk as emergent alphavirus epidemics occur across the world, as shown in La Reunion with CHIKV. Better understanding of the alphaviral lifecycle and the viral proteins involved may lead to potential targets for treatment, as well as novel vaccine targets. For the first time, through the use of time course infections, we have characterised the replication and viral titres of 5 cell lines for propagation and study of ONNV. BHK-21 cells provide the greatest titre of all cell lines observed, while Huh7 cells released minimal virus over 72 hours. Though a number of mammalian and insect cell lines were used, cell lines more representative of ONNV's insect vectors and human target cells should be examined in a similar manner. ONNV's replication in multiple *Ae. albopictus* cell lines could have implications for ONNV vector specificity in the future and the risk an *Ae. albopictus*-competent ONNV poses for global health. Mentioned prior, *Ae. albopictus*' geographical range has altered due to globalisation and climate change, posing new global health risks by bringing CHIKV into countries with susceptible human populations (Nasci, 2014). A single amino acid substitution in the CHIKV E1 envelope protein which inferred an increase in *Ae. albopictus* vector competency; a comparison of E1 protein structures showed conservation of alanine at position 226 in ONNV; The substitution that was responsible for CHIKV's increase in *Ae. albopictus* vector competency is likely possible for ONNV (Tsetsarkin *et al.*, 2007; UniProt, 2021).

We also validated claims that anti-CHIKV nsP antibodies are effective for use against ONNV nsP proteins, a valuable tool for present and future immunofluorescence experiments. Observations of nsP3-fusion protein cleavage were seen in P3ZsG and P3mCh infectious clones which, if cleavage occurs within the cellular environment, limits the reliability of these immunofluorescent marker proteins as markers for nsP3. Anti-CHIKV nsP2/4 antibodies should be validated the future studies, to allow for identification of all components of the RC.

Through immunofluorescence, we have characterised the location of nsP1 and nsP3 in ONNV infected cells over 48 hours. nsP1 localises to the plasma membrane permanently

during infection, potentially labelling the RCs and nsP3 begins in the RC but migrates to the nuclei, forming puncta and likely supresses anti-viral stress responses produced by the cell. nsP3 was found to be unfit as a cellular marker for RCs and determining the presence of CPV-1s in ONNV infection; alternative markers were suggested for future investigation.

Finally, we used TEM and negative staining to visualise ONNV virions and computationally generated and determined the 3D structure of the ONNV virion. There were a number of setbacks which limited the accuracy and resolution of our structure, these can be rectified using more virions for reconstruction, or higher-resolution imaging such as cryo-EM. Overall, this is the first time ONNV has been imaged in such a manner. Though the methodology requires further optimisation, our structure serves as an effective proof of principle and elucidates further avenues of investigation.

This study allows for further investigations of alphavirus life-cycles, using ONNV, a BSL-2 virus as a model organism. This will be especially useful for elucidation of aspects of the CHIKV lifecycle, ONNV's closest genetic relative, through the use of studies prohibited for BSL-3 pathogens, like cryo-EM. Potential avenues of investigation could include studies of the ONNV replication virus via purification of RC-rich membranes, which would allow for investigation of their stability, their ability to replicate once isolated and nsP interactions within the RC itself. Similar investigations have been performed using SFV, displaying purified membrane fragments with RNA-synthesising activity retained (Pietila *et al.*, 2018). Previously described, cryo-EM of the ONNV virion should be performed to confirm our observations, as well as identify protein structures not visible due to low resolution.

Chapter 5: Optimisation of the ONNV Reverse Genetic System: References

Adam, M. P., Ardinger, H. H., Pagon, R. A., Wallace, S. E., Bean, L. J. H., Stephens, K. & Amemiya, A. (1993) GeneReviews.

Ahola, T., Lampio, A., Auvinen, P. & Kääriäinen, L. (1999) Semliki Forest virus mRNA capping enzyme requires association with anionic membrane phospholipids for activity. *EMBO J*, 18(11), 3164-72.

Assuncao-Miranda, I., Cruz-Oliveira, C. & Da Poian, A. T. (2013) Molecular mechanisms involved in the pathogenesis of alphavirus-induced arthritis. *Biomed Res Int*, 2013, 973516.

Baker, T. S., Olson, N. H. & Fuller, S. D. (1999) Adding the third dimension to virus life cycles: three-dimensional reconstruction of icosahedral viruses from cryo-electron micrographs. *Microbiol Mol Biol Rev*, 63(4), 862-922, table of contents.

Bakhache, W., Neyret, A., Bernard, E., Merits, A. & Briant, L. (2020) Palmitoylated Cysteines in Chikungunya Virus nsP1 Are Critical for Targeting to Cholesterol-Rich Plasma Membrane Microdomains with Functional Consequences for Viral Genome Replication. *J Virol*, 94(10).

Barzon, L. (2018) Ongoing and emerging arbovirus threats in Europe. *J Clin Virol*, 107, 38-47.

Bessaud, M., Peyrefitte, C. N., Pastorino, B. A., Gravier, P., Tock, F., Boete, F., Tolou, H. J. & Grandadam, M. (2006) O'nyong-nyong Virus, Chad. *Emerg Infect Dis*, 12(8), 1248-50.

Blackburn, N. K., Besselaar, T. G. & Gibson, G. (1995) Antigenic relationship between chikungunya virus strains and o'nyong nyong virus using monoclonal antibodies. *Res Virol*, 146(1), 69-73.

Brault, A. C., Foy, B. D., Myles, K. M., Kelly, C. L., Higgs, S., Weaver, S. C., Olson, K. E., Miller, B. R. & Powers, A. M. (2004) Infection patterns of o'nyong nyong virus in the malaria-transmitting mosquito, Anopheles gambiae. *Insect Mol Biol*, 13(6), 625-35.

Cassadou, S., Boucau, S., Petit-Sinturel, M., Huc, P., Leparc-Goffart, I. & Ledrans, M. (2014) Emergence of chikungunya fever on the French side of Saint Martin island, October to December 2013. *Euro Surveill*, 19(13).

Chan, Y. H., Teo, T. H., Torres-Ruesta, A., Hartimath, S. V., Chee, R. S., Khanapur, S., Yong, F. F., Ramasamy, B., Cheng, P., Rajarethinam, R., Robins, E. G., Goggi, J. L., Lum, F. M., Carissimo, G., Renia, L. & Ng, L. F. P. (2020) Longitudinal [18F]FB-IL-2 PET Imaging to Assess the Immunopathogenicity of O'nyong-nyong Virus Infection. *Front Immunol*, 11, 894.

Couderc, T., Chretien, F., Schilte, C., Disson, O., Brigitte, M., Guivel-Benhassine, F., Touret, Y., Barau, G., Cayet, N., Schuffenecker, I., Despres, P., Arenzana-Seisdedos, F., Michault, A., Albert, M. L. & Lecuit, M. (2008) A mouse model for Chikungunya: young age and inefficient type-I interferon signaling are risk factors for severe disease. *PLoS Pathog*, 4(2), e29.

Cristea, I. M., Carroll, J. W., Rout, M. P., Rice, C. M., Chait, B. T. & MacDonald, M. R. (2006) Tracking and elucidating alphavirus-host protein interactions. *J Biol Chem*, 281(40), 30269-78.

Cross, R. K. (1983) Identification of a unique guanine-7-methyltransferase in Semliki Forest virus (SFV) infected cell extracts. *Virology*, 130(2), 452-63.

Cross, R. K. & Gomatos, P. J. (1981) Concomitant methylation and synthesis in vitro of Semliki Forest virus (SFV) ss RNAs by a fraction from infected cells. *Virology*, 114(2), 542-54.

Davis, J. L., Hodge, H. M. & Campbell, W. E., Jr. (1971) Growth of chikungunya virus in baby hamster kidney cell (BHK-21-clone 13) suspension cultures. *Appl Microbiol*, 21(2), 338-41.

de Lamballerie, X., Leroy, E., Charrel, R. N., Ttsetsarkin, K., Higgs, S. & Gould, E. A. (2008) Chikungunya virus adapts to tiger mosquito via evolutionary convergence: a sign of things to come? *Virol J*, 5, 33.

Deresiewicz, R. L., Thaler, S. J., Hsu, L. & Zamani, A. A. (1997) Clinical and neuroradiographic manifestations of eastern equine encephalitis. *N Engl J Med*, 336(26),

1867-74.

Dhanwani, R., Khan, M., Bhaskar, A. S., Singh, R., Patro, I. K., Rao, P. V. & Parida, M. M. (2012) Characterization of Chikungunya virus infection in human neuroblastoma SH-SY5Y cells: role of apoptosis in neuronal cell death. *Virus Res*, 163(2), 563-72.

Eckei, L., Krieg, S., Bütepage, M., Lehmann, A., Gross, A., Lippok, B., Grimm, A. R., Kümmerer, B. M., Rossetti, G., Lüscher, B. & Verheugd, P. (2017) The conserved macrodomains of the non-structural proteins of Chikungunya virus and other pathogenic positive strand RNA viruses function as mono-ADP-ribosylhydrolases. *Sci Rep*, 7, 41746.

Egloff, M. P., Malet, H., Putics, A., Heinonen, M., Dutartre, H., Frangeul, A., Gruez, A., Campanacci, V., Cambillau, C., Ziebuhr, J., Ahola, T. & Canard, B. (2006) Structural and functional basis for ADP-ribose and poly(ADP-ribose) binding by viral macro domains. *J Virol*, 80(17), 8493-502.

Fokam, E. B., Levai, L. D., Guzman, H., Amelia, P. A., Titanji, V. P., Tesh, R. B. & Weaver, S. C. (2010) Silent circulation of arboviruses in Cameroon. *East Afr Med J*, 87(6), 262-8.

Fox, J. M., Long, F., Edeling, M. A., Lin, H., van Duijl-Richter, M. K. S., Fong, R. H., Kahle, K. M., Smit, J. M., Jin, J., Simmons, G., Doranz, B. J., Crowe, J. E., Fremont, D. H., Rossmann, M. G. & Diamond, M. S. (2015) Broadly Neutralizing Alphavirus Antibodies Bind an Epitope on E2 and Inhibit Entry and Egress. *Cell*, 163(5), 1095-1107.

Foy, N. J., Akhrymuk, M., Akhrymuk, I., Atasheva, S., Bopda-Waffo, A., Frolov, I. & Frolova, E. I. (2013) Hypervariable domains of nsP3 proteins of New World and Old World alphaviruses mediate formation of distinct, virus-specific protein complexes. *J Virol*, 87(4), 1997-2010.

Friedman, R. M., Levin, J. G., Grimley, P. M. & Berezesky, I. K. (1972) Membrane-associated replication complex in arbovirus infection. *J Virol*, 10(3), 504-15.

Frolova, E. I., Gorchakov, R., Pereboeva, L., Atasheva, S. & Frolov, I. (2010) Functional Sindbis virus replicative complexes are formed at the plasma membrane. *J Virol*, 84(22), 11679-95.

Fros, J. J., Liu, W. J., Prow, N. A., Geertsema, C., Ligtenberg, M., Vanlandingham, D. L., Schnettler, E., Vlak, J. M., Suhrbier, A., Khromykh, A. A. & Pijlman, G. P. (2010) Chikungunya virus nonstructural protein 2 inhibits type I/II interferon-stimulated JAK-STAT signaling. *J Virol*, 84(20), 10877-87.

Fros, J. J., van der Maten, E., Vlak, J. M. & Pijlman, G. P. (2013) The C-terminal domain of chikungunya virus nsP2 independently governs viral RNA replication, cytopathicity, and inhibition of interferon signaling. *J Virol*, 87(18), 10394-400.

Gao, Y., Goonawardane, N., Ward, J., Tuplin, A. & Harris, M. (2019) Multiple roles of the non-structural protein 3 (nsP3) alphavirus unique domain (AUD) during Chikungunya virus genome replication and transcription. *PLoS Pathog*, 15(1), e1007239.

Ghildiyal, R., Gupta, S., Gabrani, R., Joshi, G., Gupta, A., Chaudhary, V. K. & Gupta, V. (2019) In silico study of chikungunya polymerase, a potential target for inhibitors. *Virusdisease*, 30(3), 394-402.

Göertz, G. P., McNally, K. L., Robertson, S. J., Best, S. M., Pijlman, G. P. & Fros, J. J. (2018) The Methyltransferase-Like Domain of Chikungunya Virus nsP2 Inhibits the Interferon Response by Promoting the Nuclear Export of STAT1. *J Virol*, 92(17).

Gorchakov, R., Frolova, E., Sawicki, S., Atasheva, S., Sawicki, D. & Frolov, I. (2008) A new role for ns polyprotein cleavage in Sindbis virus replication. *J Virol*, 82(13), 6218-31.
Götte, B., Liu, L. & McInerney, G. M. (2018) The Enigmatic Alphavirus Non-Structural Protein 3 (nsP3) Revealing Its Secrets at Last. *Viruses*, 10(3).

Gottipati, K., Woodson, M. & Choi, K. H. (2020) Membrane binding and rearrangement by chikungunya virus capping enzyme nsP1. *Virology*, 544, 31-41.

Gould, E. A. & Higgs, S. (2009) Impact of climate change and other factors on emerging arbovirus diseases. *Trans R Soc Trop Med Hyg*, 103(2), 109-21.

Grandadam, M., Caro, V., Plumet, S., Thiberge, J. M., Souares, Y., Failloux, A. B., Tolou, H. J., Budelot, M., Cosserat, D., Leparc-Goffart, I. & Despres, P. (2011) Chikungunya virus, southeastern France. *Emerg Infect Dis*, 17(5), 910-3.

Grimley, P. M., Berezesky, I. K. & Friedman, R. M. (1968) Cytoplasmic structures associated with an arbovirus infection: loci of viral ribonucleic acid synthesis. *J Virol*, 2(11), 1326-38.
Grimley, P. M., Levin, J. G., Berezesky, I. K. & Friedman, R. M. (1972) Specific membranous structures associated with the replication of group A arboviruses. *J Virol*, 10(3), 492-503.
Guo, F. & Jiang, W. (2014) Single particle cryo-electron microscopy and 3-D reconstruction of viruses. *Methods Mol Biol*, 1117, 401-43.

Haddow, A. J. D., C. J.; Walker, A. J. (1960) O'nyong-nyong fever: An epidemic virus disease in East Africa 1. Introduction. *Trans R Soc Trop Med Hyg*, 54(6), 517-522.

Hahn, Y. S., Strauss, E. G. & Strauss, J. H. (1989) Mapping of RNA- temperature-sensitive mutants of Sindbis virus: assignment of complementation groups A, B, and G to nonstructural proteins. *J Virol*, 63(7), 3142-50.

Helenius, A., Kartenbeck, J., Simons, K. & Fries, E. (1980) On the entry of Semliki forest virus into BHK-21 cells. *J Cell Biol*, 84(2), 404-20.

Hellström, K., Kallio, K., Utt, A., Quirin, T., Jokitalo, E., Merits, A. & Ahola, T. (2017) Partially Uncleaved Alphavirus Replicase Forms Spherule Structures in the Presence and Absence of RNA Template. *J Virol*, 91(18).

Henss, L., Yue, C., Von Rhein, C., Tschismarov, R., Lewis-Ximenez, L. L., Dölle, A., Baylis, S. A. & Schnierle, B. S. (2020) Analysis of Humoral Immune Responses in Chikungunya Virus (CHIKV)-Infected Patients and Individuals Vaccinated With a Candidate CHIKV Vaccine. *J Infect Dis*, 221(10), 1713-1723.

Jones, R., Bragagnolo, G., Arranz, R. & Reguera, J. (2021) Capping pores of alphavirus nsP1 gate membranous viral replication factories. *Nature*, 589(7843), 615-619.

Josseran, L., Paquet, C., Zehgnoun, A., Caillere, N., Le Tertre, A., Solet, J. L. & Ledrans, M. (2006) Chikungunya disease outbreak, Reunion Island. *Emerg Infect Dis*, 12(12), 1994-5.

Kading, R. C., Borland, E. M., Cranfield, M. & Powers, A. M. (2013) Prevalence of antibodies to alphaviruses and flaviviruses in free-ranging game animals and nonhuman primates in the greater Congo basin. *J Wildl Dis*, 49(3), 587-99.

Kallio, K., Hellström, K., Jokitalo, E. & Ahola, T. (2016) RNA Replication and Membrane Modification Require the Same Functions of Alphavirus Nonstructural Proteins. *J Virol*, 90(3), 1687-92.

Kamer, G. & Argos, P. (1984) Primary structural comparison of RNA-dependent polymerases from plant, animal and bacterial viruses. *Nucleic Acids Res*, 12(18), 7269-82.

Keene, K. M., Foy, B. D., Sanchez-Vargas, I., Beaty, B. J., Blair, C. D. & Olson, K. E. (2004) RNA interference acts as a natural antiviral response to O'nyong-nyong virus (Alphavirus; Togaviridae) infection of Anopheles gambiae. *Proc Natl Acad Sci U S A*, 101(49), 17240-5.

Khan, A. H., Morita, K., Parquet, M. D. C., Hasebe, F., Mathenge, E. G. M. & Igarashi, A. (2002) Complete nucleotide sequence of chikungunya virus and evidence for an internal polyadenylation site. *J Gen Virol*, 83(Pt 12), 3075-3084.

Kiwanuka, N., Sanders, E. J., Rwaguma, E. B., Kawamata, J., Ssengooba, F. P., Najjemba, R., Were, W. A., Lamunu, M., Bagambisa, G., Burkot, T. R., Dunster, L., Lutwama, J. J., Martin, D. A., Cropp, C. B., Karabatsos, N., Lanciotti, R. S., Tsai, T. F. & Campbell, G. L. (1999) O'nyong-nyong fever in south-central Uganda, 1996-1997: clinical features and validation of a clinical case definition for surveillance purposes. *Clin Infect Dis*, 29(5), 1243-50.

Kraemer, M. U. G., Reiner, R. C., Jr., Brady, O. J., Messina, J. P., Gilbert, M., Pigott, D. M., Yi, D., Johnson, K., Earl, L., Marczak, L. B., Shirude, S., Davis Weaver, N., Bisanzio, D., Perkins, T. A., Lai, S., Lu, X., Jones, P., Coelho, G. E., Carvalho, R. G., Van Bortel, W., Marsboom, C., Hendrickx, G., Schaffner, F., Moore, C. G., Nax, H. H., Bengtsson, L., Wetter, E., Tatem, A. J., Brownstein, J. S., Smith, D. L., Lambrechts, L., Cauchemez, S., Linard, C., Faria, N. R., Pybus, O. G., Scott, T. W., Liu, Q., Yu, H., Wint, G. R. W., Hay, S. I. & Golding, N. (2019) Past and future spread of the arbovirus vectors Aedes aegypti and Aedes albopictus. *Nat Microbiol*, 4(5), 854-863.

Kumar, S., Kumar, A., Mamidi, P., Tiwari, A., Kumar, S., Mayavannan, A., Mudulli, S., Singh, A. K., Subudhi, B. B. & Chattopadhyay, S. (2018) Chikungunya virus nsP1 interacts directly with nsP2 and modulates its ATPase activity. *Sci Rep*, 8(1), 1045.

Labadie, K., Larcher, T., Joubert, C., Mannioui, A., Delache, B., Brochard, P., Guigand, L., Dubreil, L., Lebon, P., Verrier, B., de Lamballerie, X., Suhrbier, A., Cherel, Y., Le Grand, R.

& Roques, P. (2010) Chikungunya disease in nonhuman primates involves long-term viral persistence in macrophages. *J Clin Invest*, 120(3), 894-906.

LaBeaud, A. D., Banda, T., Brichard, J., Muchiri, E. M., Mungai, P. L., Mutuku, F. M., Borland, E., Gildengorin, G., Pfeil, S., Teng, C. Y., Long, K., Heise, M., Powers, A. M., Kitron, U. & King, C. H. (2015) High rates of o'nyong nyong and Chikungunya virus transmission in coastal Kenya. *PLoS Negl Trop Dis*, 9(2), e0003436.

Lanciotti, R. S., Ludwig, M. L., Rwaguma, E. B., Lutwama, J. J., Kram, T. M., Karabatsos, N., Cropp, B. C. & Miller, B. R. (1998) Emergence of epidemic O'nyong-nyong fever in Uganda after a 35-year absence: genetic characterization of the virus. *Virology*, 252(1), 258-68.

Lastarza, M. W., Grakoui, A. & Rice, C. M. (1994) Deletion and duplication mutations in the C-terminal nonconserved region of Sindbis virus nsP3: effects on phosphorylation and on virus replication in vertebrate and invertebrate cells. *Virology*, 202(1), 224-32.

Lee, S., Owen, K. E., Choi, H. K., Lee, H., Lu, G., Wengler, G., Brown, D. T., Rossmann, M. G. & Kuhn, R. J. (1996) Identification of a protein binding site on the surface of the alphavirus nucleocapsid and its implication in virus assembly. *Structure*, 4(5), 531-41.

Leung, J. Y., Ng, M. M. & Chu, J. J. (2011) Replication of alphaviruses: a review on the entry process of alphaviruses into cells. *Adv Virol*, 2011, 249640.

Levinson, R. S., Strauss, J. H. & Strauss, E. G. (1990) Complete sequence of the genomic RNA of O'nyong-nyong virus and its use in the construction of alphavirus phylogenetic trees. *Virology*, 175(1), 110-23.

Lindh, E., Argentini, C., Remoli, M. E., Fortuna, C., Faggioni, G., Benedetti, E., Amendola, A., Marsili, G., Lista, F., Rezza, G. & Venturi, G. (2019) The Italian 2017 Outbreak Chikungunya Virus Belongs to an Emerging Aedes albopictus-Adapted Virus Cluster Introduced From the Indian Subcontinent. *Open Forum Infect Dis*, 6(1), ofy321.

Maciel-de-Freitas, R., Avendanho, F. C., Santos, R., Sylvestre, G., Araújo, S. C., Lima, J. B., Martins, A. J., Coelho, G. E. & Valle, D. (2014) Undesirable consequences of insecticide resistance following Aedes aegypti control activities due to a dengue outbreak. *PLoS One*, 9(3), e92424.

Malet, H., Coutard, B., Jamal, S., Dutartre, H., Papageorgiou, N., Neuvonen, M., Ahola, T., Forrester, N., Gould, E. A., Lafitte, D., Ferron, F., Lescar, J., Gorbalenya, A. E., de Lamballerie, X. & Canard, B. (2009) The crystal structures of Chikungunya and Venezuelan equine encephalitis virus nsP3 macro domains define a conserved adenosine binding pocket. *J Virol*, 83(13), 6534-45.

Mancini, E. J., Clarke, M., Gowen, B. E., Rutten, T. & Fuller, S. D. (2000) Cryo-electron microscopy reveals the functional organization of an enveloped virus, Semliki Forest virus. *Mol Cell*, 5(2), 255-66.

Marhoul, Z. & Pudney, M. (1972) A mosquito cell line (MOS. 55) from Anopheles gambiae larva. *Trans R Soc Trop Med Hyg*, 66(1), 183-4.

Martinet, J. P., Ferte, H., Failloux, A. B., Schaffner, F. & Depaquit, J. (2019) Mosquitoes of North-Western Europe as Potential Vectors of Arboviruses: A Review. *Viruses*, 11(11).

McPherson, R. L., Abraham, R., Sreekumar, E., Ong, S. E., Cheng, S. J., Baxter, V. K., Kistemaker, H. A., Filippov, D. V., Griffin, D. E. & Leung, A. K. (2017) ADP-ribosylhydrolase activity of Chikungunya virus macrodomain is critical for virus replication and virulence. *Proc Natl Acad Sci U S A*, 114(7), 1666-1671.

Meertens, L., Hafirassou, M. L., Couderc, T., Bonnet-Madin, L., Kril, V., Kümmerer, B. M., Labeau, A., Brugier, A., Simon-Loriere, E., Burlaud-Gaillard, J., Doyen, C., Pezzi, L., Goupil, T., Rafasse, S., Vidalain, P. O., Bertrand-Legout, A., Gueneau, L., Juntas-Morales, R., Ben Yaou, R., Bonne, G., de Lamballerie, X., Benkirane, M., Roingeard, P., Delaugerre, C., Lecuit, M. & Amara, A. (2019) FHL1 is a major host factor for chikungunya virus infection. *Nature*, 574(7777), 259-263.

Meshram, C. D., Agback, P., Shiliaev, N., Urakova, N., Mobley, J. A., Agback, T., Frolova, E. I. & Frolov, I. (2018) Multiple Host Factors Interact with the Hypervariable Domain of Chikungunya Virus nsP3 and Determine Viral Replication in Cell-Specific Mode. *J Virol*, 92(16).

Muller, H. M., Dimopoulos, G., Blass, C. & Kafatos, F. C. (1999) A hemocyte-like cell line established from the malaria vector Anopheles gambiae expresses six prophenoloxidase genes. *J Biol Chem*, 274(17), 11727-35.

Mutso, M., Morro, A. M., Smedberg, C., Kasvandik, S., Aquilimeba, M., Teppor, M., Tarve, L., Lulla, A., Lulla, V., Saul, S., Thaa, B., McInerney, G. M., Merits, A. & Varjak, M. (2018) Mutation of CD2AP and SH3KBP1 Binding Motif in Alphavirus nsP3 Hypervariable Domain Results in Attenuated Virus. *Viruses*, 10(5).

Nasci, R. S. (2014) Movement of chikungunya virus into the Western hemisphere. *Emerg Infect Dis*, 20(8), 1394-5.

Neuvonen, M., Kazlauskas, A., Martikainen, M., Hinkkanen, A., Ahola, T. & Saksela, K. (2011) SH3 domain-mediated recruitment of host cell amphiphysins by alphavirus nsP3 promotes viral RNA replication. *PLoS Pathog*, 7(11), e1002383.

Panas, M. D., Ahola, T. & McInerney, G. M. (2014) The C-terminal repeat domains of nsP3 from the Old World alphaviruses bind directly to G3BP. *J Virol*, 88(10), 5888-93.

Panas, M. D., Varjak, M., Lulla, A., Eng, K. E., Merits, A., Karlsson Hedestam, G. B. & McInerney, G. M. (2012) Sequestration of G3BP coupled with efficient translation inhibits stress granules in Semliki Forest virus infection. *Mol Biol Cell*, 23(24), 4701-12.

Parrott, M. M., Sitarski, S. A., Arnold, R. J., Picton, L. K., Hill, R. B. & Mukhopadhyay, S. (2009) Role of conserved cysteines in the alphavirus E3 protein. *J Virol*, 83(6), 2584-91.

Partidos, C. D., Paykel, J., Weger, J., Borland, E. M., Powers, A. M., Seymour, R., Weaver, S. C., Stinchcomb, D. T. & Osorio, J. E. (2012) Cross-protective immunity against o'nyong-nyong virus afforded by a novel recombinant chikungunya vaccine. *Vaccine*, 30(31), 4638-43.

Peränen, J., Rikkonen, M., Liljeström, P. & Kääriäinen, L. (1990) Nuclear localization of Semliki Forest virus-specific nonstructural protein nsP2. *J Virol*, 64(5), 1888-96.
Peter, B. J., Kent, H. M., Mills, I. G., Vallis, Y., Butler, P. J., Evans, P. R. & McMahon, H. T. (2004) BAR domains as sensors of membrane curvature: the amphiphysin BAR structure. *Science*, 303(5657), 495-9.

Pezzi, L., Diallo, M., Rosa-Freitas, M. G., Vega-Rua, A., Ng, L. F. P., Boyer, S., Drexler, J. F., Vasilakis, N., Lourenco-de-Oliveira, R., Weaver, S. C., Kohl, A., de Lamballerie, X., Failloux, A. B. & GloPID-R chikungunya, o. n.-n. a. M. v. W. G. (2020) GloPID-R report on chikungunya, o'nyong-nyong and Mayaro virus, part 5: Entomological aspects. *Antiviral Res*,

174, 104670.

Pezzi, L., LaBeaud, A. D., Reusken, C. B., Drexler, J. F., Vasilakis, N., Diallo, M., Simon, F., Jaenisch, T., Gallian, P., Sall, A., Failloux, A. B., Weaver, S. C., de Lamballerie, X. & GloPID-R chikungunya, o. n.-n. a. M. v. W. G. (2019a) GloPID-R report on chikungunya, o'nyong-nyong and Mayaro virus, part 2: Epidemiological distribution of o'nyong-nyong virus. *Antiviral Res*, 172, 104611.

Pezzi, L., Reusken, C. B., Weaver, S. C., Drexler, J. F., Busch, M., LaBeaud, A. D., Diamond, M. S., Vasilakis, N., Drebot, M. A., Siqueira, A. M., Ribeiro, G. S., Kohl, A., Lecuit, M., Ng, L. F. P., Gallian, P., de Lamballerie, X. & GloPID-R Chikungunya, O. n.-n. a. M. v. W. G. (2019b) GloPID-R report on Chikungunya, O'nyong-nyong and Mayaro virus, part I: Biological diagnostics. *Antiviral Res*, 166, 66-81.

Pialoux, G., Gauzere, B. A., Jaureguiberry, S. & Strobel, M. (2007) Chikungunya, an epidemic arbovirosis. *Lancet Infect Dis*, 7(5), 319-27.

Pietila, M. K., Hellstrom, K. & Ahola, T. (2017) Alphavirus polymerase and RNA replication. *Virus Res*, 234, 44-57.

Pietila, M. K., van Hemert, M. J. & Ahola, T. (2018) Purification of Highly Active Alphavirus Replication Complexes Demonstrates Altered Fractionation of Multiple Cellular Membranes. *J Virol*, 92(8).

Powers, A. M., Brault, A. C., Tesh, R. B. & Weaver, S. C. (2000) Re-emergence of Chikungunya and O'nyong-nyong viruses: evidence for distinct geographical lineages and distant evolutionary relationships. *J Gen Virol*, 81(Pt 2), 471-9.

Pyke, A. T., Moore, P. R. & McMahon, J. (2018) New insights into chikungunya virus emergence and spread from Southeast Asia. *Emerg Microbes Infect*, 7(1), 26.

Queyriaux, B., Simon, F., Grandadam, M., Michel, R., Tolou, H. & Boutin, J. P. (2008) Clinical burden of chikungunya virus infection. *Lancet Infect Dis*, 8(1), 2-3.

Reeves, W. C., Hutson, G. A., Bellamy, R. E. & Scrivani, R. P. (1958) Chronic latent infections of birds with Western equine encephalomyelitis virus. *Proc Soc Exp Biol Med*,

97(4), 733-6.

Roberts, G. C., Zothner, C., Remenyi, R., Merits, A., Stonehouse, N. J. & Harris, M. (2017) Evaluation of a range of mammalian and mosquito cell lines for use in Chikungunya virus research. *Sci Rep*, 7(1), 14641.

Robin, S., Ramful, D., Le Seach, F., Jaffar-Bandjee, M. C., Rigou, G. & Alessandri, J. L. (2008) Neurologic manifestations of pediatric chikungunya infection. *J Child Neurol*, 23(9), 1028-35.

Rodriguez-Andres, J., Rani, S., Varjak, M., Chase-Topping, M. E., Beck, M. H., Ferguson, M. C., Schnettler, E., Fragkoudis, R., Barry, G., Merits, A., Fazakerley, J. K., Strand, M. R. & Kohl, A. (2012) Phenoloxidase activity acts as a mosquito innate immune response against infection with Semliki Forest virus. *PLoS Pathog*, 8(11), e1002977.

Rubach, J. K., Wasik, B. R., Rupp, J. C., Kuhn, R. J., Hardy, R. W. & Smith, J. L. (2009) Characterization of purified Sindbis virus nsP4 RNA-dependent RNA polymerase activity in vitro. *Virology*, 384(1), 201-8.

Rwaguma, E. B., Lutwama, J. J., Sempala, S. D., Kiwanuka, N., Kamugisha, J., Okware, S., Bagambisa, G., Lanciotti, R., Roehrig, J. T. & Gubler, D. J. (1997) Emergence of epidemic O'nyong-nyong fever in southwestern Uganda, after an absence of 35 years. *Emerg Infect Dis*, 3(1), 77.

Salonen, A., Vasiljeva, L., Merits, A., Magden, J., Jokitalo, E. & Kääriäinen, L. (2003) Properly folded nonstructural polyprotein directs the semliki forest virus replication complex to the endosomal compartment. *J Virol*, 77(3), 1691-702.

Saxton-Shaw, K. D., Ledermann, J. P., Borland, E. M., Stovall, J. L., Mossel, E. C., Singh, A. J., Wilusz, J. & Powers, A. M. (2013) O'nyong nyong virus molecular determinants of unique vector specificity reside in non-structural protein 3. *PLoS Negl Trop Dis*, 7(1), e1931.

Schessl, J., Zou, Y., McGrath, M. J., Cowling, B. S., Maiti, B., Chin, S. S., Sewry, C., Battini, R., Hu, Y., Cottle, D. L., Rosenblatt, M., Spruce, L., Ganguly, A., Kirschner, J., Judkins, A. R., Golden, J. A., Goebel, H. H., Muntoni, F., Flanigan, K. M., Mitchell, C. A. & Bönnemann, C. G. (2008) Proteomic identification of FHL1 as the protein mutated in human reducing

body myopathy. *J Clin Invest*, 118(3), 904-12.

Scholte, F. E., Tas, A., Albulescu, I. C., Žusinaite, E., Merits, A., Snijder, E. J. & van Hemert, M. J. (2015) Stress granule components G3BP1 and G3BP2 play a proviral role early in Chikungunya virus replication. *J Virol*, 89(8), 4457-69.

Schuffenecker, I., Iteman, I., Michault, A., Murri, S., Frangeul, L., Vaney, M. C., Lavenir, R., Pardigon, N., Reynes, J. M., Pettinelli, F., Biscornet, L., Diancourt, L., Michel, S., Duquerroy, S., Guigon, G., Frenkiel, M. P., Brehin, A. C., Cubito, N., Despres, P., Kunst, F., Rey, F. A., Zeller, H. & Brisse, S. (2006) Genome microevolution of chikungunya viruses causing the Indian Ocean outbreak. *PLoS Med*, 3(7), e263.

Schulte, T., Liu, L., Panas, M. D., Thaa, B., Dickson, N., Götte, B., Achour, A. & McInerney, G. M. (2016) Combined structural, biochemical and cellular evidence demonstrates that both FGDF motifs in alphavirus nsP3 are required for efficient replication. *Open Biol*, 6(7).

Seymour, R. L., Rossi, S. L., Bergren, N. A., Plante, K. S. & Weaver, S. C. (2013) The role of innate versus adaptive immune responses in a mouse model of O'nyong-nyong virus infection. *Am J Trop Med Hyg*, 88(6), 1170-9.

Shathasivam, T., Kislinger, T. & Gramolini, A. O. (2010) Genes, proteins and complexes: the multifaceted nature of FHL family proteins in diverse tissues. *J Cell Mol Med*, 14(12), 2702-20.

Shin, G., Yost, S. A., Miller, M. T., Elrod, E. J., Grakoui, A. & Marcotrigiano, J. (2012) Structural and functional insights into alphavirus polyprotein processing and pathogenesis. *Proc Natl Acad Sci U S A*, 109(41), 16534-9.

Singh, H., Mudgal, R., Narwal, M., Kaur, R., Singh, V. A., Malik, A., Chaudhary, M. & Tomar, S. (2018) Chikungunya virus inhibition by peptidomimetic inhibitors targeting virus-specific cysteine protease. *Biochimie*, 149, 51-61.

Spuul, P., Balistreri, G., Kääriäinen, L. & Ahola, T. (2010) Phosphatidylinositol 3-kinase-, actin-, and microtubule-dependent transport of Semliki Forest Virus replication complexes from the plasma membrane to modified lysosomes. *J Virol*, 84(15), 7543-57.

Spuul, P., Salonen, A., Merits, A., Jokitalo, E., Kääriäinen, L. & Ahola, T. (2007) Role of the amphipathic peptide of Semliki forest virus replicase protein nsP1 in membrane association and virus replication. *J Virol*, 81(2), 872-83.

Spyr, C. A., Kasermann, F. & Kempf, C. (1995) Identification of the pore forming element of Semliki Forest virus spikes. *FEBS Lett*, 375(1-2), 134-6.

Staples, J. E. & Fischer, M. (2014) Chikungunya virus in the Americas--what a vectorborne pathogen can do. *N Engl J Med*, 371(10), 887-9.

Strauss, J. H. & Strauss, E. G. (1994) The alphaviruses: gene expression, replication, and evolution. *Microbiol Rev*, 58(3), 491-562.

Sudeep, A. B., Vyas, P. B., Parashar, D. & Shil, P. (2019) Differential susceptibility & replication potential of Vero E6, BHK-21, RD, A-549, C6/36 cells & Aedes aegypti mosquitoes to three strains of chikungunya virus. *Indian J Med Res*, 149(6), 771-777.
Suhrbier, A., Jaffar-Bandjee, M. C. & Gasque, P. (2012) Arthritogenic alphaviruses--an overview. *Nat Rev Rheumatol*, 8(7), 420-9.

Sun, S., Xiang, Y., Akahata, W., Holdaway, H., Pal, P., Zhang, X., Diamond, M. S., Nabel, G. J. & Rossmann, M. G. (2013) Structural analyses at pseudo atomic resolution of Chikungunya virus and antibodies show mechanisms of neutralization. *Elife*, 2, e00435.
Tappe, D., Kapaun, A., Emmerich, P., Campos Rde, M., Cadar, D., Gunther, S. & Schmidt-Chanasit, J. (2014) O'nyong-nyong virus infection imported to Europe from Kenya by a traveler. *Emerg Infect Dis*, 20(10), 1766-7.

Thaa, B., Biasiotto, R., Eng, K., Neuvonen, M., Götte, B., Rheinemann, L., Mutso, M., Utt, A., Varghese, F., Balistreri, G., Merits, A., Ahola, T. & McInerney, G. M. (2015) Differential Phosphatidylinositol-3-Kinase-Akt-mTOR Activation by Semliki Forest and Chikungunya Viruses Is Dependent on nsP3 and Connected to Replication Complex Internalization. *J Virol*, 89(22), 11420-37.

Tomar, S., Hardy, R. W., Smith, J. L. & Kuhn, R. J. (2006) Catalytic core of alphavirus nonstructural protein nsP4 possesses terminal adenylyltransferase activity. *J Virol*, 80(20), 9962-9.

Tossavainen, H., Aitio, O., Hellman, M., Saksela, K. & Permi, P. (2016) Structural Basis of the High Affinity Interaction between the Alphavirus Nonstructural Protein-3 (nsP3) and the SH3 Domain of Amphiphysin-2. *J Biol Chem*, 291(31), 16307-17.

Tsetsarkin, K. A., Chen, R., Leal, G., Forrester, N., Higgs, S., Huang, J. & Weaver, S. C. (2011) Chikungunya virus emergence is constrained in Asia by lineage-specific adaptive landscapes. *Proc Natl Acad Sci U S A*, 108(19), 7872-7.

Tsetsarkin, K. A., Vanlandingham, D. L., McGee, C. E. & Higgs, S. (2007) A single mutation in chikungunya virus affects vector specificity and epidemic potential. *PLoS Pathog*, 3(12), e201.

UniProt, C. (2021) UniProt: the universal protein knowledgebase in 2021. *Nucleic Acids Res*, 49(D1), D480-D489.

Varjak, M., Zusinaite, E. & Merits, A. (2010) Novel functions of the alphavirus nonstructural protein nsP3 C-terminal region. *J Virol*, 84(5), 2352-64.

Vu, D. M., Jungkind, D. & Angelle Desiree, L. (2017) Chikungunya Virus. *Clin Lab Med*, 37(2), 371-382.

Wada, Y., Orba, Y., Sasaki, M., Kobayashi, S., Carr, M. J., Nobori, H., Sato, A., Hall, W. W. & Sawa, H. (2017) Discovery of a novel antiviral agent targeting the nonstructural protein 4 (nsP4) of chikungunya virus. *Virology*, 505, 102-112.

Wahlberg, J. M., Bron, R., Wilschut, J. & Garoff, H. (1992) Membrane fusion of Semliki Forest virus involves homotrimers of the fusion protein. *J Virol*, 66(12), 7309-18.
Weaver, S. C. & Reisen, W. K. (2010) Present and future arboviral threats. *Antiviral Res*, 85(2), 328-45.

Weiss, B., Nitschko, H., Ghattas, I., Wright, R. & Schlesinger, S. (1989) Evidence for specificity in the encapsidation of Sindbis virus RNAs. *J Virol*, 63(12), 5310-8.

Wiebe, A., Longbottom, J., Gleave, K., Shearer, F. M., Sinka, M. E., Massey, N. C., Cameron, E., Bhatt, S., Gething, P. W., Hemingway, J., Smith, D. L., Coleman, M. & Moyes, C. L. (2017) Geographical distributions of African malaria vector sibling species and

evidence for insecticide resistance. *Malar J*, 16(1), 85.

Williams, M. C., Woodall, J. P. & Gillett, J. D. (1965) O'nyong-Nyong Fever: An Epidemic Virus Diesease in East Africa. Vii. Virus Isolations from Man and Serological Studies up to July 1961. *Trans R Soc Trop Med Hyg*, 59, 186-97.

Wilson, M. E. & Schlagenhauf, P. (2016) Aedes and the triple threat of DENV, CHIKV, ZIKV--Arboviral risks and prevention at the 2016 Rio Olympic games. *Travel Med Infect Dis*, 14(1), 1-4.

Woodruff, A. W., Bowen, E. T. & Platt, G. S. (1978) Viral infections in travellers from tropical Africa. *Br Med J*, 1(6118), 956-8.

Wu, D., Zhang, Y., Zhouhui, Q., Kou, J., Liang, W., Zhang, H., Monagin, C., Zhang, Q., Li, W., Zhong, H., He, J., Li, H., Cai, S., Ke, C. & Lin, J. (2013) Chikungunya virus with E1-A226V mutation causing two outbreaks in 2010, Guangdong, China. *Virol J*, 10, 174.
Zarrinpar, A., Bhattacharyya, R. P. & Lim, W. A. (2003) The structure and function of proline recognition domains. *Sci STKE*, 2003(179), RE8.

Yap, M. L., Klose, T., Urakami, A., Hasan, S. S., Akahata, W., Rossman, M. G. (2017) Structural Studies of Chikungunya virus maturation. *PNAS*, 114(52), 13703-13707.